USGS
science for a changing world

Two-Dimensional Seismic Velocities and Structural Variations at Three British Columbia Hydro and Power Authority (BC Hydro) Dam Sites, Vancouver Island, British Columbia, Canada

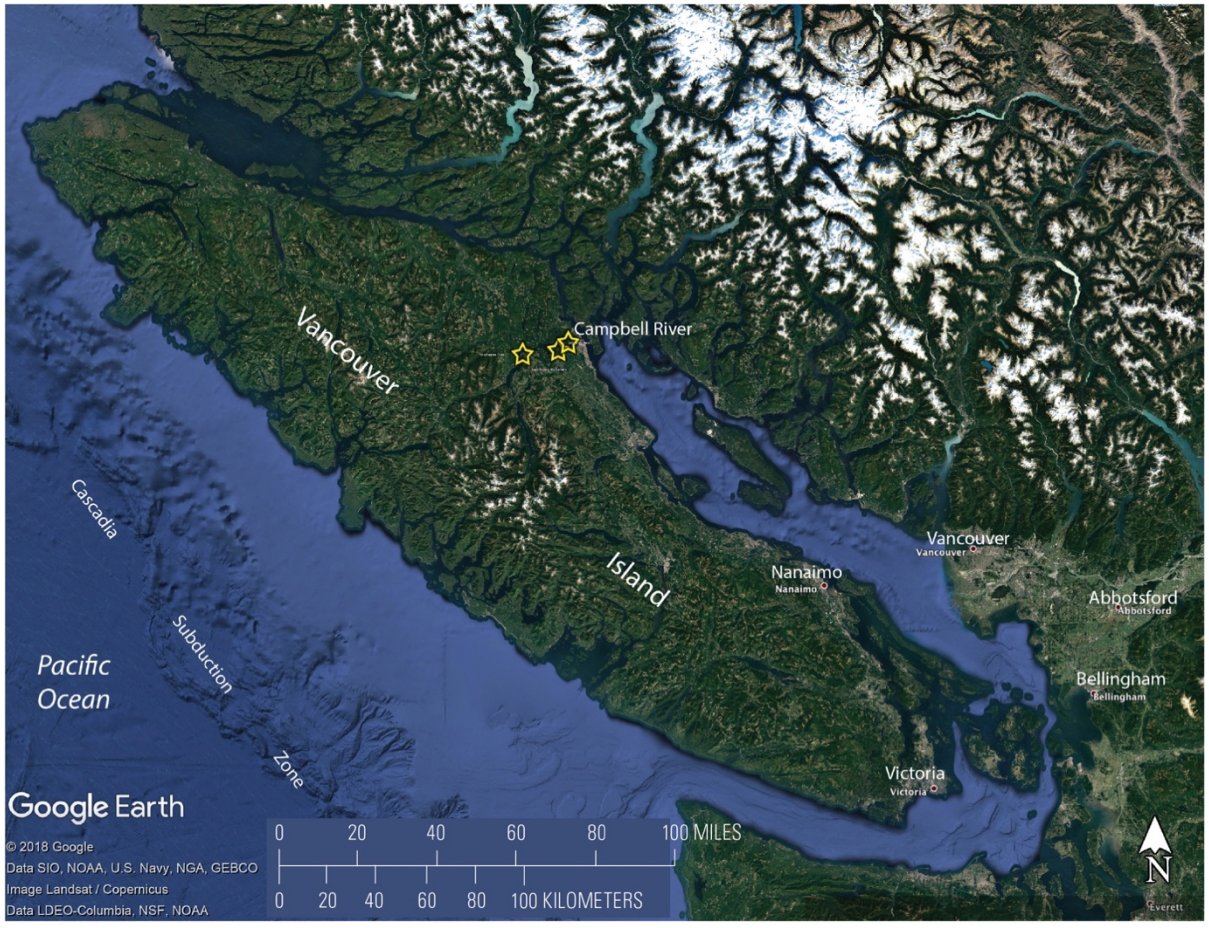

Open-File Report 2019–1015

U.S. Department of the Interior
U.S. Geological Survey

Cover. Map of Vancouver Island, British Columbia, Canada, showing three BC Hydro dam sites (John Hart, Ladore, and Strathcona Dams; stars) at which seismic velocities and two-dimensional structural variations were examined.

Two-Dimensional Seismic Velocities and Structural Variations at Three British Columbia Hydro and Power Authority (BC Hydro) Dam Sites, Vancouver Island, British Columbia, Canada

By Rufus D. Catchings, Kofi O. Addo, Mark R. Goldman, Joanne H. Chan, Robert R. Sickler, and Coyn J. Criley

Open-File Report 2019–1015

U.S. Department of the Interior
U.S. Geological Survey

U.S. Department of the Interior
DAVID BERNHARDT, Acting Secretary

U.S. Geological Survey
James F. Reilly II, Director

U.S. Geological Survey, Reston, Virginia: 2019

Suggested citation:
Catchings, R.D., Addo, K.O., Goldman, M.R., Chan, J.H., Sickler, R.R., and Criley, C.J., 2019, Two-dimensional seismic velocities and structural variations at three British Columbia Hydro and Power Authority (BC Hydro) dam sites, Vancouver Island, British Columbia, Canada: U.S. Geological Survey Open-File Report 2019–1015, 125 p., https://doi.org/10.3133/ofr20191015.

ISSN 2331-1258 (online)

Acknowledgments

We thank Keith Galvin, Freddie Jackson, Nicholas Ogasa, Brandon Smythe, Steve Watson, Alan Yong, and Edward Zhang for field assistance in acquiring the data. We thank Maria Garcia and Ray Chickite for medical assistance, and we thank several additional British Columbia Hydro and Power Authority (BC Hydro) staff for field and office support. We thank Robert Fornasier and Jane Meyer for logistical and administrative support. This work was completed under the authority of a 2011 agreement relating to scientific and technical cooperation in the Earth sciences between the U.S. Geological Survey (U.S. Department of the Interior) and British Columbia Hydro and Power Authority of British Columbia, Canada. We especially thank the Incorporated Research Institutions for Seismology (IRIS) Portable Array Seismic Studies of the Continental Lithosphere (PASSCAL) Instrument Center for providing seismic-recording equipment.

Contents

Figures

Tables

Conversion Factors

International System of Units to U.S. customary units

Multiply	By	To obtain
	Length	
meter (m)	3.281	foot (ft)
kilometer (km)	0.6214	mile (mi)
	Flow rate	
meter per second (m/s)	3.281	foot per second (ft/s)
	Mass	
kilogram (kg)	2.205	pound avoirdupois (lb)

U.S. customary units to International System of Units

Multiply	By	To obtain
	Length	
mile (mi)	1.609	kilometer (km)
	Mass	
pound, avoirdupois (lb)	0.4536	kilogram (kg)

Abbreviations

1D	one dimensional
2D	two dimensional
3D	three dimensional
AWD	accelerated weight drop
BC Hydro	British Columbia Hydro and Power Authority (a Canadian provincial Crown Corporation)
BRF	Beaufort Range Fault
g	acceleration due to gravity at the Earth's surface
Hz	hertz
MASW	multichannel analysis of surface waves using Rayleigh waves
MALW	multichannel analysis of surface waves using Love waves
MAS_RW	multichannel analysis of surface waves for Rayleigh waves (same as MASW)
MAS_LW	multichannel analysis of surface waves for Love waves (same as MALW)
M_w	moment magnitude
USGS	U.S. Geological Survey
V_P	P-wave or compressional-wave velocity
V_S	S-wave or shear-wave velocity
$V_{S(z)}$	time-averaged shear-wave velocities as a function of depth (*z*)
V_{S30}	time-averaged shear-wave velocity in the upper 30 meters of the subsurface
V_{S150}	time-averaged shear-wave velocity in the upper 150 meters of the subsurface
z	model depth

Two-Dimensional Seismic Velocities and Structural Variations at Three British Columbia Hydro and Power Authority (BC Hydro) Dam Sites, Vancouver Island, British Columbia, Canada

By Rufus D. Catchings,[1] Kofi O. Addo,[2] Mark R. Goldman,[1] Joanne H. Chan,[1] Robert R. Sickler,[1] and Coyn J Criley[1]

Executive Summary

In June 2017, we acquired seismic data along five linear profiles at three British Columbia Hydro and Power Authority (BC Hydro, a Canadian provincial Crown Corporation) dam sites (John Hart, Ladore, and Strathcona Dams) on Vancouver Island, British Columbia, Canada. We also attempted to acquire linear seismic profiles at two additional BC Hydro dam sites (Ruskin Dam and Stave Falls Dam) east of the City of Vancouver, British Columbia, Canada; however, due to a seismograph programming error, little active-source data from Ruskin Dam and Stave Falls Dam were recorded. Thus, results from Ruskin Dam and Stave Falls Dam are not included in this report.

At the three dam sites with successful data acquisition, we acquired both active- and passive-source data. Data acquisition details for each of the three dam sites varied in terms of seismic sources, the number of seismographs, and seismic profile length and orientation. However, for active-source acquisition at each dam site, we acquired one or more linear seismic profiles ranging in length from about 150 to 400 meters (m), and along each profile, seismograph spacing was either 3 or 5 m (see appendix 1). All data were recorded in three components (vertical and two horizontals). To greatly increase the resolution of the seismic velocity structure along these profiles, we co-located active sources at each seismograph.

Typically, for site characterization purposes, surface-based seismic velocity measurements are one dimensional (1D) and are averaged over large distances (~50 to ~100 m), with active seismic sources ("shots") typically placed at each end (and sometimes the middle) of a linear seismic profile that is at least 100 m long. Such acquisition methods result in shot spacings ranging from 50 to >100 m and rather low resolution (for example, see Odum and others, 2003; Pegah and Liu, 2016). However, for this study active-source spacing was as much as 33 times greater than spacing typically used for site characterization. Furthermore, we present two-dimensional (2D) models, instead of 1D models. In addition, most other studies simply record the vertical component of the wavefield, but in this study, we

[1]U.S. Geological Survey.
[2]BC Hydro, Burnaby British Columbia, Canada.

acquired three-component (P- and S-wave) data. The dense shot and seismograph spacings (see appendixes 1 and 2) and three-component data allow for multiple 2D evaluations and much greater resolution of the velocity structure at any point along the seismic profiles. Furthermore, we acquired passive (ambient noise) surface-wave data at each of the sites, but our initial analysis suggests the Earth's structure and topography at the sites on Vancouver Island are less than ideal to extract S-wave velocities from the passive surface-wave data (see appendix 3). The variety of data acquired and the number of evaluation methods used allow us to infer 2D structure, composition, and physical state of subsurface materials, in addition to evaluating the 2D, time-averaged, S-wave velocities.

From the active-source data acquired at the three Vancouver Island dam sites, we developed 2D compressional-wave velocity (V_P) models and shear-wave velocity (V_S) models from body waves and 2D V_S models from surface waves using two principle analysis techniques (multichannel analysis of surface waves (MASW) for Rayleigh waves (referred to as MASW or MAS_RW) and MASW for Love waves (referred to as MALW or MAS_LW). From the V_S models, we calculated the time-averaged V_S of the upper 30 m (V_{S30}) of the subsurface at regular lateral intervals (1 or 5 m intervals) along each V_S model. For longer (deeper) profiles, we calculated time-averaged V_S to depths as much as 150 m (V_{S150}) at regular lateral intervals (1 or 5 m intervals) along the V_S models. From the tomography models, we developed 2D time-averaged shear-wave velocity at all model depths, z, ($V_{S(z)}$) below the surface topography. In this report, we focus on the tomographic models, as they appear to be more reliable than models determined from surface waves, which are strongly affected by lateral variations in topography, velocity, and structure along most seismic profiles. However, we include the surface-wave-determined (MAS_RW/MAS_LW) models within this report. For tomographic analysis, we also calculated V_P/V_S ratios and Poisson's ratios, and we infer that the top of the water table varies laterally along each seismic profile, factors which can be useful in evaluating time-averaged V_{S30} using other techniques. The 2D velocity models are also useful in inferring 2D lateral variations in shallow crustal structure along the seismic profiles.

At John Hart Dam, our seismic profile trended along the middle earthfill dam (one of several dam structures at John Hart Dam), which consists of as much as 45 m of sediment overlying basaltic rock, as indicated by previously published information (Lou and others, 1991) and by our velocity models. Tomographic analyses of the data from John Hart Dam show that V_P ranges from about 750 meters per second (m/s) in the near-surface to about 5,750 m/s at a depth of about 100 m, with significant lateral variations. V_S ranges from about 300 m/s to 1,700 m/s in the upper 50 m to as much as 2,700 m/s at a depth of about 150 m. Calculations of V_{S30} and V_{S150} vary depending on the data analysis method (tomography, MAS_RW, MAS_LW) used to calculate V_S, but we determined tomographic values of V_{S30} and V_{S150} at the John Hart Dam strong-motion recording site to be 577 m/s and 1,032 m/s, respectively. Lateral variations in tomographic V_{S30} along the length of the profile ranged from 465 m/s to 917 m/s, with an average value of 559 m/s. Near the intersection of our seismic profile with a newly constructed tunnel, we modeled high V_P, but relatively low V_S, which may indicate saturated and highly fractured basaltic rocks (or some material other than solid basalt) at depth. Alternatively, the modeled low V_S may result from possible inaccurate first-arrival measurements in a very localized set of shot gathers (see Data Limitations section); however, we note that the models derived from surface-wave data, which are independent from the first-arrival refractions, also indicate low V_S values in the same location. Our models also indicate a localized zone of high V_P/V_S and Poisson's ratios (as much as 4.4 and 0.47, respectively) that also may (if correct) indicate water saturation and rock damage (Catchings and others, 2014), with the zone extending from near the intersection of the seismic profile and the tunnel (at depth) to the center of the earthfill dam near the surface.

At Ladore Dam, our seismic profile was oriented approximately perpendicular to the dam, laterally offset by about 60 m to the northeast. V_P and V_S are highly variable, especially near the dam. Modeled tomographic velocities range from about 750 m/s (V_P) and 400 m/s (V_S) near the surface to about 6,500 m/s (V_P) and 2,300 m/s (V_S) at about 35-m depth, respectively. Our calculations of V_{S30} are highly variable laterally, and V_{S30} also varies with data-analysis methodology (tomographic, MAS_RW, MAS_LW). For all methods, we found V_{S30} values range from 575 m/s to 2,163 m/s laterally along the seismic profile. There is a near-vertical discontinuity that offsets high- and low-velocity rocks across a topographic slope near the dam. We also observe prominent near-vertical discontinuities in V_P, V_S, and V_P/V_S and Poisson's ratios across the topographic slope, and we speculate that this observed large lateral change in subsurface materials and topographic variation may be fault related, given that a geologic fault has been mapped in the vicinity of the dam (Geosciences BC, 2013). Generally, large lateral variations in seismic velocities due to faults or other factors are an important consideration for site characterization studies, as they can strongly affect potential ground motions.

We acquired three seismic profiles at Strathcona Dam, one along the roadway (Roadway profile) extending from the dam, a second along the spillway (Spillway profile), and a third along the campground (Campground profile) at the base of the dam. The data along each of the Strathcona seismic profiles include significant cultural noise, which makes it difficult to analyze the Strathcona profiles with all three techniques. As a result, velocity models are less well determined at Strathcona Dam that at either John Hart Dam or Ladore Dam.

Along the Strathcona Roadway profile, V_P and V_S also vary laterally and vertically, with modeled tomographic velocities ranging from about 1,000 m/s (V_P) and 400 m/s (V_S) in the near surface to about 4,750 m/s (V_P) and 3,200 m/s (V_S) at depths of approximately 40 m. Generally, we observe lower velocities near the dam. Our calculated V_P/V_S and Poisson's ratios determined from tomography are highly variable (1.5–2.5 and 0.05–0.4, respectively) and may indicate variable lithologies and physical conditions in the subsurface. Alternatively, the variable ratios may have resulted from highly averaged V_P or V_S values in a discrete area of our model that resulted from imprecise first-arrival measurements at the corresponding location along the seismic profile. Our calculated V_{S30} values vary laterally along the Roadway seismic profile and also vary with data analysis methodology (tomographic, MAS_RW, MAS_LW), ranging laterally from 311 to 1,551 m/s.

Along the Strathcona Spillway profile, V_P and V_S also vary laterally and vertically, with modeled tomographic velocities ranging from about 1,500 m/s (V_P) and 1,200 m/s (V_S) in the near surface to about 5,600 m/s (V_P) and 3,300 m/s (V_S) at approximately 40 m depth. Our calculated V_P/V_S and Poisson's ratios are highly variable (0.95–1.80 and 0.01–0.21, respectively) and likely reflect variable lithologies and physical conditions but could also reflect localized zones where either the V_P or V_S model is not precisely determined. On the basis of the V_S tomography model, we calculated V_{S30} to range laterally from 2,128 to 2,594 m/s, but we note that there is uncertainty in the tomographic model because of weak first arrivals. Due to the high rock velocities and the short length of the seismic profiles, even small (a few milliseconds) errors in arrival-time measurements can locally alter the modeled velocities. As a result of inconsistent dispersion curves observed along the Spillway profile, MAS_RW/MAS_LW-based V_S is not well determined.

Along the Strathcona Campground profile, V_P and V_S vary laterally and vertically. Due to noise conditions (See appendix 1, fig. 48), only V_P (1,500–6,000 m/s) could be modeled in the upper 55 m using the tomography data, as the S-wave first-arrivals were not evident beyond about 20 m laterally from the source. As a result, we were not able to calculate tomographic V_P/V_S and Poisson's ratios along the Campground profile. Coherent dispersion curves were apparent only with the Love-wave data; thus,

V_S (400–1,900 m/s) was calculated only on the basis of MAS_LW (Love waves). Lateral variations in MAS_LW-based V_{S30} values range from 577 to 692 m/s along the Campground seismic profile.

Evaluating V_S with surface-wave methods in geologically complex areas and along certain engineered structures (such as dams) can be difficult due to the 1D Earth assumption inherent in the surface-wave method (Kim and others, 2001; Min and Kim, 2006; Karl and others, 2011; Zeng and others, 2012; Cardarelli and others, 2014). In such environments, the use of multiple types of seismic data can be valuable in obtaining reasonable results (Ivanov and others, 2009; 2017; Cardarelli and others, 2014), and using multicomponent (P-wave, S-wave, Rayleigh-wave, and Love Wave) seismic data (acquired with multiple sources), combined with multiple seismic analysis techniques (P and S tomography, MAS_RW, and MAS_LW), can further improve the results (Ivanov and others, 2009; 2017; Yong and others, 2013; Cardarelli and others, 2014; Pegah and Liu, 2016; Catchings and others, 2017; Martin and others, 2017). Such complex geological or engineered structures exist along each of our seismic profiles at the BC Hydro dam sites.

Overall, we found the seismic velocities (V_P and V_S) to be highly variable in the our study area due to variations in sediments, sedimentary rocks, and basement rocks. In the vicinity of the three dams where we acquired data, we found near-surface sediments (V_P=750 to 1,500 m/s; V_S=300 to 800 m/s) to range in thickness from ~0 to 45 m from site to site. We found basement velocities to be generally high, both with respect to V_P and V_S. V_P of basement rocks ranges from a minimum of about 1,500 m/s to a maximum of about 6,500 m/s in the upper 100 m, and V_S of basement rocks ranges from a minimum of about 800 m/s to a maximum of about 3,300 m/s in the upper 100 m. We observed strong lateral variations in V_{S30} at individual sites and among the sites. Our calculated V_{S30} values also varied with the data analysis method; from tomography, MAS_RW, and MAS_LW, we found the range of V_{S30} values to be 465–2,594 m/s, 198–2,163 m/s, and 263–1,625 m/s, respectively, among all sites.

Introduction

British Columbia Hydro and Power Authority (BC Hydro) is a Canadian provincial Crown Corporation that reports to the British Columbia Ministry of Energy and Mines and is regulated by the British Columbia Utilities Commission. BC Hydro generates and distributes electricity in the province of British Columbia, providing service to approximately 1.8 million people. On Vancouver Island, BC Hydro operates six electricity-generating facilities—Strathcona, Ladore, John Hart, Jordan River, Puntledge, and Ash River generating stations. In June 2017, we conducted five seismic investigations at three of those facilities—Strathcona, Ladore, and John Hart Dams (fig. 1*A*,*B,C*).

A

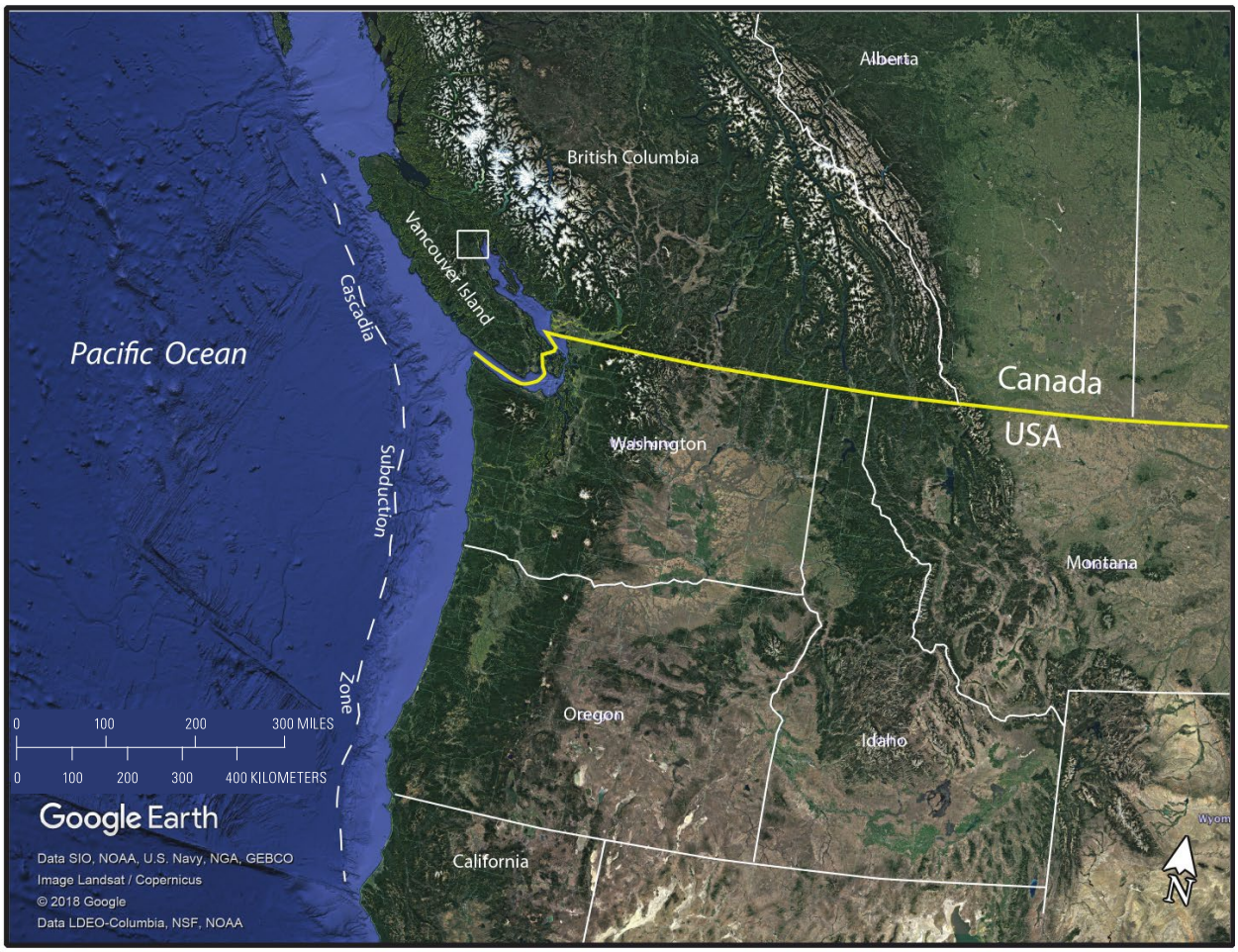
Alberta
British Columbia
Vancouver Island
Cascadia
Subduction
Zone
Pacific Ocean
Canada
USA
Washington
Montana
Oregon
Idaho
California
0 100 200 300 MILES
0 100 200 300 400 KILOMETERS
Google Earth
Data SIO, NOAA, U.S. Navy, NGA, GEBCO
Image Landsat / Copernicus
© 2018 Google
Data LDEO-Columbia, NSF, NOAA
N

B


Bloedel
Heriot Bay
Quathiaski Cove
John Hart Dam
Campbell River
Yaculta
Ladore Dam
Strathcona Dam
Quinsam
0 1 2 3 4 5 MILES
0 1 2 3 4 5 KILOMETERS
N
Google Earth
Data SIO, NOAA, U.S. Navy, NGA, GEBCO
Image © 2018 DigitalGlobe
Image © 2018 CNES / Airbus

C

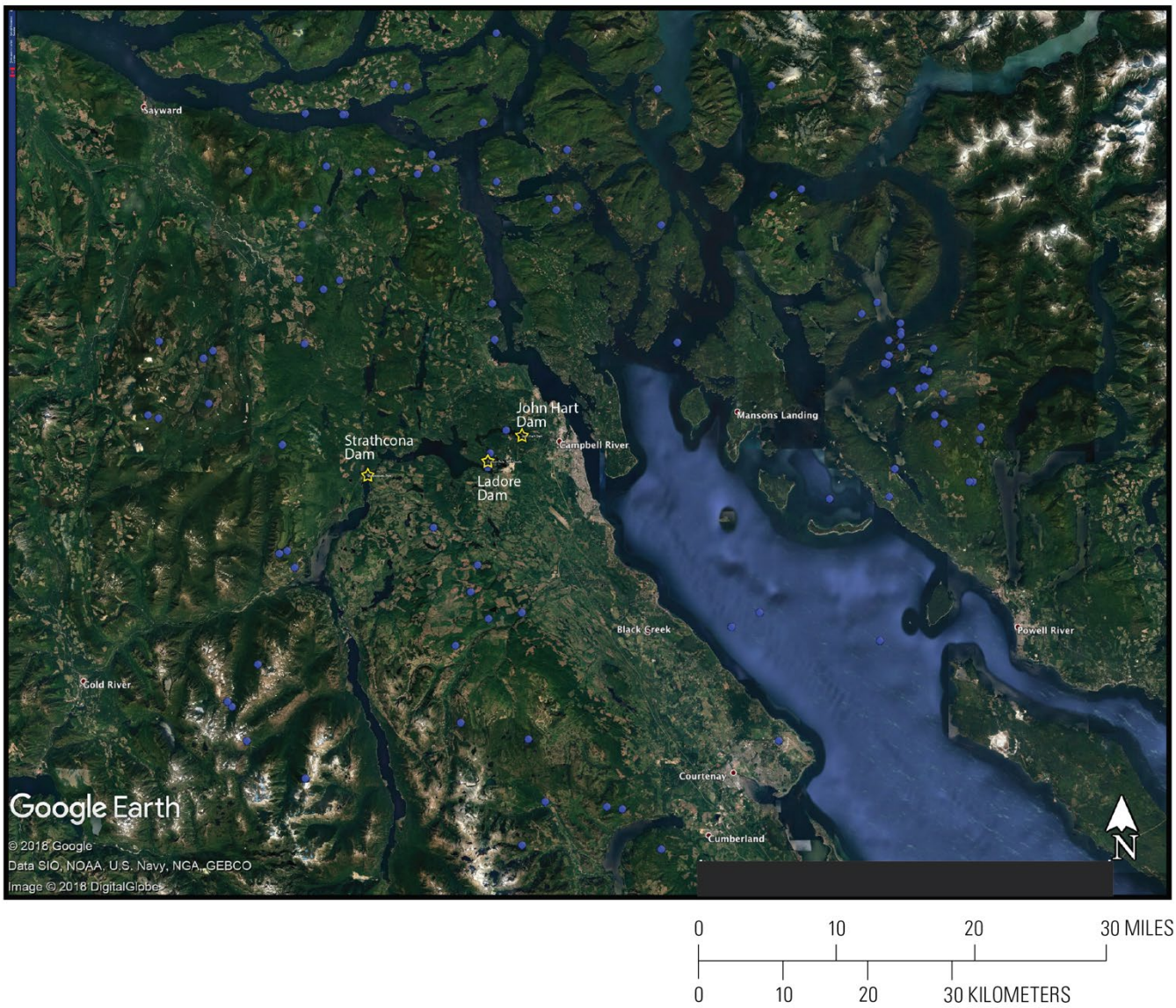

Figure 1. Satellite images of the study area where seismic data were collected along five linear profiles at three British Columbia Hydro and Power Authority (BC Hydro) dam sites, Vancouver Island, British Columbia, Canada. *A*, Image of the northwestern United States, southwestern Canada, and the adjoining eastern Pacific Ocean. Our study area is shown in the white rectangle on Vancouver Island, in southwestern British Columbia. The general trend of the Cascadia Subduction Zone is shown offshore, trending from northern California to the northern part of Vancouver Island. *B,* Close-up view of the white rectangle shown in figure 2*A*. Yellow stars show the locations of three dams of the Campbell River system discussed in this report. *C*, An expanded image of the study area with the locations of the dams (yellow stars) and earthquakes (blue dots) recorded within 50 kilometers of downtown Campbell River during the period January 1, 1985, to July 5, 2018 (from Natural Resources Canada, 2018). (Images from Google Earth®.)

Vancouver Island is subject to strong shaking from regional and local earthquake sources. To better understand potential seismic shaking hazards at BC Hydro power-generating stations on Vancouver Island, the U.S. Geological Survey (USGS), in collaboration with BC Hydro, conducted a series of seismic investigations to measure shallow-depth, shear-wave velocities and shallow-crustal velocity structure at those generating stations. In this report, we present two-dimensional (2D) models of compressional-wave velocity (V_P), shear-wave velocity (V_S), time-averaged shear-wave velocity to 30 meters (m) depth (V_{S30}), time-averaged shear-wave velocity as a function of depth (z) ($V_{S(z)}$), V_P/V_S ratios, and Poisson's ratios along most seismic profiles acquired at the Strathcona, Ladore, and John Hart electrical-power-generating stations (dams).

Tectonic Setting and Geology

Vancouver Island and southwestern British Columbia are bordered on the west by the Cascadia Subduction Zone (figs. 1*A* and 2), a convergent plate boundary that extends from northern California to northern Vancouver Island, approximately 1,000 kilometers (km). The Cascadia Subduction Zone may be capable of generating earthquakes that exceed magnitude 9.0. The last great earthquake on the Cascadia Subduction Zone occurred in the year 1700 (Satake and others, 1996; Yamaguchi and others, 1997; Atwater and others, 2015), and paleoseismic studies indicate that great earthquakes occur on average, every ~240 to 500 years (Goldfinger and others, 2012). Thus, presently, the Cascadia Subduction Zone is theoretically capable of generating a large-magnitude earthquake that could affect power-generating stations on Vancouver Island.

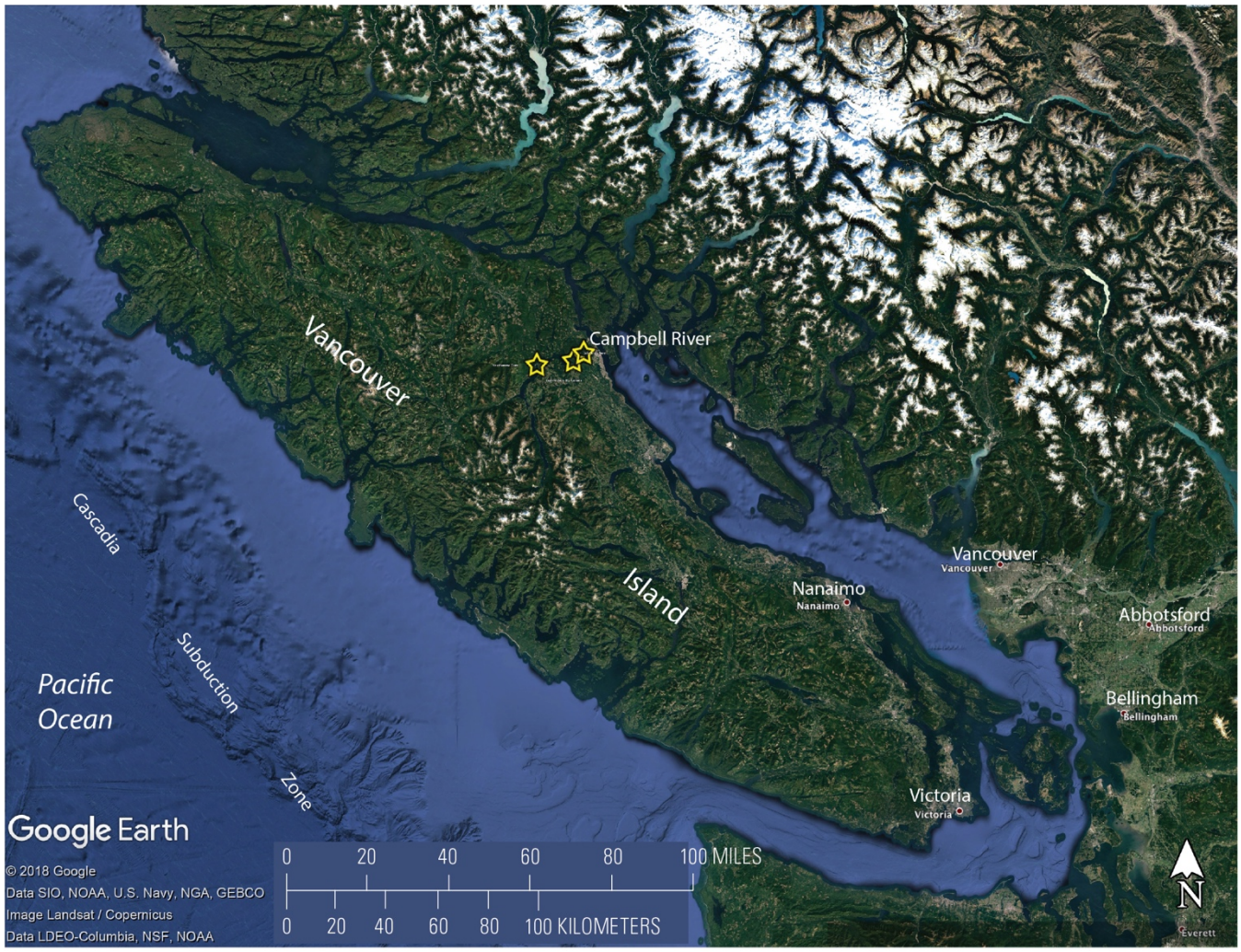

Figure 2. Satellite image of Vancouver Island, British Columbia, Canada, with the locations of the three British Columbia Hydro and Power Authority (BC Hydro) dams in our study area (yellow stars). The northern part of the Cascadia Subduction Zone can be seen offshore of Vancouver Island. (Image from Google Earth®.)

In addition to the regional hazards posed by the Cascadia Subduction Zone, locally there are crustal faults on Vancouver Island that are capable of generating significant earthquakes. The most prominent known fault on Vancouver Island is the Beaufort Range Fault (BRF), which trends northwesterly, extending to our general study area, and is believed to have been the causative fault of the June 23, 1946, moment magnitude (M_w) 7.5 Vancouver Island earthquake (Rogers and Hasegawa, 1978). The BRF extends to within at least 10 km of Strathcona Dam and is no farther than 30 km from the other dams evaluated in this study (Geosciences BC, 2013). However, the causative fault is not well determined. Initial determinations of the epicenter of the 1946 Vancouver Island earthquake placed it closer to the City of Campbell River, possibly on a fault other than the BRF. According to the Natural Resources of Canada (2018), between 1985 and 2018, there have been 96 recorded earthquakes (magnitude 2 or less) within 50 km of downtown Campbell River, three of which have epicenters in the immediate vicinity (~ 2 km) of John Hart Dam or Ladore Dam (fig. 1*C*). Hypocenters of the proximal earthquakes range in depth from 0 to 54.5 km.

A combination of thrust, normal, and undetermined faults is mapped in the area of the three dam sites investigated in this study (fig. 3; Geosciences BC, 2013). These faults generally range in orientation from northwest to northeast. A mapped normal fault trends through the vicinity of Ladore Dam, and a mapped fault (unknown slip direction) also extends beneath the alluvial cover slightly northwest of Strathcona Dam. Alluvium largely covers the surface near John Hart Dam, making it difficult to map basement faults there, but a normal fault is mapped within 1.5 km of the dam (Geosciences BC, 2013). We are unaware of the recency of slip on the faults in our study area; however, the combination of regional Cascadia Subduction Zone-related earthquakes, as well as local earthquakes (discussed above) beneath Vancouver Island, suggest the dams may be subject to strong seismic shaking (Lou and others, 1991; BC Hydro, 2012a,b; Lawrence and others, 2014; McCann and others, 2014). Therefore, we undertook these seismic surveys to better characterize the site response and path effects near the subject dams of this study.

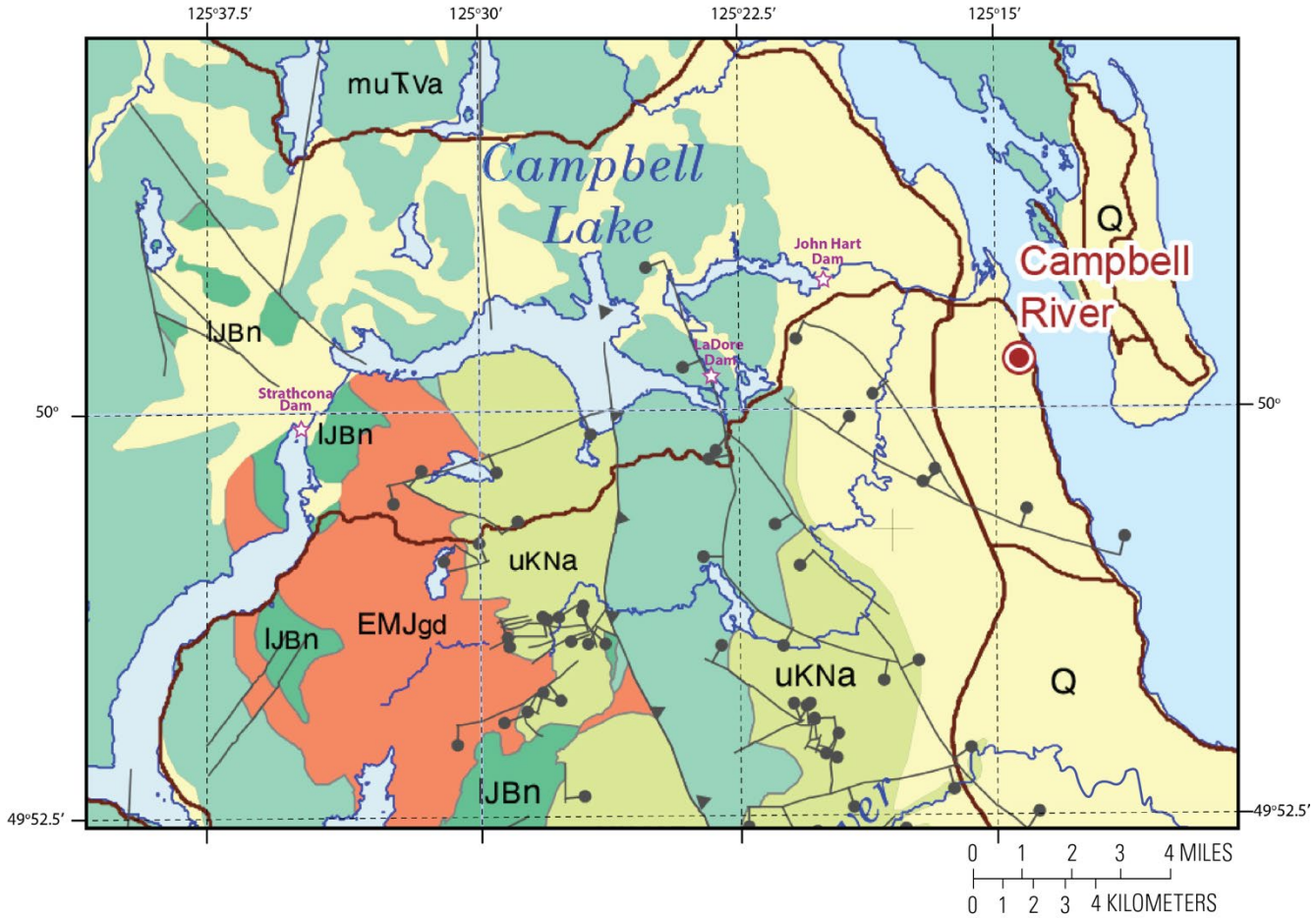

Figure 3. Geologic map of the study area, Vancouver Island, British Columbia, Canada. The locations of John Hart, Ladore, and Strathcona Dams are shown by the magenta and white stars. Faults are shown as thin black lines. Fault with barbs indicate thrust faults, faults with round paddles indicate normal faults. Geologic units—Q, (Quaternary cover), uKNa (upper Cretaceous Nanaimo Group), IJBn (Lower Jurassic Bonanza Group), muTVa (Middle to Upper Triassic Vancouver Group and equivalents), and EMJgd (Early to Middle Jurassic granodiorite). For descriptions of the units, see the text. (Map from Geosciences BC, 2013.)

The geology of Vancouver Island is highly variable, with rocks ranging from Paleozoic to Cenozoic (fig. 3). Many of the valleys are covered at the surface by glacial and fluvial deposits. According to Geosciences BC (2013), deposits and rocks in the immediate study area consist of:

1. Quaternary cover (Q): Alluvium, glaciofluvial gravels and sand, till.
2. Upper Cretaceous Nanaimo Group (uKNa)—Boulder, cobble and pebble conglomerate, coarse to fine sandstone, siltstone, shale, and coal.
3. Lower Jurassic Bonanza Group (lJBn)—Massive amygdaloidal and pillowed basalt to andesite flows, dacite to rhyolite massive or laminated lava, green and maroon tuff, feldspar crystal tuff, breccia; tuffaceous sandstone, argillite, pebble conglomerate, and minor limestone and calcareous siltstone.
4. Middle to Upper Triassic Vancouver Group and equivalents (muTVa)—Basalt pillowed flows, pillow breccia, hyaloclastite tuff and breccia, massive amygdaloidal flows, minor tuffs, interflow sediment and limestone lenses; grey to black, micritic and stylolitic limestone, calcareous siltstone, minor oolitic and bioclastic limestone, garnet-epidote-diopside skarn; thinly bedded black argillite, siltstone and shale, calcareous argillite, grey and black limestone, shaly limestone, coralline limestone, minor tuffaceous sandstone, grit, and breccia.
5. Early to Middle Jurassic granodiorite (EMJgd).

Seismic Surveys and Acquisition

In June 2017, we acquired one seismic survey at John Hart Dam, one seismic survey at Ladore Dam, and three seismic surveys at Strathcona Dam (fig. 1*B,C*). Our seismic surveys consisted of active-source P- and S-wave refraction surveys, active-source surface-wave surveys, and ambient noise surveys (not fully analyzed here). We used multiple sources to acquire the active-source data, including (1) a 500 pound (lb) (227 kilogram, kg) vertical accelerated weight drop (AWD), (2) a 100-lb (45 kg) vertical AWD, (3) a 100-lb (45 kg) angled AWD, (4) a 10-lb (4.5 kg) hammer and plate combination, (5) a 3-lb (1.4 kg) hammer and plate combination, and (6) a Betsy Seisgun® (with 400-grain (26-gram) black powder shells). The 100-lb (45-kg) angled weight drop and the two hammer/plate combinations were used to generate shear waves, and the other active-sources were used to generate both compressional waves for V_P measurements and surface waves for V_S measurements. Timing (~ 0.1 millisecond, ms, accuracy) was determined electronically by completing a closed circuit when the hammer (or AWD) contacted the metal strike plate.

The active-source data were recorded using three Reftek® RT-125 single-channel seismographs (mated with a Sercel® L-28, 3-component sensor) at each recording station. The passive-source data were recorded using both the above-described seismographs and Reftek® RT-130 3-component seismographs (also mated with the 4.5-hertz (Hz), Sercel® L-28, 3-component sensors). For all surveys, we used a sampling rate of 4 ms, which we subsequently found to be lower than desirable for the relatively high-frequency data that were transmitted during most of the seismic surveys on Vancouver Island. However, the lower sampling rate allowed for multiple 1-day-long surveys between programming of the seismographs and data downloading. S-waves, P-waves, and surface-waves were recorded along all linear seismic profiles. For passive-source surveying, we used the same arrays, and (or) we deployed seismographs in either 100-m-long, L-shaped arrays or triangular arrays (100 m each side). Details on the seismic data and acquisition parameters are available in Goldman and others (2018).

John Hart Dam Seismic Survey

John Hart Dam is located about 5 km west-northwest of downtown Campbell, Vancouver Island, BC (fig. 1*B,C*). The dam impounds John Hart Lake and releases water into the Campbell River, which flows into downtown Campbell River. According to Lou and others (1991), John Hart Dam (at the time of our data acquisition) consisted of a main concrete dam, a power intake dam, and three earthfill sections—a north earthfill dam, a middle earthfill dam, and a south earthfill dam. Our seismic profile at John Hart Dam was located along the middle earthfill dam, southeast of the main concrete dam. We acquired a linear, active-source seismic profile at John Hart Dam (fig. 4), along which we also recorded ambient-noise data. The seismic profile was 400 m long, extending from the main concrete dam southeastward along the crest of the middle earthfill dam to just southwest of the power intake dam. Elevation varied by about 6 m along the length of the seismic profile. Noise levels were relatively high, owing to water flow over the spillway and to ongoing underground drilling. The surface along the seismic profile consisted dominantly of packed gravel/alluvium that constitutes the surface of the dam fill. To generate P- and Rayleigh waves, we used a combination of a vertical 227-kg AWD, a 4.5-kg hammer, and a 1.4-kg hammer that vertically struck a metal plate on the ground surface. To generate shear body waves and Love waves along the John Hart seismic profile, we used a combination of the 45-kg angled AWD, the 4.5-kg hammer, and the 1.4-kg hammer to diagonally or horizontally strike an anchored aluminum block. At each shot point, we acquired multiple shots to increase the signal-to-noise ratio of the data, which were recorded with the RT-125 seismograph/L-28 3-component sensor combination. We also passively recorded ambient-noise data along the array of RT-125 seismographs for approximately 1 hour.

Figure 4. Satellite image of John Hart Dam, Vancouver Island, British Columbia, Canada, with the location of our seismic profile (yellow line). The green area on the north slope of the middle earthfill dam is an area where the dam has been reinforced to prevent leaks and is referred to as the "Dolphin Pool Slope." (Image from Google Earth®.)

Ladore Dam Seismic Survey

Ladore Dam is located about 9 km southwest of downtown Campbell on Vancouver Island. The dam impounds Lower Campbell Lake and releases water into John Hart Lake. Ladore Dam is a concrete structure located upstream of John Hart Dam and downstream of Strathcona Dam. Our seismic profile at Ladore Dam trended perpendicular to the face of the dam and was located about 60 m northeast of the dam at its closest point (fig. 5).

We acquired one 150-m-long, linear, active-source seismic profile and a three-dimensional (3D) triangular ambient-noise seismic survey adjacent to Ladore Dam (fig. 5). The active-source seismic profile trended northwest to southeast, approximately perpendicular to the face of the dam. The seismic profile extended from a parking lot, across a steep embankment, and along an elevated plateau, such that there were significant elevation changes over short distances (as much 10 m rise over ~50 m distance or ~11 degrees) along the seismic profile. Noise levels were relatively low, but noise sources included water flowing over the dam spillway, tree movement, and electrical power lines. The surface along the

seismic profile was variable, consisting of packed gravels within the parking area, soft soil along the steep embankment, and a thin veneer of soil/moss over basalt along the elevated plateau. To generate P- and Rayleigh waves, we used a combination of a 227-kg vertical AWD (in the parking lot), a 4.5-kg hammer, and 1.4-kg hammer that vertically struck a plate on the ground surface. To generate S- and Love waves, we used the 4.5-kg and 1.4-kg hammers to horizontally strike an anchored aluminum block. At each shot point, we acquired multiple shots to increase the signal-to-noise ratio of the data. To record ambient-noise data, we deployed a triangular array of RT-130 seismographs, in addition to the linear array of RT-125 seismographs. Both arrays recorded passively for approximately 1 hour.

Figure 5. Satellite image of the area around Ladore Dam, Vancouver Island, British Columbia, Canada. The yellow line shows the location of our seismic profile. (Image from Google Earth®.)

Strathcona Dam Seismic Surveys

Strathcona Dam, located about 23 km southwest of downtown Campbell River on Vancouver Island, is an earthfill dam that impounds Upper Campbell Lake and releases water into Lower Campbell Lake. At Strathcona Dam, we acquired three linear seismic profiles; we refer to the seismic profiles as—(1) the Strathcona Dam Roadway seismic profile, (2) the Strathcona Dam Spillway seismic profile, and (3) the Strathcona Dam Campground seismic profile (fig. 6). The three profiles were oriented southwest to northeast and were subparallel, with about 150 to 200 m of separation between each profile.

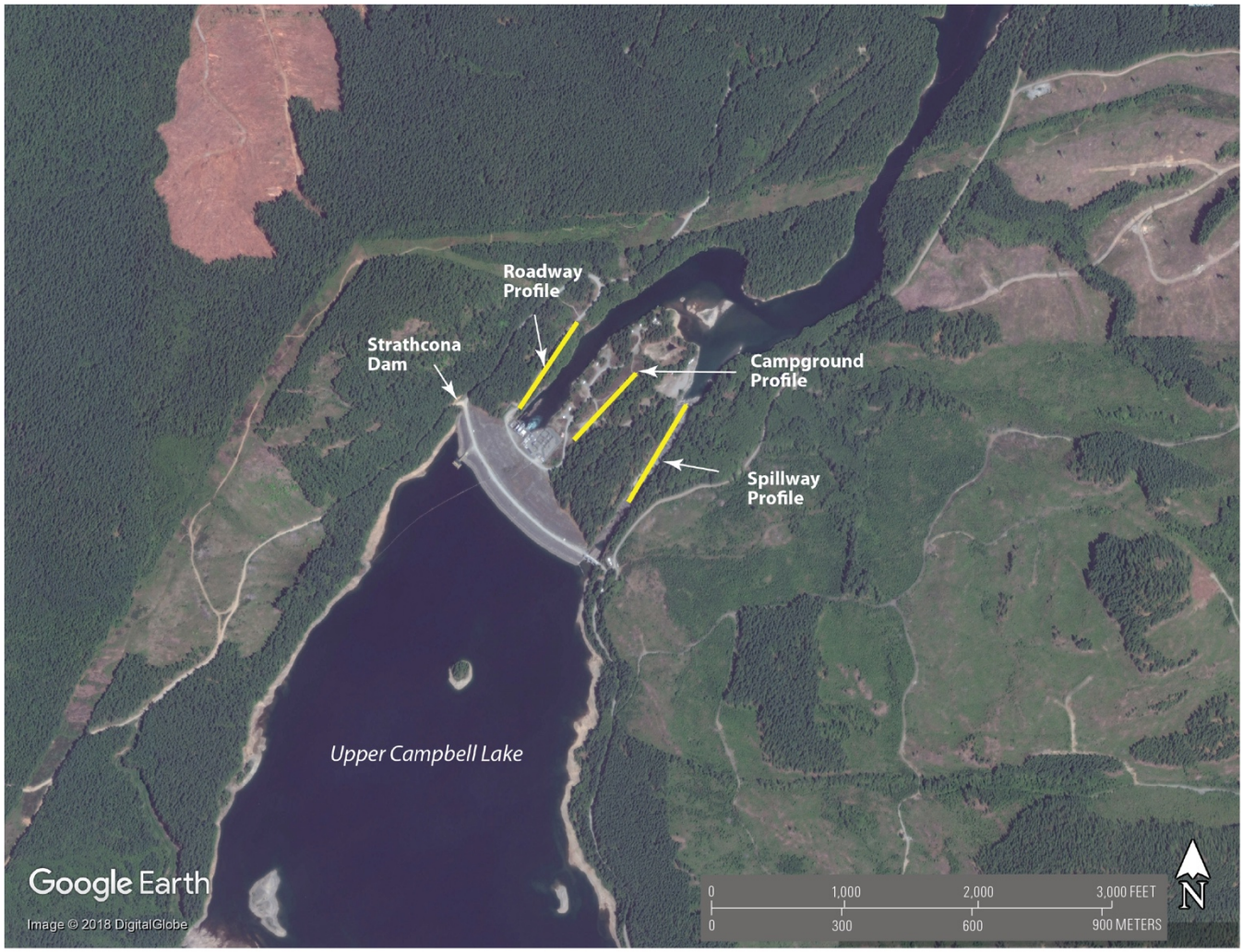

Figure 6. Satellite image of the area near Strathcona Dam, Vancouver Island, British Columbia, Canada. The yellow lines show the locations of our three seismic profiles, the Spillway profile, the Campground profile, and the Roadway profile. (Image from Google Earth®.)

Roadway Seismic Profile

The 240-m-long Roadway seismic profile followed the curves of the road leading from the base of Strathcona Dam (fig. 6), and as a result, the Roadway profile was not as linear as the other two seismic profiles at Strathcona Dam. The Roadway profile varied in elevation (12 m) along its length from near the base of the Dam toward the northeast. The road and profile extended along the edge of a steep hill that sloped downhill about 20 m to the river on the southeast side of the profile and uphill about 160 m on the northwest side. Noise levels along the seismic profile were relatively high due to the power generating station, local roadway traffic, boat traffic along the lake, and trees along the roadway. The surface along the Roadway profile consists largely of gravel that is underlain by basaltic rock. To generate P- and Rayleigh waves, we used a combination of a vertical 227-kg AWD, a 4.5-kg hammer, and a 1.4-kg hammer that vertically struck a metal plate on the ground surface. To generate S-waves along the Roadway seismic profile, we used a combination of the 45-kg angled AWD, the 4.5-kg hammer, and the 1.4-kg hammer to diagonally or horizontally strike an anchored aluminum block. At each shot point, we generated multiple shots to increase the signal-to-noise ratio of the data. Using a combination of shot stacking and the more powerful AWD, signal-to-noise ratios were higher along the Roadway seismic profile relative to the other two profiles at Strathcona Dam. We allowed the linear array of RT-125 seismographs to passively record for approximately 1 hour to obtain ambient-noise data.

Spillway Seismic Profile

A northeast-trending spillway is located on the northeastern side of Strathcona Dam, along which we acquired the 240-m-long Spillway seismic profile (fig. 6). Elevations along the length of the seismic profile vary by about 28 m, with lower elevations to the northeast. Noise levels were relatively high due to flowing water along segments of the spillway and the nearby electrical generating facilities. The seismic profile was located near the center of the spillway and was entirely on rock, which we believe to be rocks of the Vancouver Group, likely pillow basalt. To generate P- and Rayleigh waves, we used 4.5- and 1.4-kg hammers to vertically strike a metal plate placed on the ground surface. To generate shear body waves and Love waves, we used the same hammers to horizontally strike a weighted and anchored metal plate on the ground surface. The data were recorded with Reftek® RT-125 seismographs and 3-component Sercel® L-28 (4.5-Hz) sensors, which were attached to the rock surface with Plaster of Paris. To record ambient noise, we recorded for approximately 1 hour along the linear array of RT-125 seismographs.

Campground Seismic Profile

The 215-m-long Campground seismic profile was located approximately 150 to 200 m west of and subparallel to the Spillway seismic profile (fig. 6). There were only small (~2 m) elevation changes along the Campground seismic profile. However, relative to the Spillway seismic profile, elevations along the Campground seismic profile were as much as 30 m higher on the southern end of the profile and as much as 5 m lower on the northern end of the profile. Noise levels were relatively high, owing to the power-generating station, flowing water in the spillway, and overhead powerlines along the profile. The surface along the Campground seismic profile consisted of a thin layer of alluvium, possibly overlying broken rocks (rubble) and rocks similar to those seen along the Spillway seismic profile. The southwestern end of the seismic profile consisted of pockets of sand that were more than 1 m thick, but other alluvial materials were considerably less than 1 m thick along parts of the seismic profile. Where the alluvium was more than 0.3 m thick, we used a Betsy Seisgun® to generate P- and Rayleigh-wave

data, but where rock and rubble were too shallow to use a seisgun, we used 4.5- and 1.4-kg hammers to vertically strike a metal plate. To generate shear body waves and Love waves, we used the same hammers to horizontally strike a weighted and anchored plate. The linear-array data were recorded with the RT-125 seismograph/L-28 sensor combination. To record ambient noise, we deployed Reftek® RT-130, 3-component seismographs in a triangular array and the RT-125 seismographs in a linear array. Ambient-noise data were recorded for approximately 1 hour.

Data

The seismographs recorded continuously for approximately 5 days, resulting in a large volume of data. For the combined active and passive seismic surveys, we noted specific shot times and recording windows while in the field, and when in the laboratory, we cut the continuous shot records into usable windows for data processing. Active-source shot records were typically about 2 seconds in length, and the data were organized into shot gathers. The passive-source records were usually about 1 hour in length and were organized into a series of individual records.

Data Processing and Modeling

We processed active-source data for the linear profiles using ProMax®, an interactive seismic data processing package, and we developed stacked shot gathers for data processing. We also filtered the data to remove unreasonably high or low frequencies.

We evaluated the active-source data using multiple methods, including (1) V_P refraction tomography, (2) V_S refraction tomography, (3) multichannel analysis of surface waves (MASW) for Rayleigh waves (referred to as MASW or MAS_RW), and (4) MASW for Love waves (referred to as MASLW or MAS_LW). Refraction tomography methods have been used since the later 1980s and are typically applied to both V_P and V_S data. Similarly, the MASW method can be applied to Rayleigh- and Love-wave (surface wave) data. The MASW method was originally applied to Rayleigh waves (Xia and others, 1999; Park and others, 1999; Miller and others, 1999; Xia and others 2002; Hayashi and Suzuki, 2004) and is generally referred to as the MASW method in the scientific literature, but the method has also been referred to as the MAS_RW method (Yong and other, 2013; Martin and others, 2017; Chan and others, 2018). The MASW method has also be applied to Love waves and has been referred to as the MALW method (Yuan, 2011; Xia and others, 2012; Xia, 2014; Catchings and others, 2017; Hu and others, 2018), but the MALW method has also been referred to as the MAS_LW method (Yong and others, 2013; Martin and others, 2017; Chan and others, 2018). In this report, we use the MAS_RW and MAS_LW descriptors to differentiate between the MASW method when applied to Rayleigh and Love waves, respectively.

Having both body waves (P- and S-waves) and surface waves (Raleigh and Love waves) allowed us to develop multiple types of 2D seismic models and images, including (1) V_P refraction tomography, (2) V_S refraction tomography, (3) V_P/V_S ratio models, (4) Poisson's ratio models, (5) MAS_RW (Rayleigh wave) V_S models, (6) MAS_LW (Love wave) V_S models, and (7) $V_{S(z)}$ models (time-averaged V_S at all model depths). In addition, although not processed for this report, some of the body-wave data may also be suitable for seismic reflection analysis.

We developed our refraction tomography models using the code of Hole (1992) and the Rayleigh- and Love-wave V_S models using a version of the MASW method (Park and others, 1999) that was developed by Hayashi and Suzuki (2004) and Hayashi (2008) and is available in the Geometrics® 2D SeisImager™ software package.

The active-source data included a shot at each sensor, which resulted in a large number of shot gathers and a high degree of redundancy, whereby there were potentially thousands of first arrivals that could be inverted to develop the velocity models. For example, for profiles with 80 shots and 80 recording locations, there were as many as 6,400 P-wave and 6,400 S-wave seismograms available for model inversion. Although three-component data were acquired for all seismic profiles, in most cases, we analyzed only the vertical-component (P-wave body waves and Rayleigh surface waves) and the horizontally transverse (S-wave body wave and Love surface waves) component of the data. For all tomographic analyses, we used grid spacings that matched our shot and sensor spacing. Our starting velocity models were developed from 1D analysis of shot gathers along the seismic profile. We used multiple starting models that converged to a consistent final model, usually with small (<5 percent) variations among the final models. For MAS_RW analysis, the SeisImager^{TM} algorithm constructs common mid-point correlations to develop 1D dispersion curves and 1D V_S models for each shot point along the seismic profiles, and by laterally combining those V_S models, a 2D V_S model is developed for each seismic profile.

Data Limitations

Acquiring usable seismic data near the dam sites on Vancouver Island can be challenging because of noise (electrical and mechanical) produced by power generation and flowing water, highly 3D velocity and structural variations, and significant topographic variations. As a result, all data evaluation methods used in this study have some limitations.

Data from each of the seismic profiles included a fair amount of noise for individual shots (see appendix 1), which makes it difficult to evaluate body waves. However, we recorded multiple shots at each shot point in the field, and in the lab, we stacked those shots. This usually resulted in sizeable increases in signal-to-noise ratios, but for some profiles, the overall data quality would have benefitted from stacking additional shots at each shot point and (or) using a larger seismic source. The hard rock in our study area transmitted high-frequency refracted arrivals, which are typically low in amplitude. On some shot gathers, the combination of low amplitudes and high-noise levels made it difficult to accurately measure first arrivals, which are required for tomographic inversion. In an attempt to overcome this difficulty, we used reciprocal arrivals to more accurately measure high-noise data. For example, in many cases, with seismic sources at a given location A, first-arrival refractions could not be accurately recorded at a distant offset location (location B), because there was a local noise source near location B. However, for sources placed at location B, clear first-arrival refractions could often be measured at location A (where there was not a strong noise source). Because the travel time from source A to recorder B has to be exactly the same as that from source B to recorder A, it was possible to determine the first-arrival refraction at recorder B from its reciprocal time at recorder A. We used reciprocal times from appropriate shot-receiver pairs to minimize the difficulty in measuring travel times at many of the locally noisy sites, but in some cases, each component of the pairs included significant noise, making tomographic velocities along segments of some seismic profiles less well determined. If the V_P or V_S values are not well determined in an area of the velocity models, V_P/V_S and Poisson's ratios will be inaccurate in that area of the model. In this report, we point out areas of our models where V_P/V_S and (or) Poisson's ratios are higher or lower than those expected for the assumed rock types.

The use of surface-wave methods along levees, dams, hillsides, and areas with significant topographic variations can be problematic because implicit in these methods is the assumption of a 1D Earth structure (Kim and others, 2001; Min and Kim, 2006; Ivanov and others, 2009; 2017; Karl and others, 2011; Zeng and others, 2012; Caradelli and others, 2014), which is not valid for most of our

seismic profiles in this study. Such 2D or 3D complexity strongly affects surface-wave propagation and the resulting dispersion curves (see appendix 2). Two-dimensional or 3D complexities and topographic variations exist along segments of each of the seismic profiles investigated in this study. However, we suggest that the MAS_RW/MAS_LW method may be valid for less-complex segments of the seismic profiles, particularly where the velocity structure can be considered dominantly 1D (laterally) for tens of meters. Thus, we include the MAS_RW/MAS_LW models in this study and compare the derived V_S models with those derived with the tomography method.

For the passive (ambient-noise) data, we segmented the data into time sections for each seismograph deployed along the linear, triangular, or L-shaped arrays. We use Rayleigh waves from the passive data to develop dispersion curves (see appendix 3), from which we attempted to evaluate V_S. However, we found the dispersion curves to be insufficient to calculate reliable velocity models along most of the seismic arrays, except along the John Hart Dam seismic profile. As can be seen in appendix 3, the fundamental mode for most of the data was not obvious, likely the result of the complex geological structure, large lateral variations in velocity, and topographic variations that strongly affected the surface-waves. Such geological complexities strongly affect the dispersion image (Min and Kim, 2006; Karl and others, 2011; Zeng and others, 2012).

Active-Source Seismic Models

From the active-source data, we developed 2D V_P seismic models for each seismic profile and 2D V_S seismic models for all but one seismic profile. Not all data were of sufficient quality to develop useful velocity models with all the techniques for all sites. Using the V_S models developed from the various methods, we calculated V_{S30} along the length of the seismic profiles at lateral intervals ranging from 1 to 5 m along the profiles, as done by Catchings and others (2017). We also developed $V_{S(z)}$ models, time-averaged V_S at all depths laterally along the profile, where depth is relative to the surface.

John Hart Dam

For the John Hart Dam seismic profile, we developed (1) a 2D V_P refraction tomography model, (2) two 2D V_S refraction tomography models, (3) two 2-D VP/VS ratio models, (4) two 2D Poisson's ratio models, (5) two 2D V_S MAS_RW models, and (6) two 2D MAS_LW models. From the 2D V_S refraction tomography models, we developed a 2D time-averaged $V_{S(z)}$ models, which show time-averaged velocities to all depths of the models. From the combined models, we also present interpretive models.

John Hart Dam Tomography Models

We inverted the active-source data from the John Hart Dam seismic profile to develop 2D V_P and V_S refraction tomography models. The seismic data obtained from the John Hart profile included significant cultural noise, especially on the southeast end, where drilling was ongoing during data acquisition. To minimize the noise, we stacked at least 4.5-kg hammer P-wave shots at each shot point, at least two 227-kg AWD shots at each P-wave shot point, at least two 45-kg AWD shots at each S-wave shot point, and at least four 4.5-kg hammer shots at each S-wave shot point. We generated S-wave shots only at every tenth recording station (40 m spacing) along the seismic profile using the angled 45-kg AWD. Although we also used notch filters to remove cultural noise, strong noise from the drilling operations persisted on the southeastern end of the profile, but consistent first arrivals could be measured using reciprocity.

For P-wave analysis, we used 80 stacked shots recorded at 80 recording sites, resulting in as many as 6,400 P-wave and 6,400 S-wave arrivals for V_P and V_S inversion. For velocity inversion, we used a 5×5-m grid spacing, which was consistent with our shot and sensor spacing, and we developed starting velocity models from 1D analysis of shot gathers along the seismic profile. Our preferred P-wave model is shown in figure 7. V_P ranges from about 750 m/s in the near-surface to about 5,750 m/s in the upper 100 m, with significant lateral variations. Because of strong refracted arrivals from the 227-kg AWD and the use of reciprocal arrivals, we suggest the P-wave model is adequately resolved.

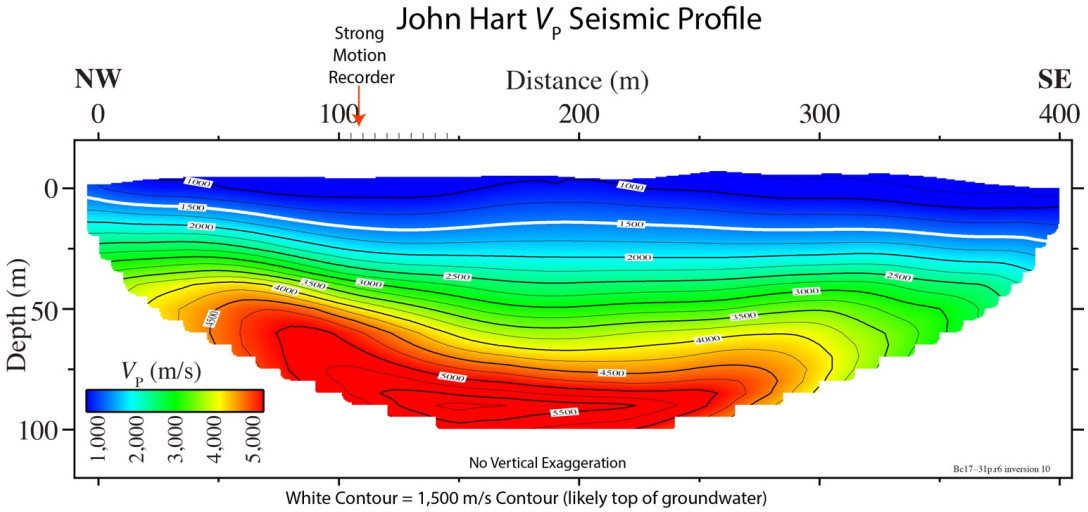

Figure 7. Diagram showing refraction tomography compressional-wave-velocity (V_P) model along the seismic profile for John Hart Dam, Vancouver Island, British Columbia, Canada (see fig. 4). White line shows the top of groundwater, as inferred by the 1,500 meters per second (m/s) velocity contour. A seismic strong motion recorder was located at approximately meter (m) 118 of our seismic profile. NW, northwest; SE, southeast.

For S-wave analysis, we developed two models (figs. 8*A* and 9*A*). One of the models used 80 stacked 4.5-kg shots (5-m spacing) and 10 stacked 45-kg shots (40-m spacing) that were recorded at 80 recording sites; this set up allowed propagation sufficient to image to about 50-m depth. V_S in the upper 50 m ranges from about 300 m/s in the shallow subsurface to about 1,700 m/s (fig. 8*A*). The other V_S model was based solely on 10 stacked 45-kg AWD shots (40-m spacing) that were recorded at 80 recording sites; these shots allowed propagation sufficient to image to 150-m depth. V_S in the upper 150-m depth ranges to as much as about 2,700 m/s (fig. 9*A*). Because of the greater number of shots and shorter distance between shot points for the first V_S model (fig. 8*A*), we suggest that the first model is better resolved at shallow depths than for the second V_S model (fig. 9*A*). However, relative to most surface-wave models, we suggest that both V_S models are relatively well resolved overall.

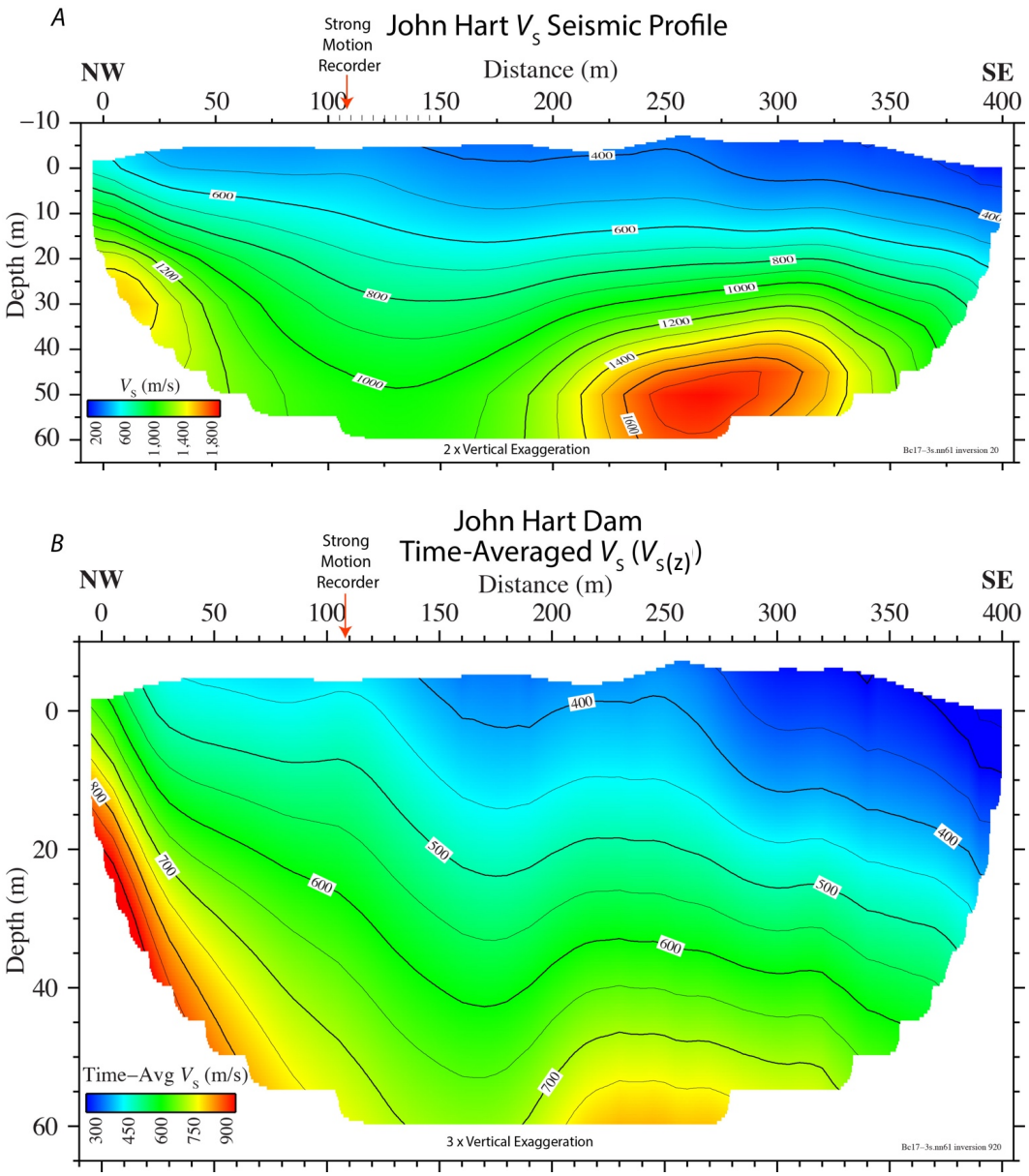

Figure 8. Diagrams showing seismic profiles for John Hart Dam, Vancouver Island, British Columbia, Canada (see fig. 4). *A*, Refraction tomography shear-wave-velocity (V_S) model to a depth of 50 meters (m) (VE2, vertical exaggeration×2). This tomographic model was derived from S-wave data acquired with an angled accelerated weight drop and small hammer and block combination. Tomographic time-averaged shear-wave velocity in the upper 30 m of the subsurface (V_{S30}) varies laterally along this model from 465 to 917 meters per second (m/s), with an average value of 559 m/s. A strong-motion recorder was located at approximately meter 118 of our seismic profile, where tomographic V_{S30} was determined to be 577 m/s. *B*, Model of 2D time-averaged shear-wave velocity as a function of depth (*z*) ($V_{S(z)}$) along the John Hart profile derived from the V_S refraction tomography model in *A*. $V_{S(z)}$ is calculated using 1-m-thick layers. The time-averaged velocities to all depths are shown graphically. Depth (*z*) is relative to the topography. NW, northwest; SE, southeast.

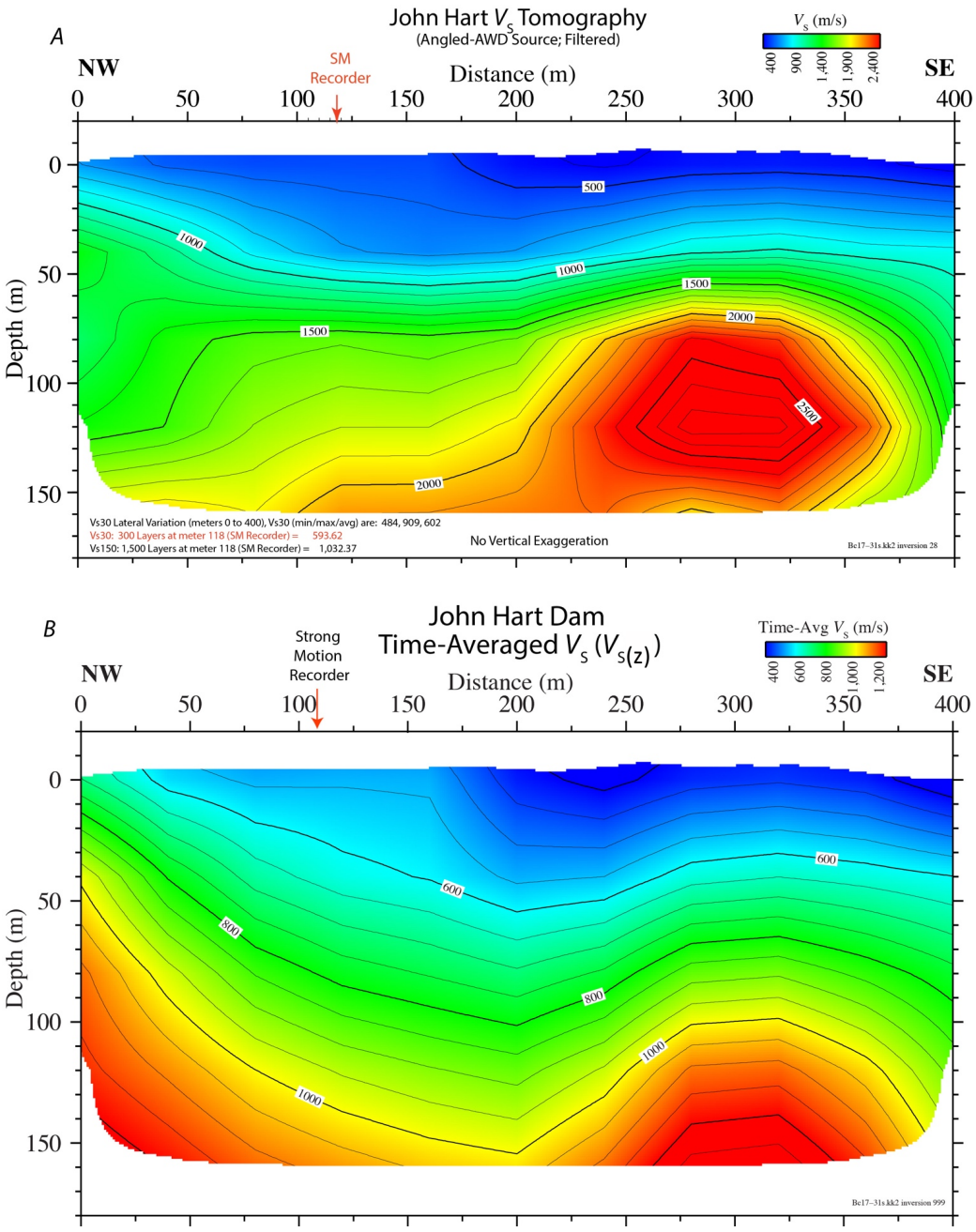

Figure 9. Diagrams showing seismic profiles for John Hart Dam, Vancouver Island, British Columbia, Canada (see fig. 4). *A*, Refraction tomography shear-wave-velocity (V_S) model to a depth of 150 meters (m). This tomographic model was derived from S-wave data acquired with an angled accelerated weight drop using 50-m shot and 5-m sensor spacing. Tomographic time-averaged shear-wave velocity in the upper 30 m of the subsurface (V_{S30}) varies laterally along this model from 484 to 909 meters per second (m/s), with an average value of 602 m/s. A strong-motion (SM) recorder was located at approximately meter 118 of our seismic profile, where tomographic V_{S30} was determined to be 594 m/s and V_{S150} was determined to be 1,032 m/s. *B*, Model of 2D time-averaged shear-wave velocity as a function of depth (*z*) ($V_{S(z)}$) along the John Hart profile derived from the V_S refraction tomography model in *A*. $V_{S(z)}$ is calculated using 1-m-thick layers. The time-averaged velocities to all depths are shown graphically. Depth (*z*) is relative to the topography. NW, northwest; SE, southeast.

John Hart Dam V_P/V_S and Poisson's Ratios

We developed shallow and deep V_P/V_S ratio models (figs. 10 and 11) and Poisson's ratio models (figs. 12 and 13) by calculating those values at each node of the tomographic V_P (fig. 7) and V_S (figs. 8*A* and 9*A*) models. V_P/V_S ratios range from 1.8 to 4.4 along the seismic profile. Ratios of about 1.8 correlate with the highest velocity rocks observed within the velocity models, suggesting competent rock at those depths. However, relatively high V_P/V_S ratios (2.0–4.4) appear to be localized in a zone from the northwest end of the profile at depth (>30 m), extending toward the surface near the central part of the profile. The modeled high V_P/V_S values at depth near the northwestern end of the seismic profile may indicate less competent rock or fracturing at those depths, but it is also possible that the V_S model lacks the requisite resolution in that limited area. However, we note that the surface-wave-based models (MAS_RW/MAS_LW) also independently infer low V_S in the same area. Similarly, Poisson's ratio is highly variable along the John Hart Dam seismic profile, with values ranging from 0.27 to 0.47. High Poisson's ratios (>0.44) may also be indicative of highly saturated rocks (Catchings and others, 2014).

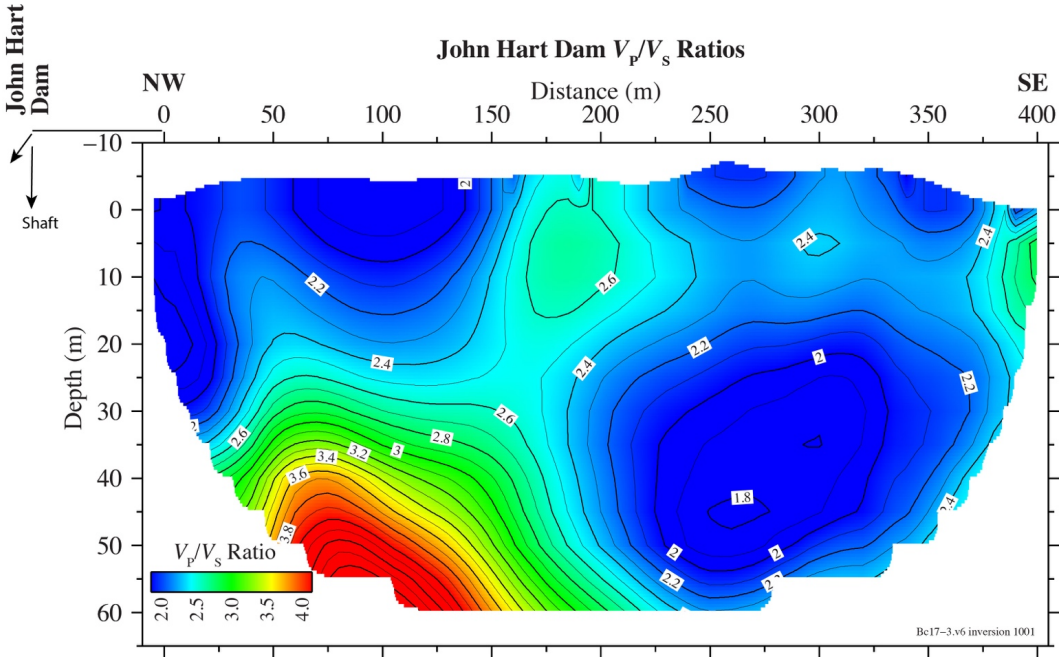

Figure 10. Diagram showing shallow-depth (~60 meters, m) model of compressional-wave-velocity/shear-wave-velocity (V_P/V_S) ratios along the seismic profile derived from a combination of the tomography V_P and V_S models for John Hart Dam, Vancouver Island, British Columbia, Canada (figs. 7 and 8*A*, respectively). Note the high V_P/V_S ratios near the bottom of the model near the northwest end of the seismic profile; a relative V_P/V_S ratio high extends from that point to the surface near the center of the profile. NW, northwest; SE, southeast.

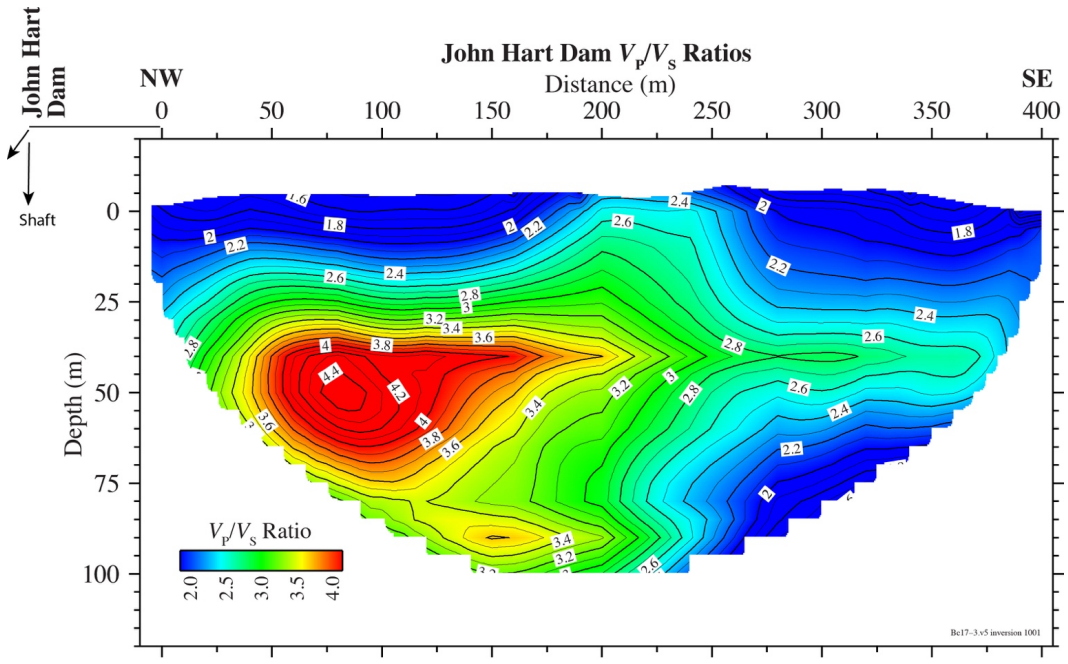

Figure 11. Diagram showing deeper (~100 meters, m) model of compressional-wave-velocity/shear-wave-velocity (V_P/V_S) ratios along the seismic profile derived from a combination of the tomography V_P and V_S models for John Hart Dam, Vancouver Island, British Columbia, Canada (figs. 7 and 9*A*, respectively). Note the high V_P/V_S ratios near the bottom of the model near the northwest end of the seismic profile; a relative V_P/V_S ratio high extends from that point to the surface near the center of the profile. NW, northwest; SE, southeast.

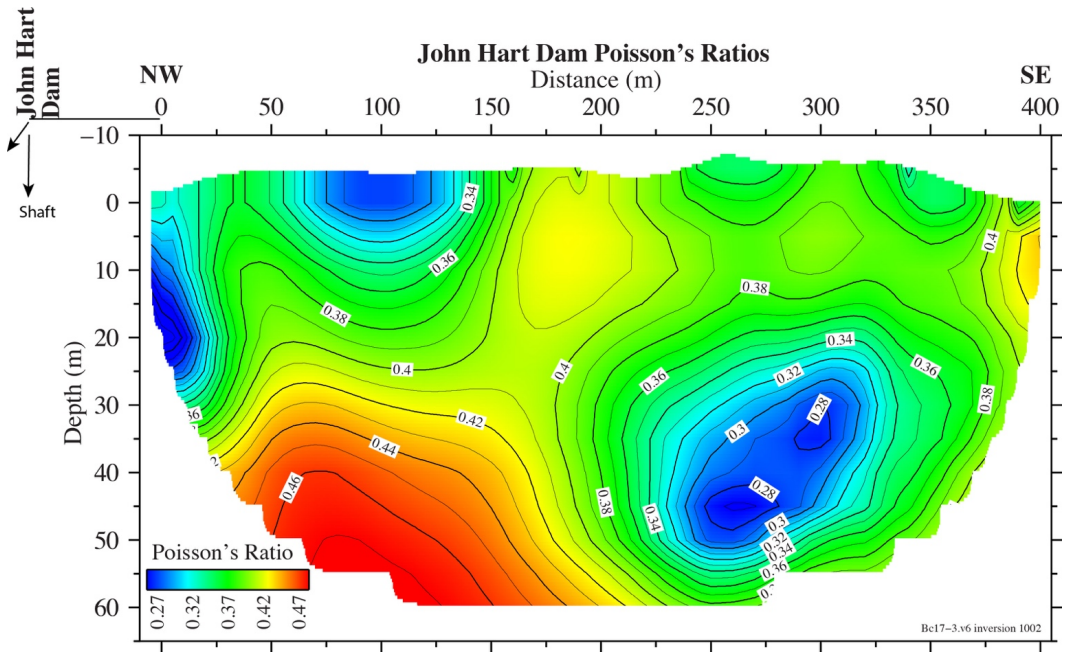

Figure 12. Diagram showing shallow-depth (~60 meters, m) model of Poisson's ratio along the seismic profile derived from a combination of the tomographic compressional-wave velocity and shear-wave-velocity (V_P and V_S, respectively) models for John Hart Dam, Vancouver Island, British Columbia, Canada (figs. 7 and 8*A*, respectively). As seen for the V_P/V_S ratio models, relatively high ratios extend from the northwestern (bottom of the model) to the surface near the center of the profile. High Poisson's ratios (~0.44) in the shallow subsurface are often correlated with a high degree of water saturation. NW, northwest; SE, southeast.

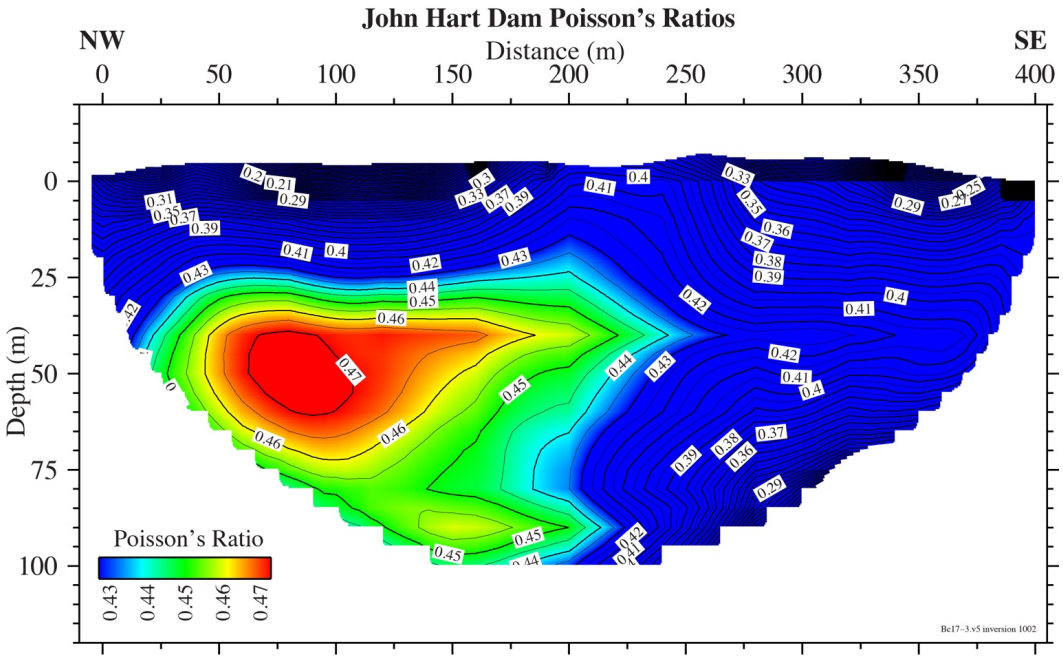

Figure 13. Diagram showing deeper (~100 meters, m) model of Poisson's ratio along the seismic profile derived from a combination of the tomographic compressional-wave-velocity and shear-wave-velocity (V_P and V_S,) models for John Hart Dam, Vancouver Island, British Columbia, Canada (figs. 7 and 9*A*, respectively). A zone of relatively high Poisson's ratios extends from depth on the northwest toward the surface near the center of the profile. NW, northwest; SE, southeast.

John Hart Dam MAS_RW and MAS_LW Models

We developed 2D V_S models along the John Hart seismic profile from the AWD-source (vertical and horizontal) data and the hammer-source (vertical and horizontal) data using the MAS_RW and MAS_LW methods. The MAS_RW models (fig. 14*A*, *B*) suggest V_S ranges from about 300 m/s in the near-surface on the southeastern end of the profile to about 1,100 m/s at depth (~90 m) on the northwestern end of the profile. One of the MAS_LW models (fig. 15*A*) suggest V_S ranges from 300 to 1,100 m/s in the upper 50 m, and another MAS_LW model (fig. 15*B*) suggests the higher velocities occur at greater depth, in the upper 90 m. However, we are mindful that large lateral variations in V_S structure and topography (as found along dams) make it difficult to extract accurate measures of V_S using surface-wave methods like MAS_RW and MAS_LW, except in areas along the seismic profile where the V_S structure can be considered 1D and where there is little topographic variation.

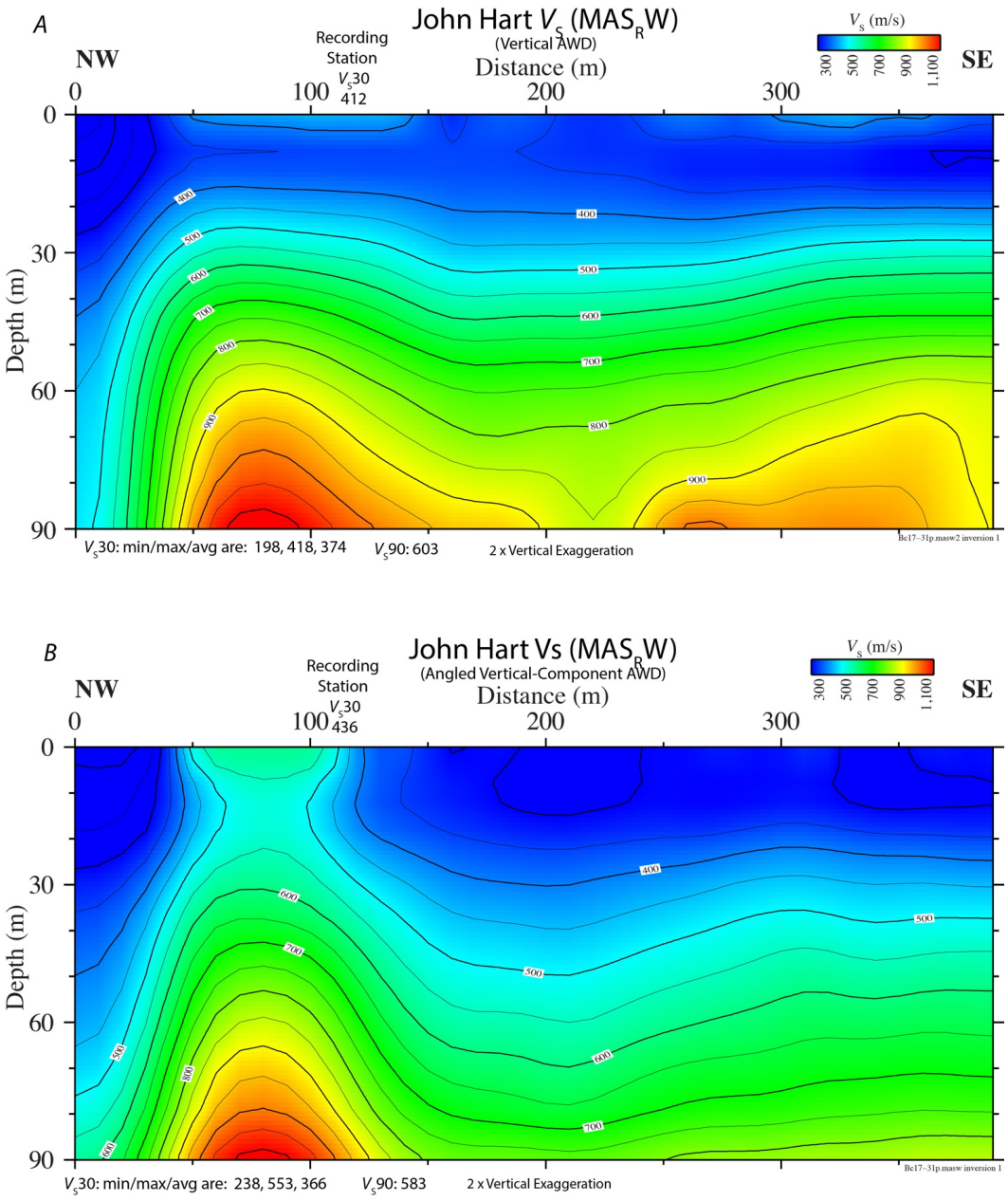

Figure 14. Diagrams showing shear-wave-velocity (V_S) model along the seismic profile derived from multichannel analysis of surface waves using Rayleigh waves (MAS_RW) for John Hart Dam, Vancouver Island, British Columbia, Canada. *A*, V_S model derived from MAS_RW. The data were derived using the 500-pound vertical accelerated weight drop (AWD) and vertical-component sensors. Lateral variations in modeled time-averaged shear-wave velocity in the upper 30 meters (m) of the subsurface (V_{S30}), as derived from the MAS_RW analysis, ranges from 198 to 418 meters per second (m/s), with an average V_{S30} of 374 meters per second (m/s). *B*, V_S model derived from MAS_RW. The data were recorded on vertical-component sensors, with a 100-pound angled accelerated weight drop source. Lateral variations in modeled V_{S30}, as derived from MAS_RW analysis, ranges from 238 to 553 m/s, with an average V_{S30} of 366 m/s. At the recording station, modeled V_{S30} is calculated to be 436 m/s. NW, northwest; SE, southeast.

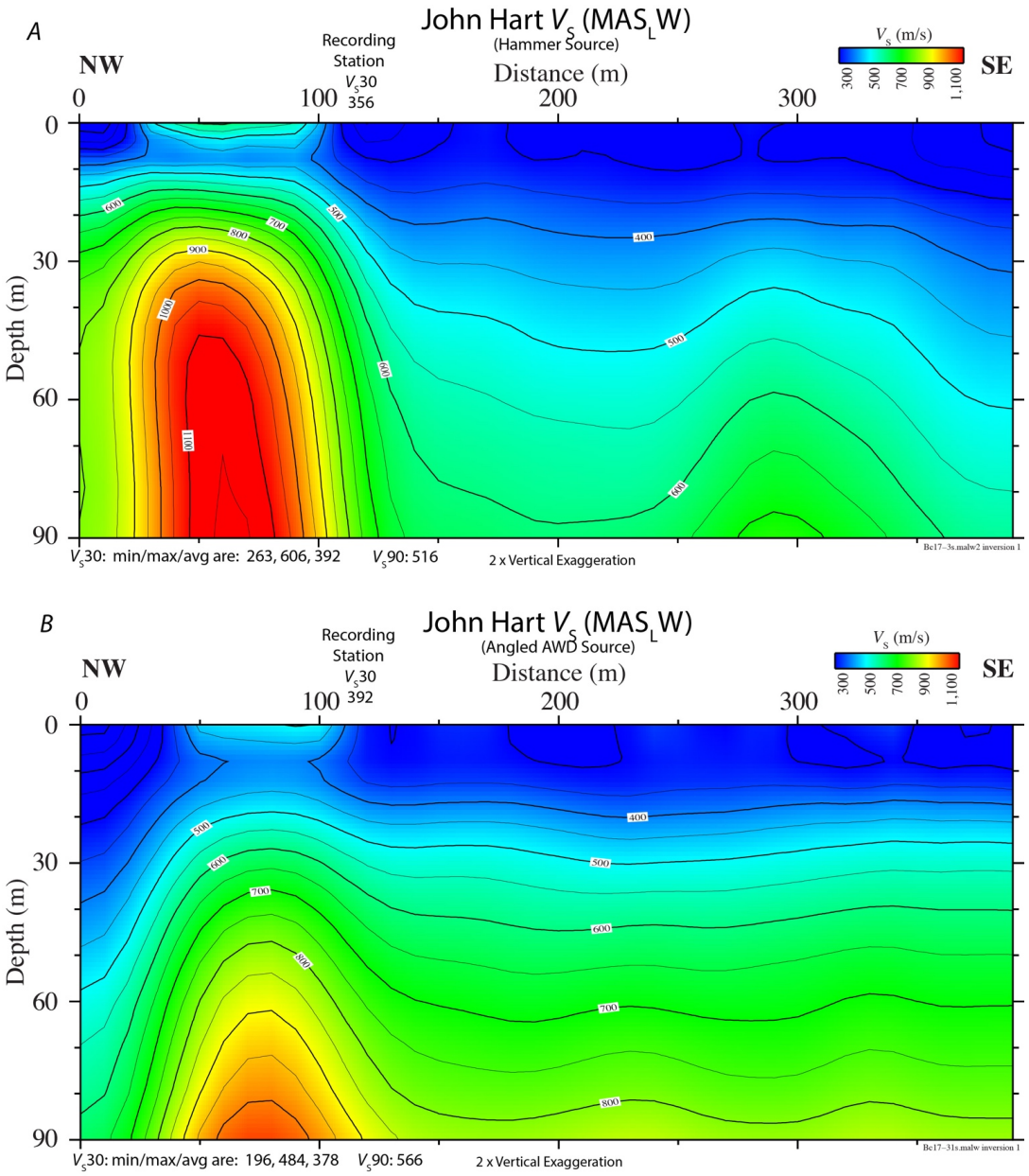

Figure 15. Diagrams showing shear-wave-velocity (V_S) model along the seismic profile derived from multichannel analysis of surface waves using Love waves (MAS$_L$W) for John Hart Dam, Vancouver Island, British Columbia, Canada. *A*, V_S model derived from MAS$_L$W. The data were derived using the 10-pound (4.5 kg) hammer source and horizontal-component sensors. Lateral variations in modeled time-averaged shear-wave velocity in the upper 30 meters (m) of the subsurface (V_{S30}) , derived from the MAS$_L$W analysis, ranges from 263 to 606 meters per second (m/s), with an average V_{S30} of 392 m/s. *B*, V_S model along the John Hart seismic profile derived from MAS$_L$W. The data were recorded on horizontal-component sensors, with a 100-pound angled accelerated weight drop (AWD) source. Lateral variations in modeled V_{S30}, as derived from MAS$_L$W analysis, ranges from 196 m/s to 484 m/s, with an average V_{S30} of 378 m/s. At the recording station, modeled V_{S30} is calculated to be 392 m/s. NW, northwest; SE, southeast.

John Hart Dam V_{S30} Calculations and Models

Using the V_S tomography models along the John Hart profile (figs. 8*A* and 9*A*), we calculated V_{S30} at 5-m lateral increments along the profile (appendix 4, table 1) where the velocity model extends to at least 30 m depth (distance meters 20 to 380). We calculated the maximum, minimum, and average tomographic V_{S30} value to be 917 m/s, 465 m/s, and 559 m/s, respectively, along the length of the profile, and we developed a 2D model of $V_{S(z)}$, whereby the time-averaged V_S at all depths (z) of the velocity model is calculated (figs. 8*A* and 9*B*). There is a strong motion seismograph located at meter 118 along the seismic profile, where we calculate tomographic V_{S30} to be 577 m/s. We also calculated time-averaged V_S at specific depths of 60 m (710 m/s) and 150 m (1,032 m/s), as can be seen in figures 8*B* and 9*B*.

Using the MAS_RW velocity model (fig. 14*A*), we calculated V_{S30} at 1-m lateral increments along the seismic profile (appendix 4, table 2). As determined from MAS_RW, we calculated the maximum, minimum, and average V_{S30} along the profile to be 418 m/s, 198 m/s, and 374 m/s, respectively. At the strong-motion seismograph (meter 118), we calculated the MAS_RW-determined V_{S30} to be 412 m/s. We also calculated MAS_RW-based $V_{S(z)}$ at greater depths, including 60 m (836 m/s) and 90 m (1,022 m/s).

Using the MAS_LW velocity model (fig. 15*A*), we calculated V_{S30} at 1-m lateral increments along the seismic profile (appendix 4, table 3). As determined from MAS_LW, we calculated the maximum, minimum, and average V_{S30} along the profile to be 606 m/s, 263 m/s, and 392 m/s, respectively. At the strong-motion seismograph (meter 118), we calculated the MAS_LW-determined V_{S30} to be 357 m/s. We also calculated MAS_LW-based $V_{S(z)}$ at greater specific depths, including 60 m (749 m/s) and 90 m (899 m/s).

Shallow Crustal Structure at John Hart Dam

When acquiring seismic data at John Hart Dam, active tunnel construction was ongoing, whereby a tunnel was being constructed from the dam to a new generating station. The tunnel originated near the northwest end of our seismic profile and extended southwestward across and sub-parallel to our seismic profile (fig. 16). The tunnel is about 10 m in diameter and was constructed within the basaltic basement rock. Blasting required to construct the tunnel would likely have altered the elastic moduli of the rock for some distance from the tunnel, such that the seismic velocities in the vicinity of the tunnel would have been affected. Our tomographic V_P models show decreases in velocity just above the tunnel (fig. 17 and 18) and where the tunnel is closest to the seismic profile (see fig. 16).

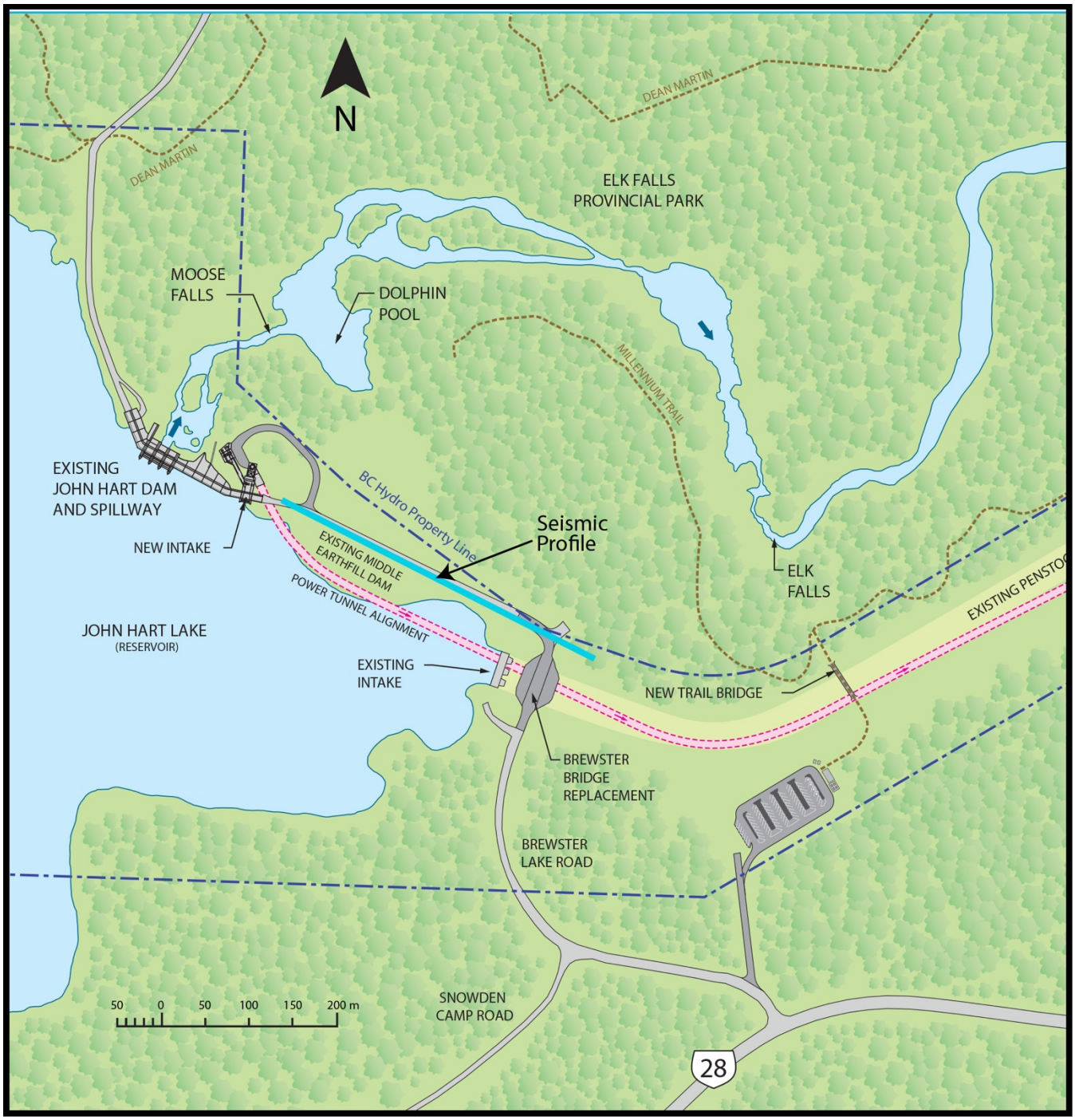

Figure 16. Map of the area around John Hart Dam, Vancouver Island, British Columbia, Canada. Our seismic profile is shown in dark blue. An approximately 10-meter (m)-diameter power tunnel, which was recently emplaced, is shown by the pink line. Note that the seismic profile and the power tunnel nearly cross near the northwest end of the seismic profile. (Map modified from British Columbia Hydro and Power Authority, BC Hydro, 2018.)

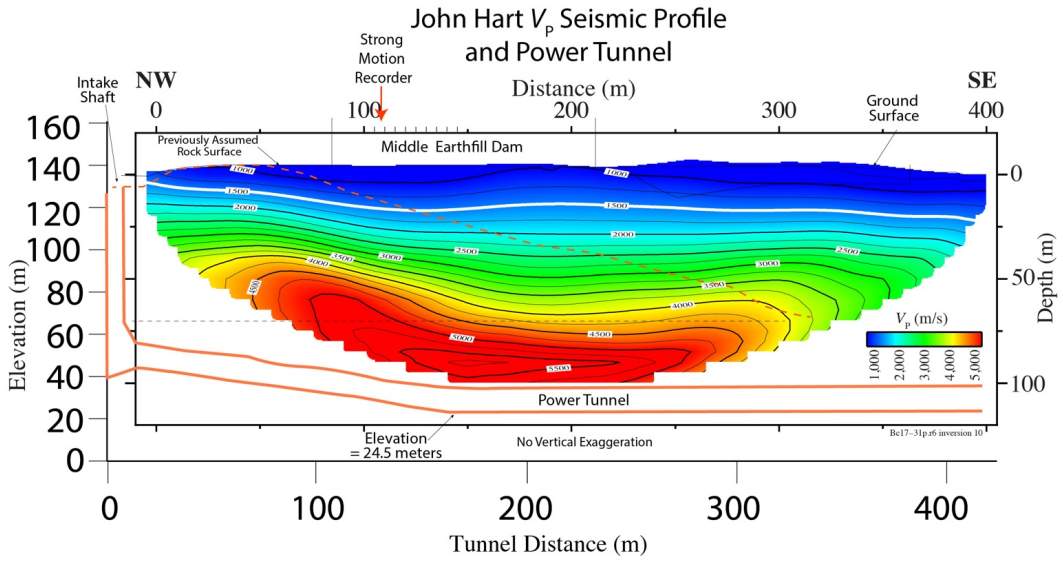

Figure 17. Diagram showing shallow tomographic compressional-wave-velocity (V_P) model (from fig. 8*A*) along the seismic profile shown relative to the power tunnel (see fig. 16) for John Hart Dam, Vancouver Island, British Columbia, Canada. The power-tunnel schematic is from engineering plans obtained from British Columbia Hydro and Power Authority (BC Hydro, written commun., 2017). White line shows the top of groundwater, as inferred by the 1,500 meter per second (m/s) velocity contour. The orange dashed line is the assumed top of hard rock from the line drawing. NW, northwest; SE, southeast; m, meters.

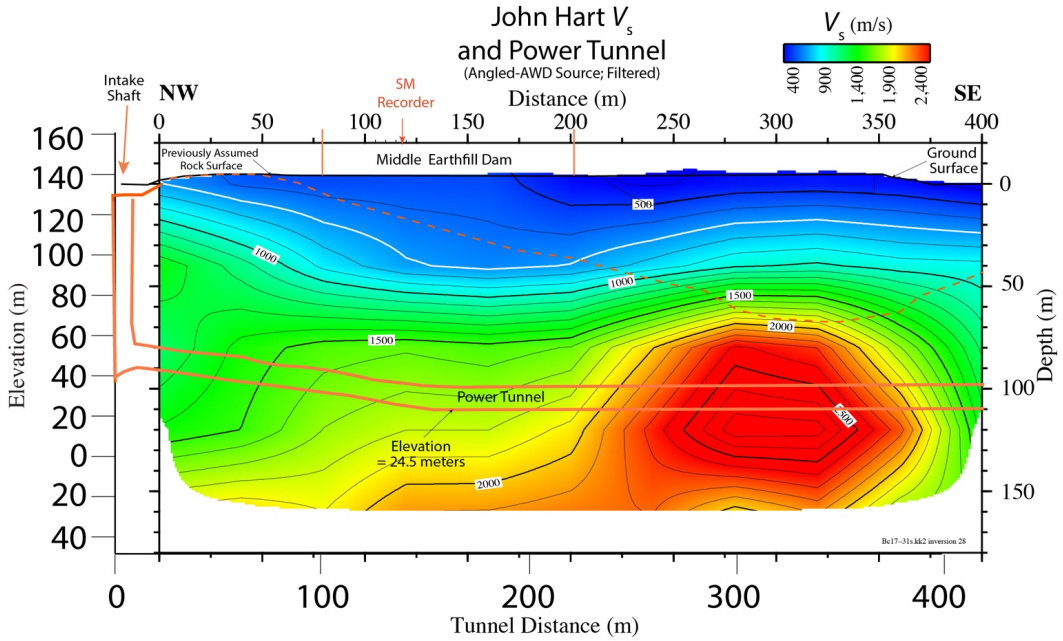

Figure 18. Diagram showing deeper tomographic shear-wave-velocity (V_S) model (from fig. 9*A*) along the seismic profile shown relative to the power tunnel (see fig. 16) for John Hart Dam, Vancouver Island, British Columbia, Canada. The power tunnel schematic is from engineering plans obtained from British Columbia Hydro and Power Authority (BC Hydro, written commun., 2017). The white line shows the top of basalt, as inferred by the 800 meter per second (m/s) velocity contour. NW, northwest; SE, southeast; SM, strong motion; m, meters.

The tomographic V_P model suggests that static groundwater (1,500 m/s velocity contour) ranges in depth from about 5 m to 22 m along the profile (fig. 17). The tomographic V_S model suggests that the depth to the top of basaltic rock, which we interpret to be V_S>800 m/s, varies along the seismic profile and is deepest near the middle of the Dolphin Pool slope (see fig. 4). We suggest it is reasonable to infer the 800 m/s velocity contour as the top of the bedrock surface because both rock and the modeled 800 m/s velocity contour occur at the surface near the northwest end of our seismic profile (fig. 17). This correlation suggests that the sedimentary overburden is as much as 45 m thick along parts of the middle earthfill dam, which is somewhat consistent with depths (45–50 m) inferred on the basis of construction records (Lou and others, 1991; figs. 19 *A*,*B*). The seismic profiles show that the earthfill section is deepest (~45 m) between meters 125 and 200 of the seismic profile (fig. 20), which includes the section directly beneath the strong motion recording station. We suggest the top of the basaltic rock near John Hart Dam is likely weathered, as shallow velocities are relatively low.

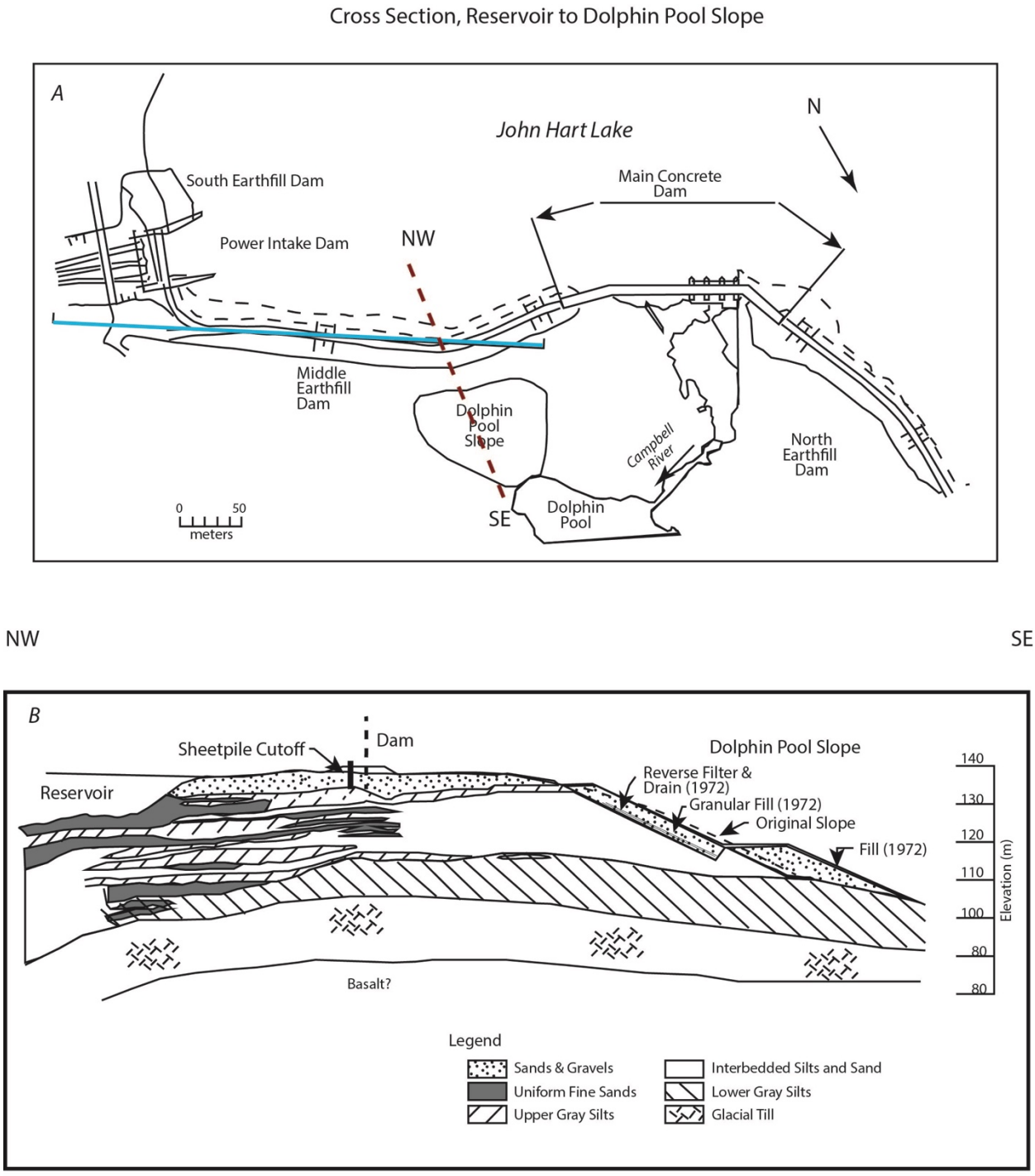

Figure 19. Map and cross section of the area near John Hart Dam, Vancouver Island, British Columbia, Canada. *A*, Map of the area. The blue line shows the approximate location of our seismic profile. The dashed red line shows the approximate location of the cross section shown in *B*. *B*, Cross section across the middle earthfill dam (see *A*). The various earthfill materials of the dam are shown to be about 45 to 50 meters (m) thick. NW, northwest; SE, southeast. (Images modified from Lou and others, 1991.)

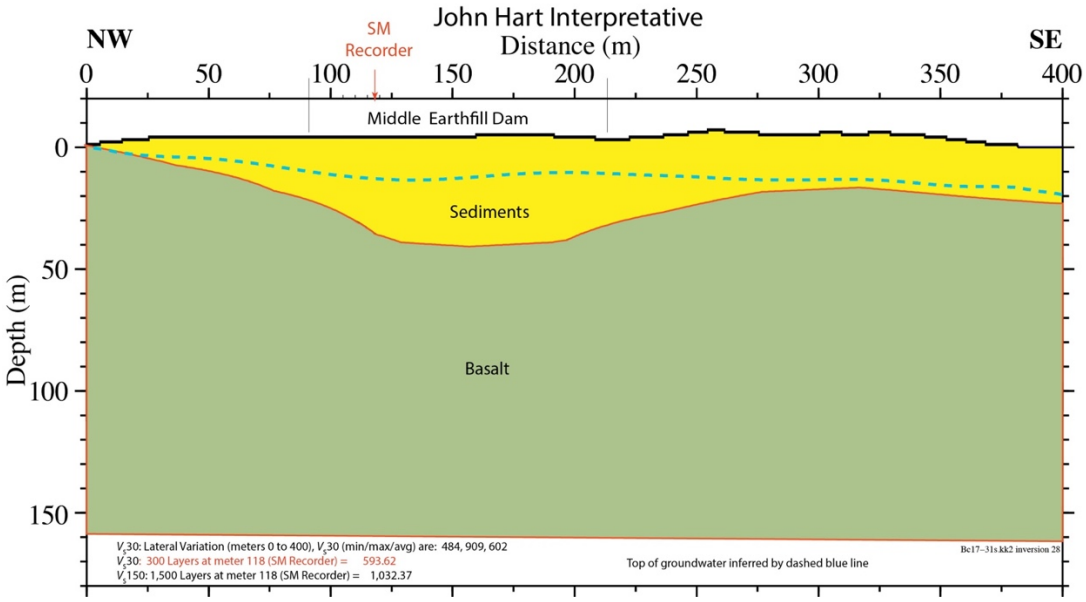

Figure 20. Diagram showing interpretative cross section along the seismic profile for John Hart Dam, Vancouver Island, British Columbia, Canada. The blue line shows the interpreted top of groundwater, as inferred by the 1,500 meter per second (m/s) contour of the compressional-wave-velocity (V_P) model. The interpreted contact between sediments and basalt is based on the 800 m/s velocity contour of the tomographic shear-wave-velocity (V_S) model (see fig. 18). NW, northwest; SE, southeast; SM, strong motion; m, meters.

Our models show a prominent zone of high V_P/V_S (figs. 10 and 11) and Poisson's ratios (figs. 12 and 13) within basaltic basement rock between meters 25 and 200 at depths ranging from 35 to 60 m. Although the V_P data representing that area of the model are of high quality, the V_S data for that area of the model are of lesser quality. Thus, the zone of high V_P/V_S and Poisson's ratios could conceivably result from lower quality of the V_S data. However, we used reciprocal pairs to bolster the quality of the picks in that part of the model; thus, we suggest that there is a reasonable possibility that this area of the model is characterized by high ratios. Generally, the V_P/V_S ratio of basalt at shallow depths is expected to be between 1.4 and 2.0, with an average of about 1.87, and Poisson's ratio is expected to be about 0.28 for unweathered basalt and as much as 0.35 for weathered basalt (Hyndman, 1979; Johnston and Christensen, 1997), but our models indicate V_P/V_S ratio values in excess of 4.0 and Poisson's ratios in excess of 0.4 in this one specific area near the northeast end of our seismic profile. Assuming our models are accurate, whereby V_P is relatively high and V_S is relatively low in that area of the model, we suggest the basement rocks there are likely fractured and water saturated. This modeled zone of high V_P/V_S and Poisson's ratios also appears to extend upward into the sediments, where it approaches the surface near meter 200 of the seismic profile. This general area of the model is near the southeastern edge of the Dolphin Pool Slope, where water leaked from the middle earthfill dam before being successfully sealed (Lou and others, 1991); it is also the general area of the middle earthfill dam where the reservoir and the newly constructed power tunnel are closest to the seismic profile (fig. 16).

We stress that a small part of the tomographic V_S model may be underdetermined, which may account for the low V_S, high V_P/V_S ratios, and high Poisson's ratios near the northwestern end of the John Hart seismic profile. However, the V_S models derived independently from surface-wave data

(using MAS_RW and MAS_LW; figs. 14 *A*, *B*, and 15 *A*, *B*, respectively) infer the same or even lower V_S values in that area of the model. This suggests that there may be some uncertainty regarding the magnitudes of the V_P/V_S and Poisson's ratios in that area of the model, but there is likely a zone of elevated V_P/V_S and Poisson's ratios in basement near the northwestern end of the John Hart profile, near the southeastern end of the concrete dam.

Ladore Dam

For the Ladore Dam seismic profile, we developed (1) a 2D V_P refraction tomography model, (2) a 2D V_S refraction tomography model, (3) a 2D V_P/V_S ratio model, (4) a 2D Poisson's ratio model, (5) a 2D V_S MAS_RW model, and (6) a 2D MAS_LW model. From the 2D V_S refraction tomography model, we developed a 2D time-averaged $V_{S(z)}$ models which shows time-averaged velocities to all depths of the models.

Ladore Dam Tomography Models

We inverted the active-source data from the Ladore Dam seismic profile to develop 2D V_P and V_S refraction tomography models (figs. 21 and 22*A*, respectively). The seismic data obtained from the Ladore seismic profile was less noisy than the seismic data from profiles acquired at the other two dam sites, but there was some noise. To minimize the existing noise, we stacked at least two P-wave shots and four S-wave shots at each shot point. On the southeastern end of the seismic profile, we used a 227-kg AWD to generate P-waves, which improved the signal-to-noise ratio of far-offset data long the profile. However, we used a 4.5-kg hammer and plate/block combination to generate seismic energy along most of the seismic profile.

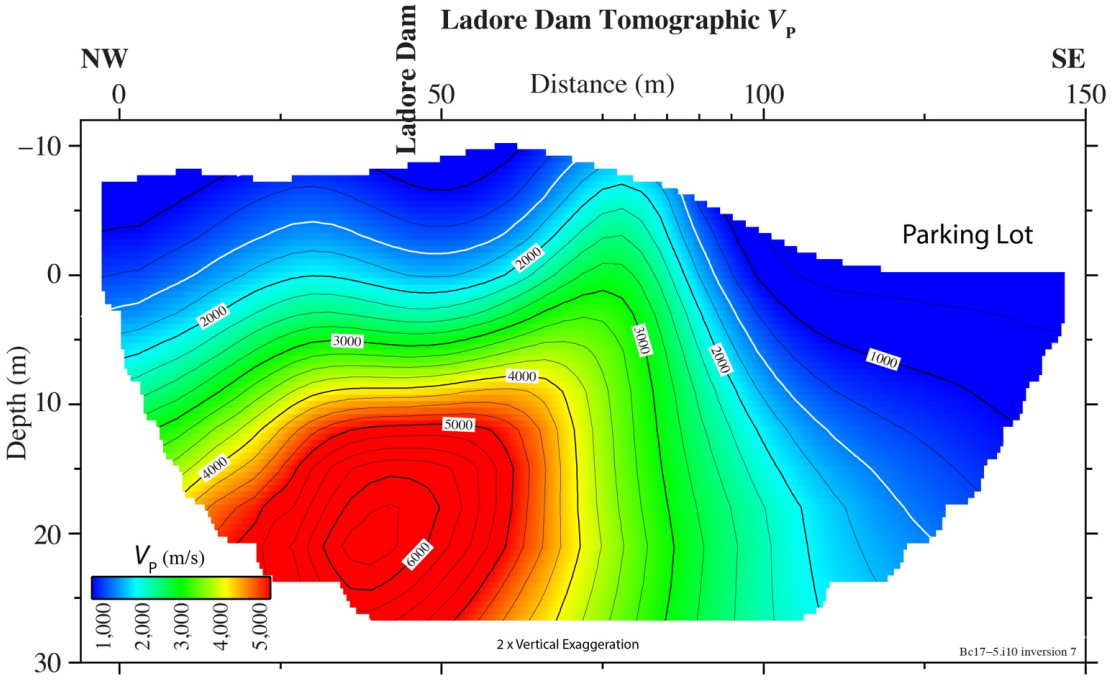

Figure 21. Diagram showing tomographic compressional-wave-velocity (V_P) model along the seismic profile for Ladore Dam ,Vancouver Island, British Columbia, Canada (see fig. 5). The top of groundwater, as inferred by the 1,500 meter per second (m/s) velocity contour, is shown in white. NW, northwest; SE, southeast; m, meters.

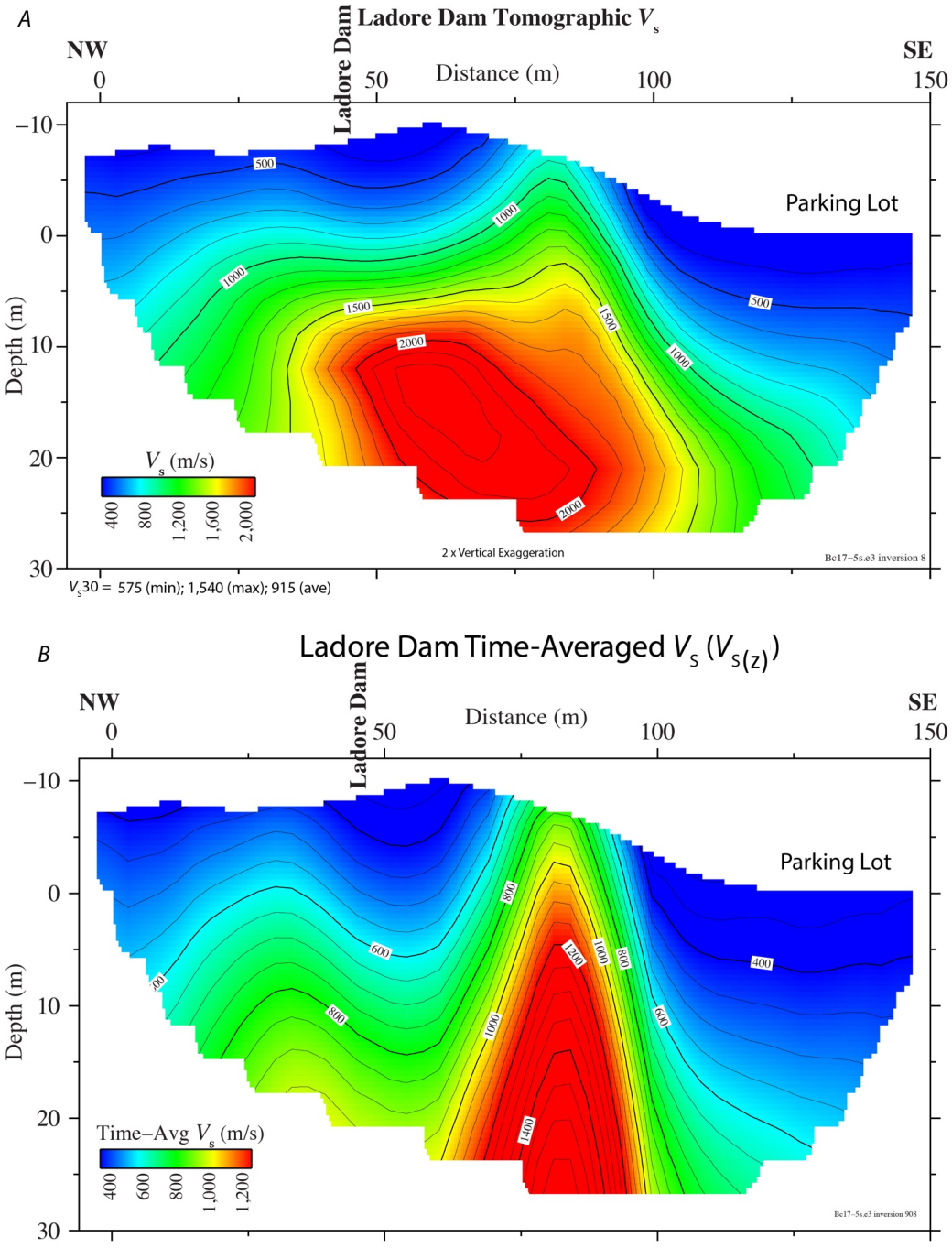

Figure 22. Diagrams showing seismic profiles for Ladore Dam, Vancouver Island, British Columbia, Canada (see fig. 5). *A*, Tomographic shear-wave-velocity (V_S) model. Lateral variations in modeled time-averaged shear-wave velocity in the upper 30 meters (m) of the subsurface (V_{S30}) along the seismic profile range from a minimum of 575 meter per second (m/s) to a maximum of 1,540 m/s, with an average of 915 m/s. *B*, Model of 2D time-averaged shear-wave velocity as a function of depth (*z*) ($V_{S(z)}$) along the profile derived from the V_S refraction tomography model in *A*. $V_{S(z)}$ is calculated using 1-m-thick layers. The time-averaged velocities to all depths are shown graphically. Depth (*z*) is relative to the topography. NW, northwest; SE, southeast; m, meters.

We used 47 shots recorded at 50 stations for the P-wave acquisition, resulting in as many as 2,350 P-wave and 2,350 S-wave arrivals available for velocity inversion. Although three-component data were acquired, we analyzed only the vertical-component and the horizontally transverse (Love-wave) component of the data for this profile. To invert the data, we used a 3×3-m grid spacing that matched our shot and sensor spacing. We developed starting velocity models from 1D analysis of shot gathers along the seismic profile. Our preferred P-wave model is shown in figure 21. Modeled V_P ranges from about 750 m/s in parts of the near-surface to about 6,500 m/s in the upper 35 m, with significant lateral variations. V_S ranges from about 400 m/s to about 2,300 m/s in the upper 30 m, with significant lateral variations in velocity (fig. 22*A*). These models inverted well and were generally consistent with respect to reciprocal arrivals. Thus, we suggest the models reasonably represent the overall velocity structure.

Both the V_P and V_S models indicate a large near-vertical velocity discontinuity from the surface to the bottom of the models near meter 100 of the seismic profile. Geologic mapping (Geosciences BC, 2013) shows a normal fault trending through the area (fig. 3), a splay of which may be related to our observed near-vertical velocity discontinuity.

Ladore Dam V_P/V_S and Poisson's Ratios Models

We developed a V_P/V_S model (fig. 23) and a Poisson's ratio model (fig. 24) by calculating those values at each node of the tomographic V_P (fig. 21) and V_S (fig. 22*A*) models. V_P/V_S ratios range from 1.3 to 3.9 along the seismic profile, with large lateral and vertical variations along the seismic profile. Poisson's ratios range from 0.03 to about 0.46, with the very low values (0.03) being inconsistent with values expected for basalt. Thus, we suggest that the zone of low V_P/V_S ratios (~1.3) and low Poisson's ratios (0.03) are not basement rocks and (or) the zone is physically altered with low-aspect-ratio cracks or fractures that are oriented perpendicular to our shear-wave propagation direction (Zhang and Bentley, 2005). Such a fracture or fault pattern is consistent with V_P and V_S models and near-vertical discontinuities in V_P/V_S and Poisson's ratios (Catchings and others, 2014, 2017) near meter 100 of the velocity model.

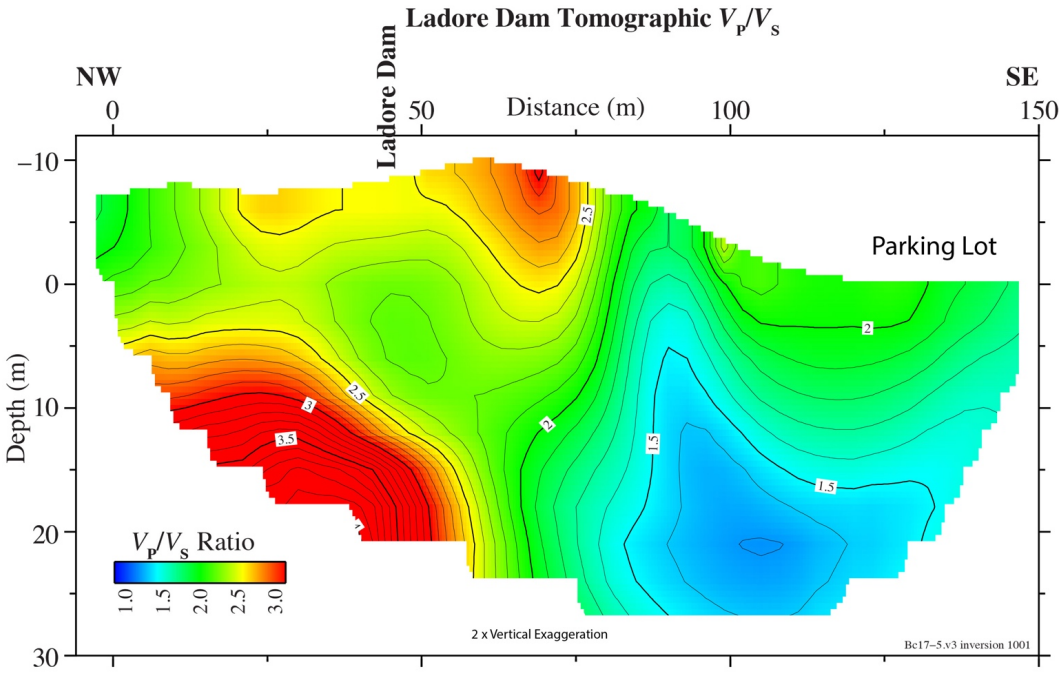

Figure 23. Diagram showing compressional-wave velocity/shear-wave-velocity (V_P/V_S) ratios along the seismic profile derived from the combined tomographic V_P (fig. 21) and V_S (fig. 22) models for Ladore Dam, Vancouver Island, British Columbia, Canada (see fig. 5). NW, northwest; SE, southeast; m, meters.

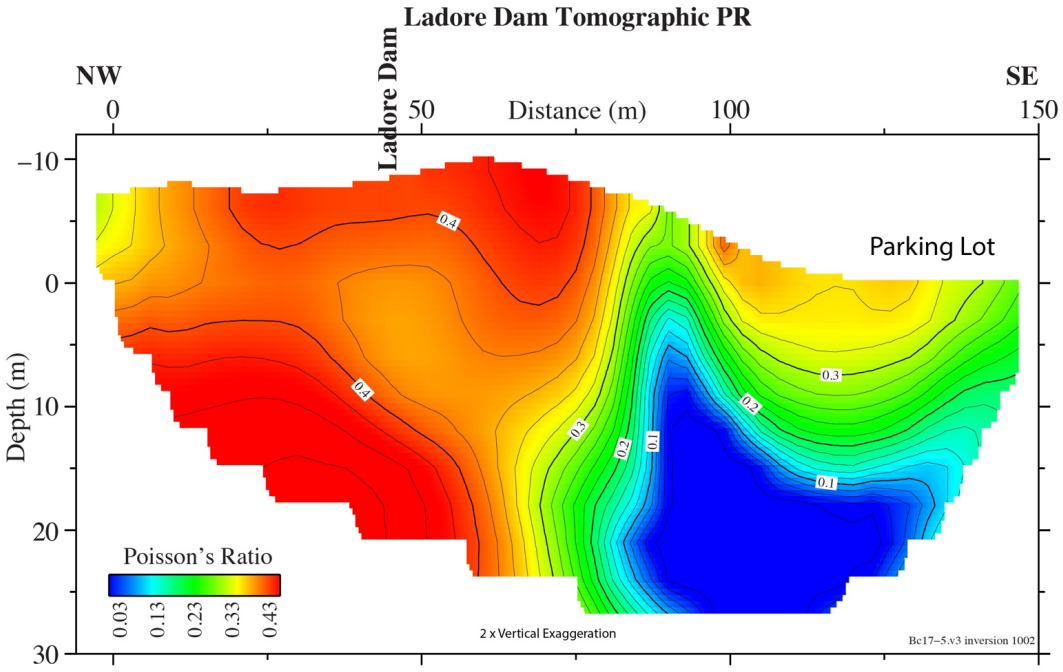

Figure 24. Diagram showing Poisson's ratios (PR) along the seismic profile derived from the combined tomographic compressional-wave-velocity (V_P) (fig. 21) and shear-wave-velocity (V_S) (fig. 22) models for Ladore Dam, Vancouver Island, British Columbia, Canada (see fig. 5). NW, northwest; SE, southeast; m, meters.

Ladore Dam MAS_RW and MAS_LW Models

We developed 2D V_S models along the Ladore Dam seismic profile using MAS_RW and MAS_LW. For the MAS_RW model (fig. 25), velocities ranged from about 500 m/s near the southeastern surface to about 5,250 m/s at 100 m depth to the northwest. The MAS_LW V_S model (fig. 26) also shows low velocities (250 m/s) at the surface on the southwest and higher velocities (3,800 m/s) to the northwest at about 90 m depth. Because of the lateral changes in elevation and the complexity of the velocity structure (as shown by tomography), surface-wave methods like MASW (for both Rayleigh and Love waves) encounter considerable difficulty in modeling lateral changes in V_S from the surface waves. However, the MAS_RW model shows similar velocity variations as the tomography model in the upper 20 m, whereby relatively low velocities (250–500 m/s) in the vicinity of the parking lot are juxtaposed against relatively high velocities (~2,000–3,000 m/s) to the northwest. Although there is less resolution in the MAS_RW and MAS_LW models, the discontinuity in velocity structure near meter 100 is consistent with observations from the tomography models.

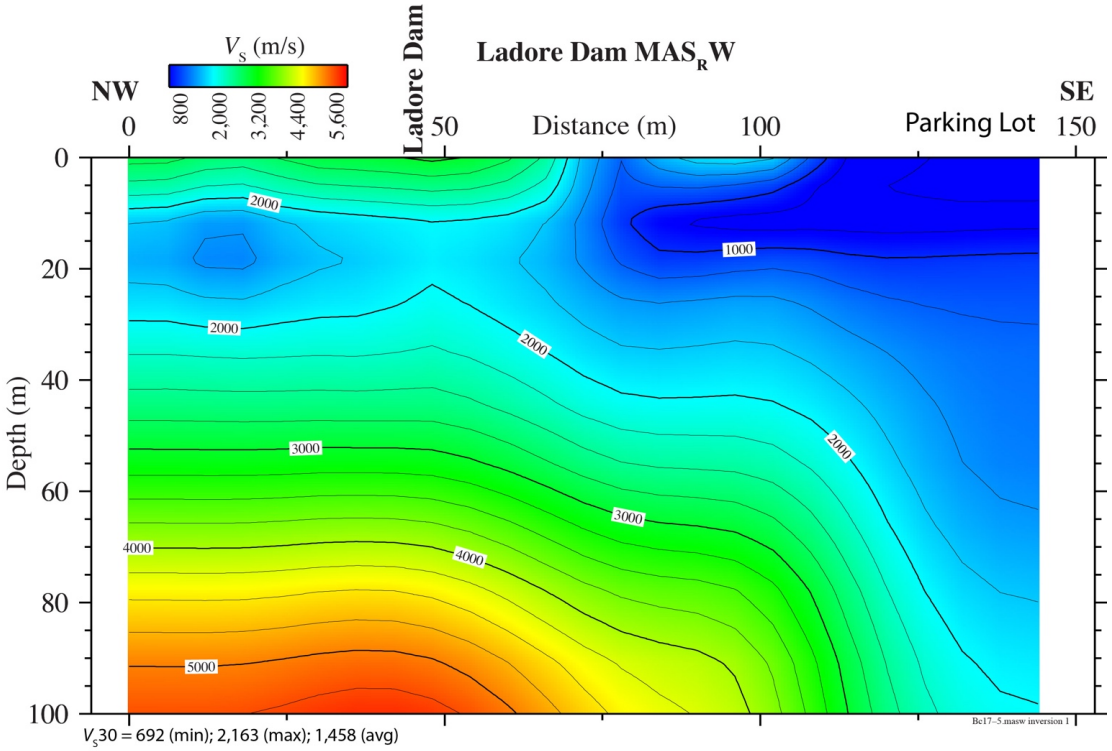

Figure 25. Diagram showing shear-wave-velocity (V_S) model along the seismic profile derived from multichannel analysis of surface waves using Rayleigh waves (MAS_RW) for Ladore Dam, Vancouver Island, British Columbia, Canada (see fig. 5). Lateral variations in V_{S30} along the seismic profile (as inferred by MAS_RW) range from a minimum of 692 meters per second (m/s) to a maximum of 2,163 m/s, with an average of 1,458 m/s. There are significant topographic and velocity variations along the seismic profile, which may affect the MAS_RW modeling. NW, northwest; SE, southeast; m, meters.

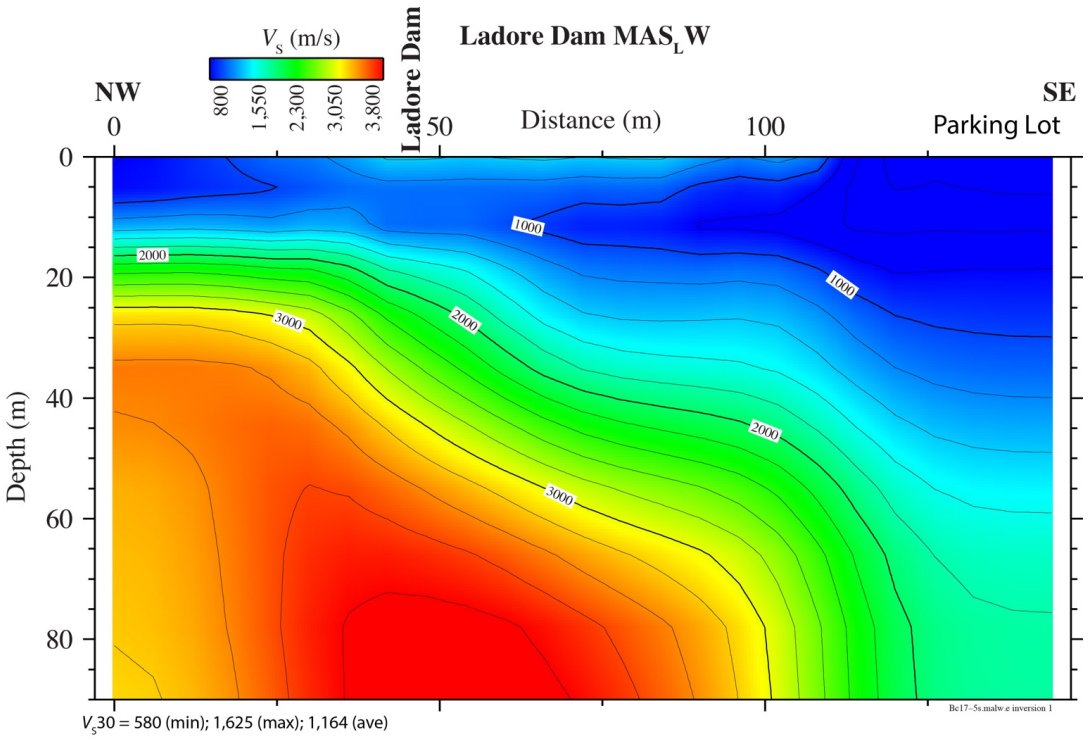

Figure 26. Diagram showing shear-wave-velocity (V_S) model along the seismic profile derived from multichannel analysis of surface waves using Love waves (MAS_LW) for Ladore Dam, Vancouver Island, British Columbia, Canada (fig. 5). Lateral variations in V_{S30} along the seismic profile (as inferred by MAS_LW) range from a minimum of 580 meters per second (m/s) to a maximum of 1,625 m/s, with an average of 1,164 m/s. There are significant topographic and velocity variations along the seismic profile, which may affect the MAS_LW modeling. NW, northwest; SE, southeast; m, meters.

Ladore Dam V_{S30} Calculations and Models

Using the V_S tomography model along the Ladore Dam profile (fig. 22*A*), we calculated V_{S30} at each meter along the profile (appendix 4, table 4) where the velocity model extended to at least 30 m depth (distance meters 54 to 99). We calculated the maximum, minimum, and average tomographic V_{S30} value along the seismic profile as 1,540 m/s, 575 m/s, and 915 m/s, and we developed a 2D model of $V_{S(z)}$, the time-averaged V_S at all depths (z) of the velocity model (fig. 22*B*). Similarly, we calculated maximum, minimum, and average V_{S30} from the MAS_RW V_S model (fig. 25) as 2,163 m/s, 692 m/s, and 1,458 m/s (appendix 4, table 5). From the MAS_LW V_S model (fig 26), we calculated the maximum, minimum, and average V_{S30} as 1,625 m/s, 580 m/s, and 1,164 m/s along the seismic profile (appendix 4, table 6).

Shallow Crustal Structure at Ladore Dam

From our tomography (V_P and V_S) models, we observe relatively high velocities (V_P=2,200 to 6,200 m/s; V_S=1,000 to 2,200 m/s) northwest of meter 100 of the seismic profile, with an abrupt, near-vertical transition to lower velocities southeast of meter 100 (figs. 21 and 22). This velocity transition occurs beneath a steeply southeast-dipping topographic slope. This steeply dipping, high-velocity/topographic feature may be fault related, as a fault has been mapped (Geosciences BC, 2013) in the immediate vicinity of Ladore Dam (fig. 3). Because both V_P and V_S can be strongly affected by

faulting (Mayer-Rosa, 1973; Healy and Peake, 1975; Aki and Lee, 1976; Wang and others, 1978; Spudich and Angstman, 1980; Mooney and Ginzburg, 1986; Jarchow and others, 1994; Catchings and others, 2002, 2014), faults in the area of the dam may explain the velocity transition. Local faults are of concern (BC Hydro 2012a, b), not only because of possible slip on the faults, but because strong shaking can be focused along them. For example, studies at other locations have shown that high-amplitude guided-wave energy can be transmitted over long distances along faults (Cormier and Spudich, 1984; Catchings and others, 2016; Li and others, 2016). Although we cannot rule out the possibility that a localized, less-well-determined part of the Ladore Dam tomographic velocity models resulted in the observed V_P/V_S and Poisson's ratio anomalies, we suggest that it is unlikely because the tomographic seismic data were relatively noise free and because we also observe similar velocities and structures from the surface-wave models, which use independent data and data analysis methods.

Relative to the central and northwest parts of the seismic profile, velocities southeast of meter 100 are generally much lower (V_P=<2,000 m/s; V_S=400 to750 m/s) and are consistent with the dominant presence of sediments in the upper 15–20 m. Furthermore, the likely depth to the top of ground water (V_P=1,500 m/s) is highly variable along the seismic profile.

Strathcona Dam

We acquired three subparallel seismic profiles at Strathcona Dam (fig. 6). The surface geology along each of the profiles differed appreciably, but the combined profiles were designed to capture the lateral variability of the seismic velocities at Strathcona Dam. Here, we present seismic models separately for each seismic profile.

Strathcona Dam Roadway Profile

For the Strathcona Dam Roadway seismic profile, we developed (1) a 2D V_P refraction tomography model, (2) a 2D V_s refraction tomography model, (3) a 2D V_P/V_s ratio model, (4) a 2D Poisson's ratio model, (5) a 2D V_s $MASW_R$ model, and (6) two 2-D $MASW_L$ models. From the 2D V_s refraction tomography model, we developed a 2D time-averaged $V_{S(z)}$ model, which shows time-averaged velocities to all depths of the models.

Strathcona Dam Roadway Tomography Models

The seismic data obtained from the Strathcona Roadway seismic profile include significant 60-hertz (Hz) noise. Although we stacked at least two AWD shots at each P- and S-wave shot point, and we applied notch filters to remove 60-Hz noise, there remained significant noise on all gathers. However, some shots had relatively strong signal-to-noise ratios, allowing arrivals to be observed along much of the seismic profile. The high-noise levels on all of the Strathcona profiles made it difficult to precisely identify first-arrival refractions to within a few (~4 ms) milliseconds, particularly at farther offsets. Because of the high velocities and the relatively short offsets of the seismic profiles, first-arrival errors of just few milliseconds can make the data difficult to invert for velocity structure. Thus, the Strathcona seismic models appear to lack the fine details typical of most similar tomographic models.

We used 79 shots recorded at 80 stations for the P-wave acquisition, resulting in as many as 6,320 P-wave and 6,320 S-wave arrivals available for velocity inversion. We used a 3×3-m grid spacing that matched our shot and sensor spacing. We developed starting velocity models from 1D analysis of shot gathers along the seismic profile, and we used multiple starting models that converged to similar final models, usually with less than 5 percent variation among the final models. Our preferred V_P model is shown in figure 27. V_P ranges from about 1,000 m/s in parts of the near-surface to about 4,750 m/s in

the upper ~40 m, with significant lateral variations. V_S ranges from about 400 m/s near the surface to about 3,200 m/s in the upper 35 m, also showing significant lateral variations in velocity (fig. 28*A*). These models appear to lack fine details of the velocity structure and are somewhat generalized, but they likely represent the overall velocities for the area.

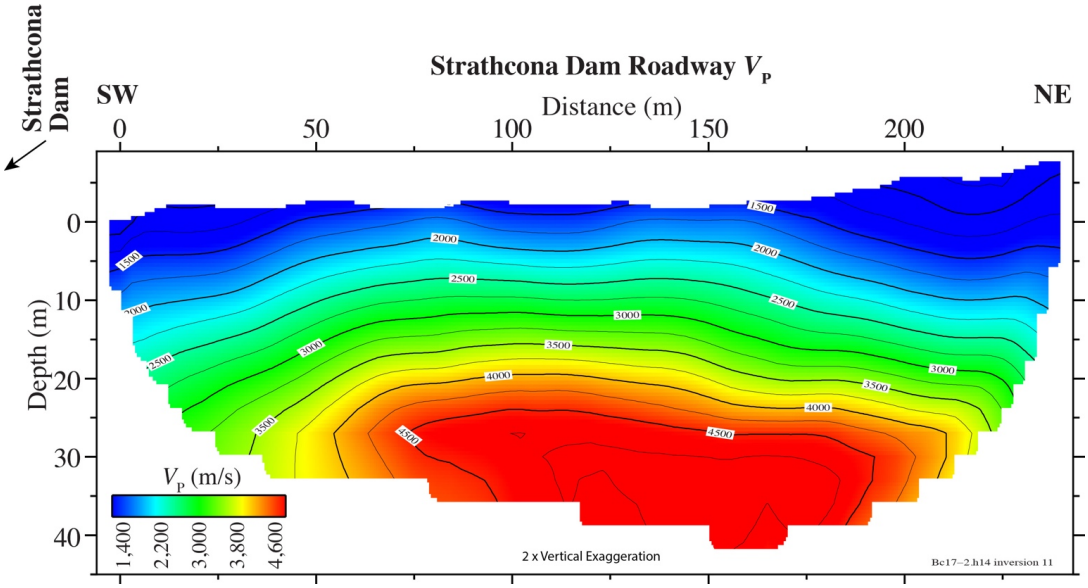

Figure 27. Diagram showing tomographic compressional-wave-velocity (V_P) model along the seismic profile for Strathcona Dam Roadway, Vancouver Island, British Columbia, Canada (see fig. 6). The top of groundwater, as inferred by the 1,500 meter per second (m/s) velocity contour, is shown in white. SW, southwest; NE, northeast; m, meters.

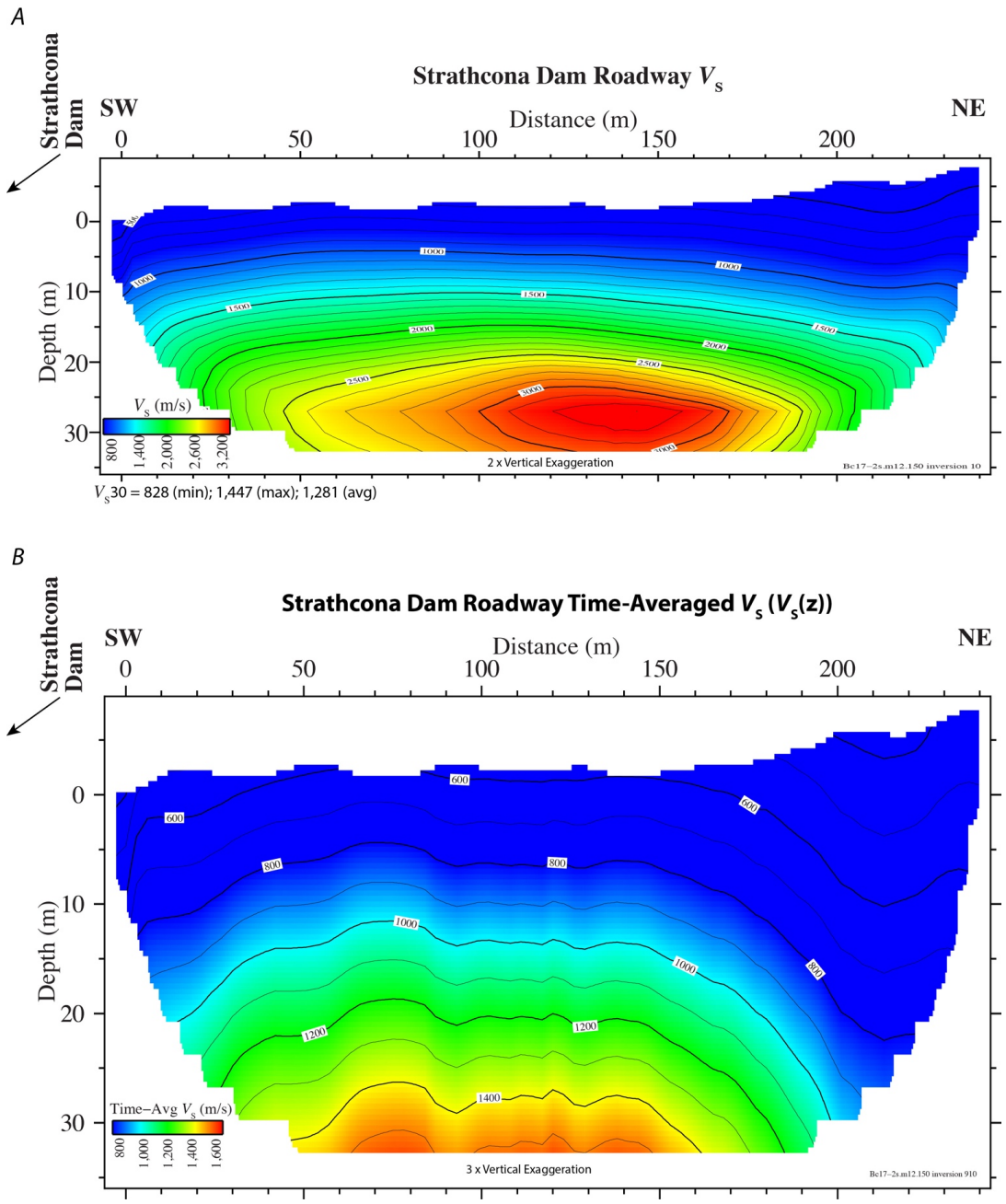

Figure 28. Diagrams showing seismic profiles for Strathcona Dam Roadway, Vancouver Island, British Columbia, Canada (see fig. 6). *A*, Tomographic shear-wave velocity (V_S) model along the seismic profile. Lateral variations in modeled time-averaged shear-wave velocity in the upper 30 meters (m) of the subsurface (V_{S30}) along the seismic profile range from a minimum of 828 meters per second (m/s) to a maximum of 1,447 m/s, with an average of 1,281 m/s. *B*, Model of 2D time-averaged shear-wave velocity as a function of depth (*z*) ($V_{S(z)}$) along the seismic profile derived from the V_S refraction tomography model in *A*. $V_{S(z)}$ is calculated using 1-m-thick layers. The time-averaged velocities to all depths are shown graphically. Depth (*z*) is relative to the topography. SW, southwest; NE, northeast.

Strathcona Dam Roadway V_P/V_S and Poisson's Ratio Models

We developed a V_P/V_S model (fig. 29) and a Poisson's ratio model (fig. 30) along the Roadway by calculating values for each at each node of the P-wave (fig. 27) and S-wave models (fig. 28*A*). V_P/V_S ratios range from 1.4 to 2.5 along the seismic profile, with the higher values near the surface likely representing road gravel and broken basalt of the roadway. Poisson's ratio (fig. 30) is variable along our profile (0.05 to 0.4). Parts of the deep seismic profile with Poisson's ratios less than about 0.14 are unusual, as typical values of Poisson's ratio for basalt are expected to be no less than 0.14. However, such low values may be consistent with other rocks, such as sandstone or schist. We cannot rule out the possibility that such low values arise from poorly determined velocities (V_P, V_S, or both) along parts of the velocity model, given the noise-contaminated data.

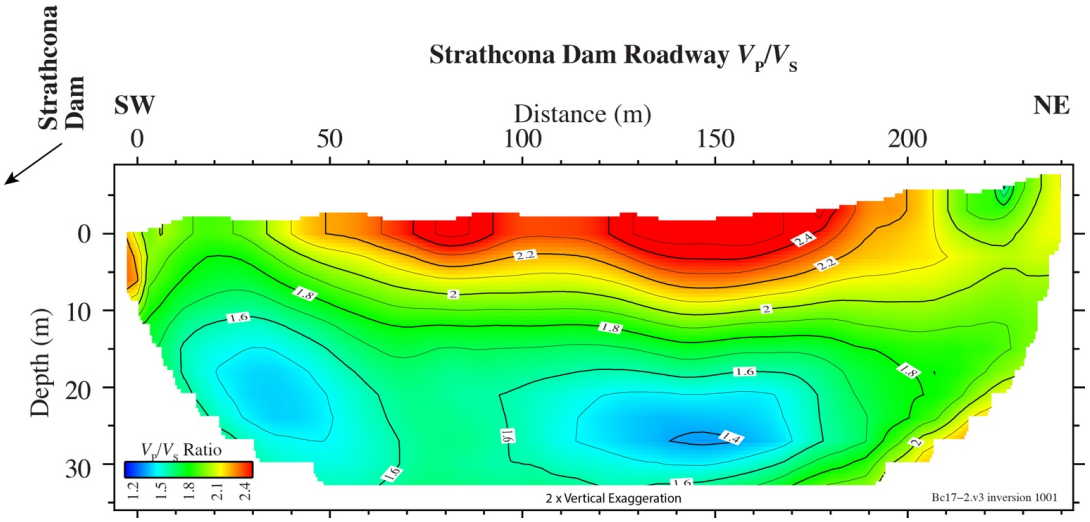

Figure 29. Diagram showing compressional-wave-velocity/shear-wave-velocity (V_P/V_S) ratios along the seismic profile derived from the combined tomographic V_P (fig. 27) and V_S (fig. 28*A*) models for Strathcona Dam Roadway, Vancouver Island, British Columbia, Canada (see fig. 6). SW, southwest; NE, northeast; m, meters.

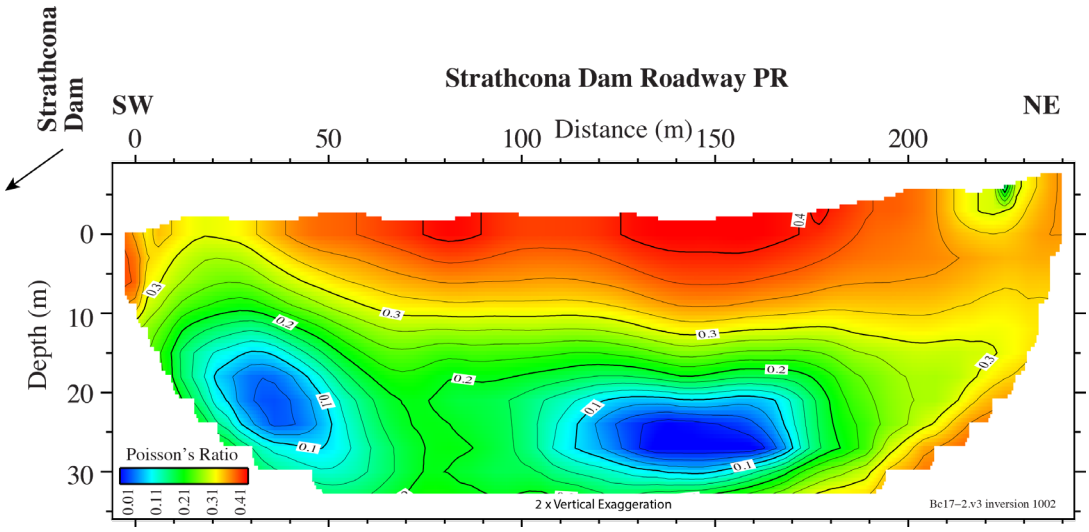

Figure 30. Diagram showing Poisson's (PR) ratios along the seismic profile derived from the combined tomographic compressional-wave-velocity (V_P) (fig. 27) and shear-wave-velocity (V_S) (fig. 28*A*) models for Strathcona Dam Roadway, Vancouver Island, British Columbia, Canada (see fig. 6). SW, southwest; NE, northeast; m, meters.

Strathcona Dam Roadway MAS_RW and MAS_LW Models

We developed 2D V_S models along the Strathcona Roadway using MAS_RW and MAS_LW. For the MAS_RW model (fig. 31), V_S ranged from about 300 m/s near the surface to about 3,300 m/s at about 90 m depth, with the lowest values near the southwestern end of the profile (nearest Strathcona Dam). Along most of the profile, MAS_RW-based, near-surface V_S ranges from about 1,000 m/s to about 1,200 m/s. For the MAS_LW models (figs. 32 and 33), modeled V_S ranges from about 400 m/s to about 3,300 m/s at 100 m depth, with lower V_S to the southwest. These surface-wave results are likely strongly affected by the steep topographic slopes along the sides of the seismic profile, the topography along the road, and the significant lateral variation in velocity seen from the tomographic profiles.

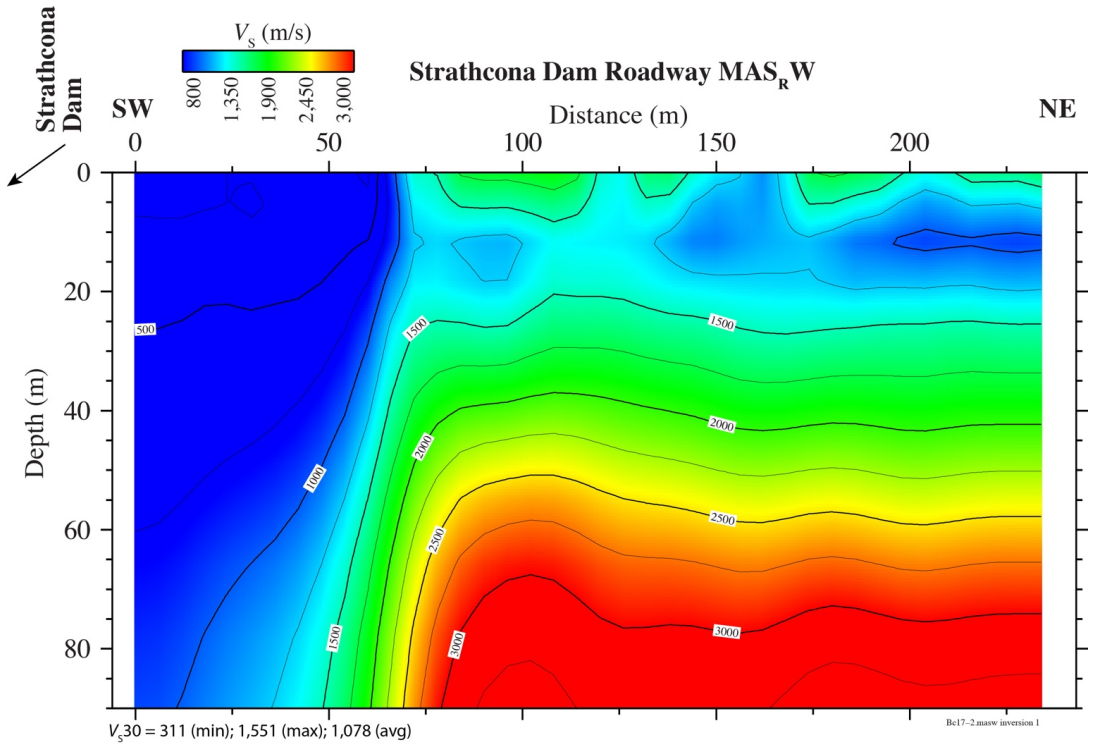

Figure 31. Diagram showing shear-wave-velocity (V_S) model along the seismic profile derived from multichannel analysis of surface waves using Rayleigh waves (MAS$_R$W) for Strathcona Dam Roadway, Vancouver Island, British Columbia, Canada (see fig. 6). Lateral variations in time-averaged shear-wave velocity in the upper 30 meters (m) of the subsurface (V_{S30}) along the seismic profile (as inferred by MAS$_R$W) range from a minimum of 311 meters per second (m/s) to a maximum of 1,551 m/s, with an average of 1,078 m/s. There are significant topographic and velocity variations along the Roadway seismic profile, which may affect the MAS$_R$W modeling. SW, southwest; NE, northeast.

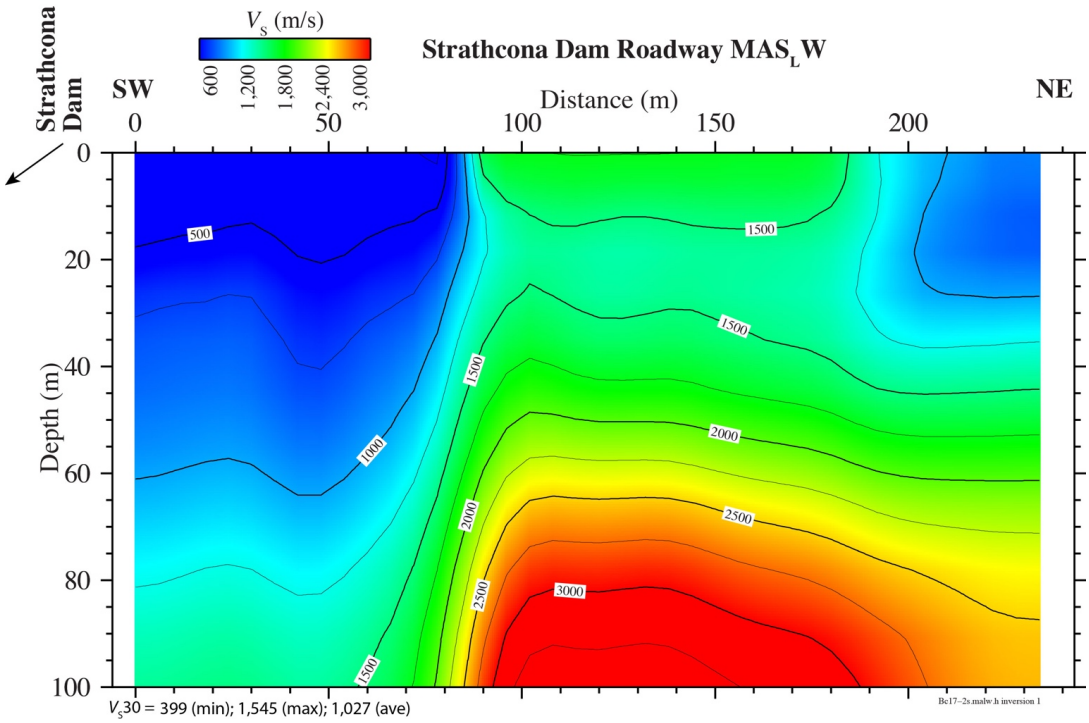

Figure 32. Diagram showing shear-wave-velocity (V_S) model along the seismic profile derived from multichannel analysis of surface waves using Love waves (MAS$_L$W) for Strathcona Dam Roadway, Vancouver Island, British Columbia, Canada (see fig. 6). Lateral variations in time-averaged shear-wave velocity in the upper 30 meters (m) of the subsurface (V_{S30}) along the seismic profile (as inferred by MAS$_L$W) range from a minimum of 399 meters per second (m/s) to a maximum of 1,545 m/s, with an average of 1,027 m/s. There are significant topographic and velocity variations along the seismic profile, which may affect the MAS$_L$W modeling. SW, southwest; NE, northeast.

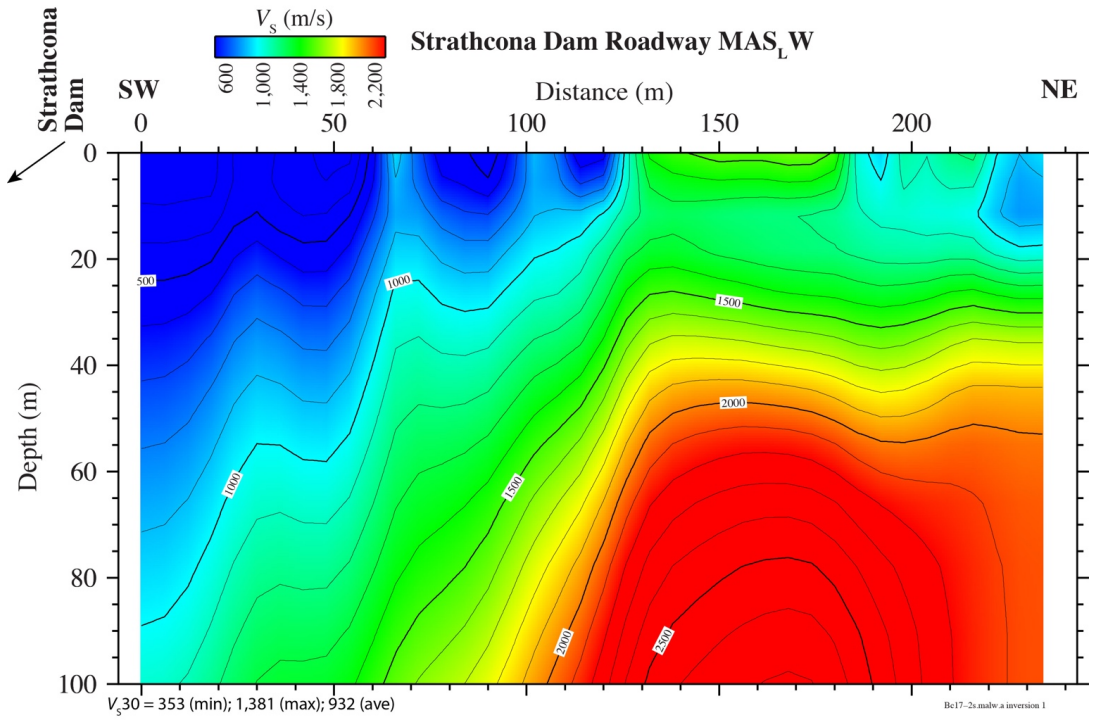

Figure 33. Diagram showing alternative shear-wave-velocity (V_S) model along the seismic profile derived from multichannel analysis of surface waves using Love waves (MAS$_L$W) for Strathcona Dam Roadway, Vancouver Island, British Columbia, Canada (see fig. 6). Lateral variations in V_{S30} along the Roadway seismic profile (as inferred by MAS$_L$W) range from a minimum of 353 meters per second (m/s) to a maximum of 1,381 m/s, with an average of 932 m/s. There are significant topographic and velocity variations along the Roadway seismic profile, which may affect the MAS$_L$W modeling. SW, southwest; NE, northeast.

Strathcona Dam Roadway V_{S30} Calculations and Models

Using the V_S tomography model along the spillway (fig. 28*A*), we calculated V_{S30} at each lateral meter along the profile (appendix 4, table 7) where the velocity model extended to at least 30 m depth. We calculated the maximum, minimum, and average V_{S30} values as 1,447 m/s, 828m/s, and 1,281 m/s, respectively, and we developed a 2D model of $V_{S(z)}$ whereby the time-averaged V_S at all depths (z) of the velocity model are calculated (fig. 28*B*). Similarly, we calculated V_{S30} from the MAS$_R$W model (fig. 31) and calculated maximum, minimum, and average values of 1,551 m/s, 311 m/s, and 1,078 m/s, respectively (appendix 4, table 8). We used the north and east components of the data to calculate dispersion curves for the Roadway seismic profile. For the MAS$_L$W (Love, transverse component) model (fig 32), we calculated V_{S30} as 1,545 m/s (maximum), 399 m/s (minimum) and 1,027 m/s (average) along the seismic profile (appendix 4, table 9). For the MAS$_L$W (Love, parallel component) model (fig. 33), we calculated V_{S30} as 1,381 m/s (maximum), 353 m/s (minimum), and 932 m/s (average) (appendix 4, table 10).

Strathcona Dam Spillway Profile

For the Strathcona Dam Spillway seismic profile, we developed (1) two 2D V_P refraction tomography models, (2) two 2D V_S refraction tomography models, (3) a 2D V_P/V_S ratio model, (4) a 2D Poisson's ratio model, (5) a 2D V_S MAS$_R$W model, and (6) a 2D MAS$_L$W model. From the 2D V_S

refraction tomography models, we developed two 2D time-averaged $V_{S(z)}$ models, which shows time-averaged velocities to all depths of the models.

Strathcona Dam Spillway Tomography Models

For the Strathcona Dam Spillway active-source data, we developed 2D V_P and V_S refraction tomography models. The seismic data obtained from the spillway was highly reverberative and included significant 60-Hz noise (appendix 1, fig. 47). To minimize the noise, we stacked multiple shots at each shot point, whereby each shot gather consisted of at least four stacked shots. We also used notch filters to remove as much of the 60-Hz noise as was practical. Nevertheless, significant noise persisted, particularly at the farther offsets. In addition, the refracted P-wave phases were generally higher in frequency and weaker in amplitude, owing to the fact that the seismic source was generated directly on the hard rock surface and the sensor was also located on the rock surface.

Two P-wave models for the Strathcona Dam Spillway seismic profile are shown in figures 34 and 36. Based on first-arrival P-wave measurements, which were not well determined in most cases, our modeled tomographic V_P ranges from about 1,500 m/s in parts of the near-surface to about 5,600 m/s in the upper 40 m+, with significant lateral variations. We also developed two V_S models for the spillway seismic profiles. Our modeled V_S ranges from about 1,200 m/s to about 3,300 m/s in the upper 30 m, also showing significant lateral variations in velocity (figs. 35*A* and 37*A*). These V_S models inverted well and were generally consistent with respect to reciprocal arrivals; however, we caution that the relatively weak (high frequency) first arrivals (of both P- and S-waves) were difficult to accurately measure, such that our models may lack fine details. Nevertheless, we suggest the models are generally representative of the range of velocities, but details of the velocity structure may be inaccurately captured due to the background noise associated with the data. Because of the relatively high near-surface velocities and the relatively poor data quality (see appendix 1; fig. 47), it was difficult to differentiate between the P- and S-wave arrivals at near offsets. As a result, V_S in the upper few meters of the subsurface may be less well determined than V_P.

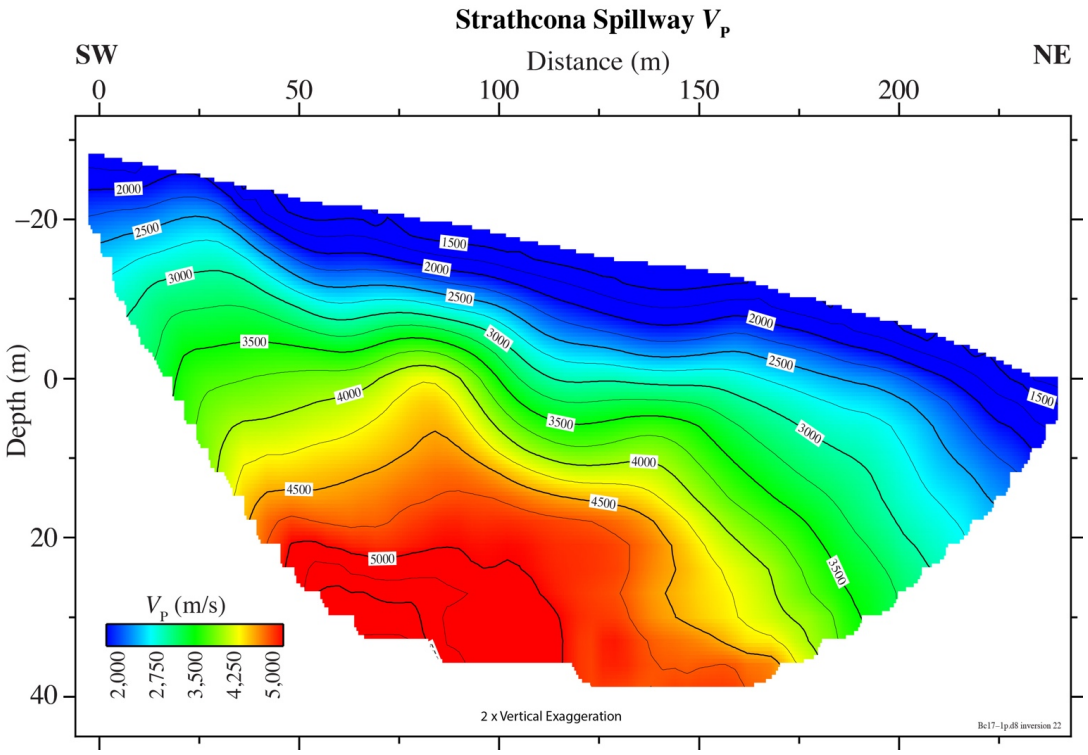

Figure 34. Diagram showing tomographic compressional-wave velocity (V_P) model along the seismic profile Strathcona Dam Spillway, Vancouver Island, British Columbia, Canada (see fig. 6). The top of groundwater, as inferred by the 1,500 meters per second (m/s) velocity contour, is shown in white. SW, southwest; NE, northeast; m, meters.

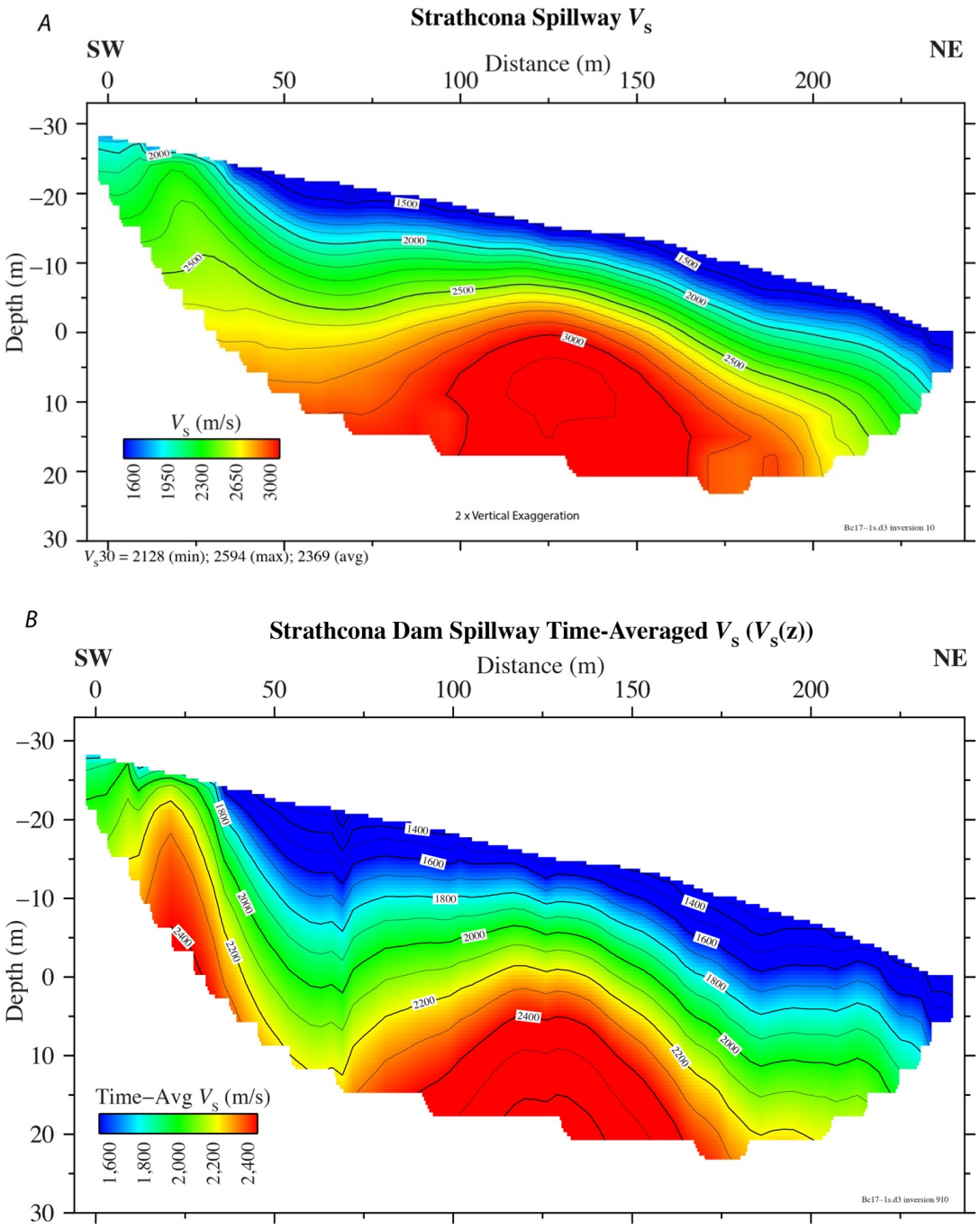

Figure 35. Diagrams showing seismic profiles for Strathcona Dam Spillway, Vancouver Island, British Columbia, Canada (see fig. 6). *A*, Tomographic shear-wave-velocity (V_S) model along the seismic profile. Lateral variations in time-averaged shear-wave velocity in the upper 30 meters (m) of the subsurface (V_{S30}) along the seismic profile range from a minimum of 2,128 meters per second (m/s) to a maximum of 2,594 m/s, with an average of 2,369 m/s. *B*, Alternative model of 2D time-averaged shear-wave velocity as a function of depth (*z*) ($V_{S(z)}$) along the Spillway seismic profile derived from the V_S refraction tomography model in *A*. $V_{S(z)}$ is calculated using 1-m-thick layers. The time-averaged velocities to all depths are shown graphically. Depth (*z*) is relative to the topography. SW, southwest; NE, northeast.

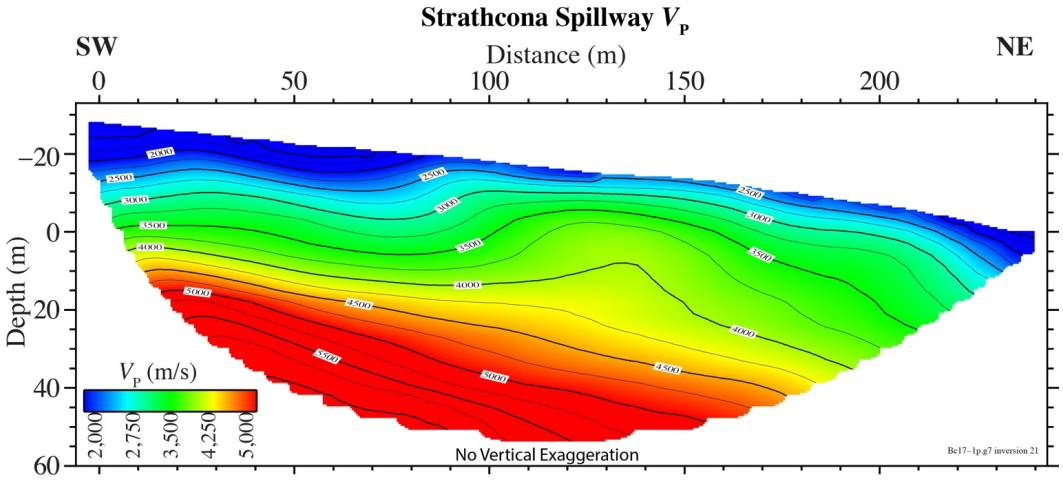

Figure 36. Diagram showing alternative tomographic compressional-wave-velocity (V_P) model along the seismic profile for Strathcona Dam Spillway, Vancouver Island, British Columbia, Canada (see fig. 6). SW, southwest; NE, northeast; m, meters.

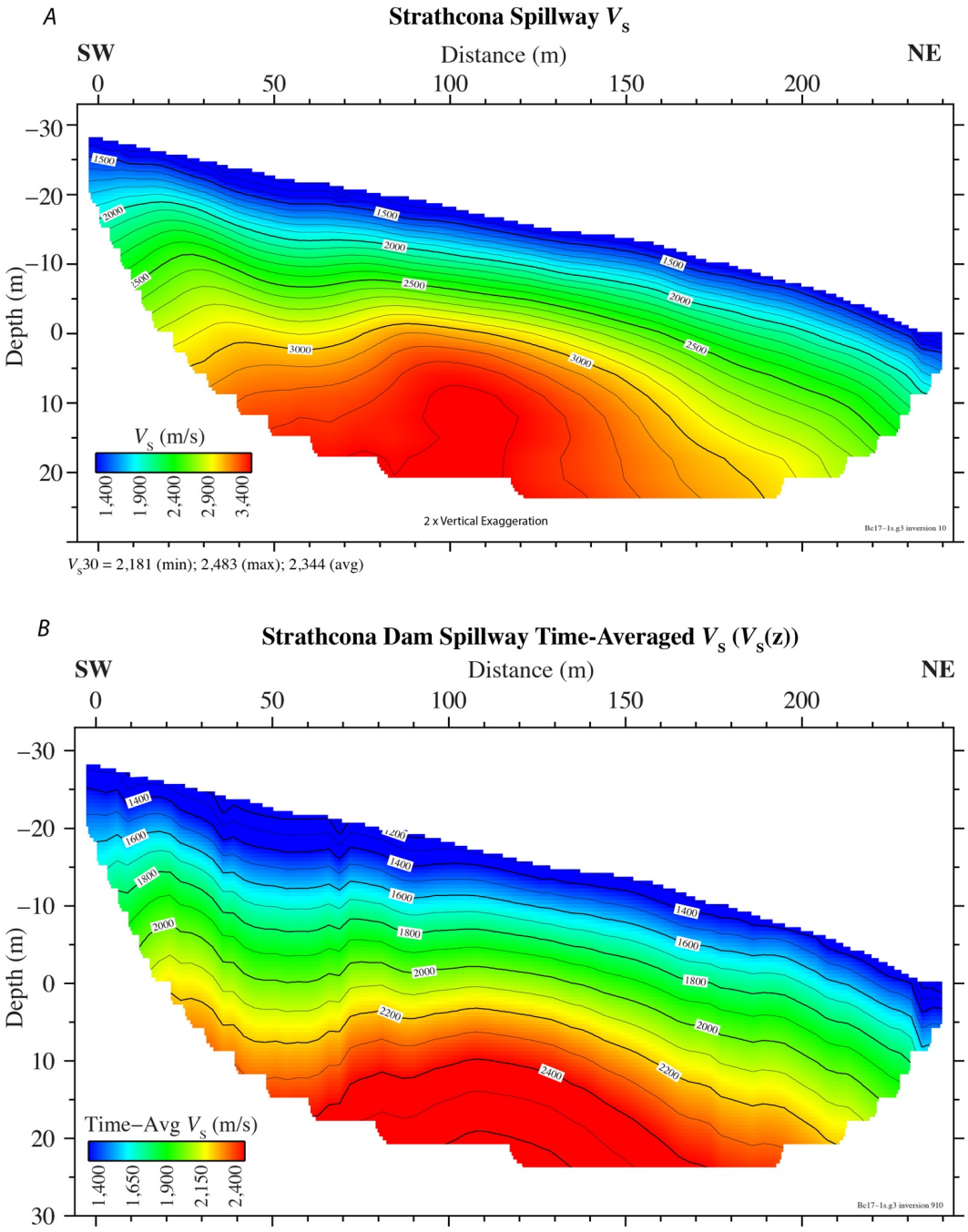

Figure 37. Diagrams showing seismic profiles for Strathcona Dam Spillway, Vancouver Island, British Columbia, Canada (see fig. 6). *A*, Alternative tomographic shear-wave-velocity (V_S) model along the seismic profile. Lateral variations in time-averaged shear-wave velocity in the upper 30 meters (m) of the subsurface (V_{S30}) along the seismic profile range from a minimum of 2,181 meters per second (m/s) to a maximum of 2,483 m/s, with an average of 2,344 m/s. *B*, Alternative model of 2D time-averaged shear-wave velocity as a function of depth (*z*) ($V_{S(z)}$) along the seismic profile derived from the V_S refraction tomography model in *A*. $V_{S(z)}$ is calculated using 1-m-thick layers. The time-averaged velocities to all depths are shown graphically. Depth (*z*) is relative to the topography. SW, southwest; NE, northeast.

Strathcona Dam Spillway Tomographic V_P/V_S and Poisson's Ratio Models

We developed a V_P/V_S ratio model (fig. 38) and a Poisson's ratio model (fig. 39) from preferred the V_P (fig. 34) and *Vs* models (fig. 35*A*). Our models suggest that V_P/V_S ratios range from about 1.1 to about 1.8, and Poisson's ratios range from about 0.01 to about 0.28. However, we believe that the V_P and V_S models for the Spillway profile may not be well determined, and as a result, the V_P/V_S ratio and Poisson's ratio models may be in error in parts of the models.

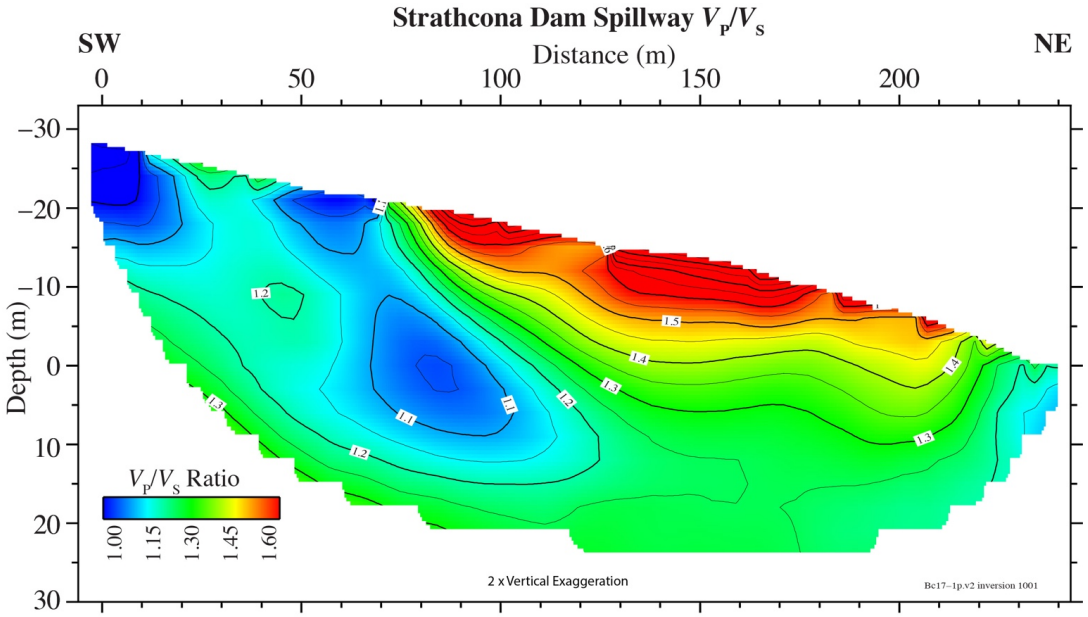

Figure 38. Diagram showing compressional-wave velocity/shear-wave-velocity (V_P/V_S) ratios along the seismic profile derived from the combined tomographic V_P (fig. 34) and V_S (fig. 35) models for Strathcona Dam Spillway, Vancouver Island, British Columbia, Canada (see fig. 6). SW, southwest; NE, northeast; m, meters.

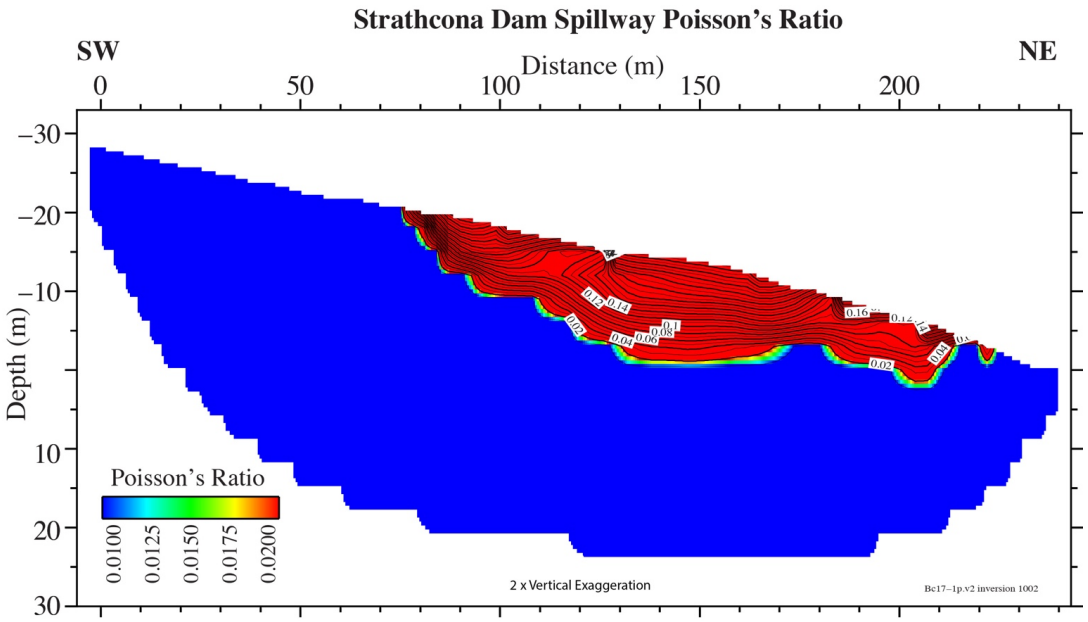

Figure 39. Diagram showing Poisson's ratios along the seismic profile derived from the combined tomographic compressional-wave velocity (V_P) (fig. 34) and shear-wave-velocity (V_S) (fig. 35) models for Strathcona Dam Spillway, Vancouver Island, British Columbia, Canada (see fig. 6). SW, southwest; NE, northeast; m, meters.

Strathcona Dam Spillway $MASW_R$ and $MASW_L$ Models

We attempted to develop 2D V_S models along the Strathcona Spillway using $MASW_R$ (fig. 40) and $MASW_L$ (fig. 41); however, clear dispersion curves (appendix 2) could not be developed from the Rayleigh- and Love-wave data for the Spillway profile; therefore, we have low confidence in the surface-wave-based Spillway velocity models. In addition, there was considerable topographic relief along the seismic profile, which strongly affects the surface-wave-based V_S results.

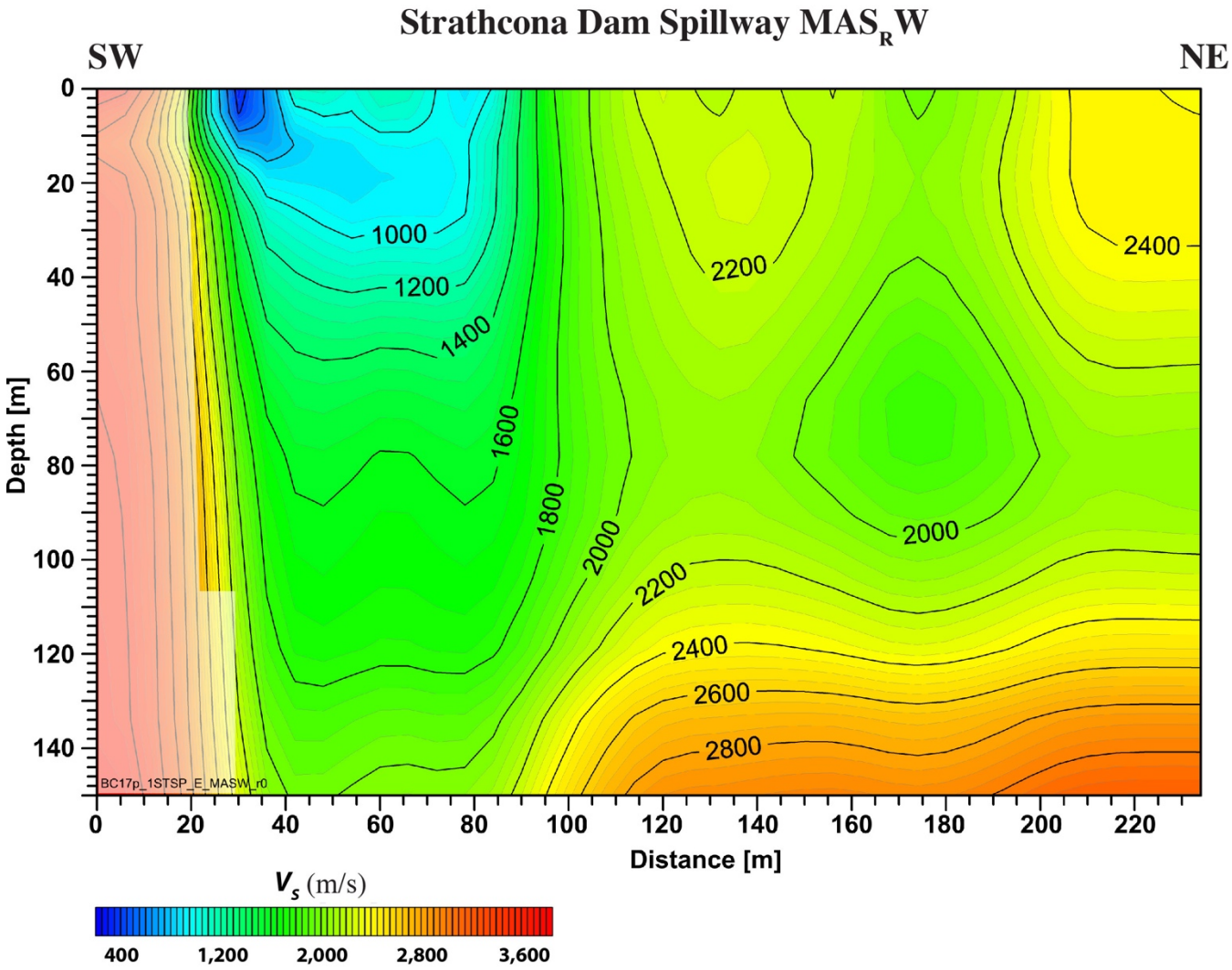

Figure 40. Diagram showing shear-wave-velocity (V_S) model along the seismic profile derived from multichannel analysis of surface waves using Rayleigh waves (MAS_RW) for Strathcona Dam Spillway, Vancouver Island, British Columbia, Canada (see fig. 6). SW, southwest; NE, northeast; m, meters; m/s, meters per second.

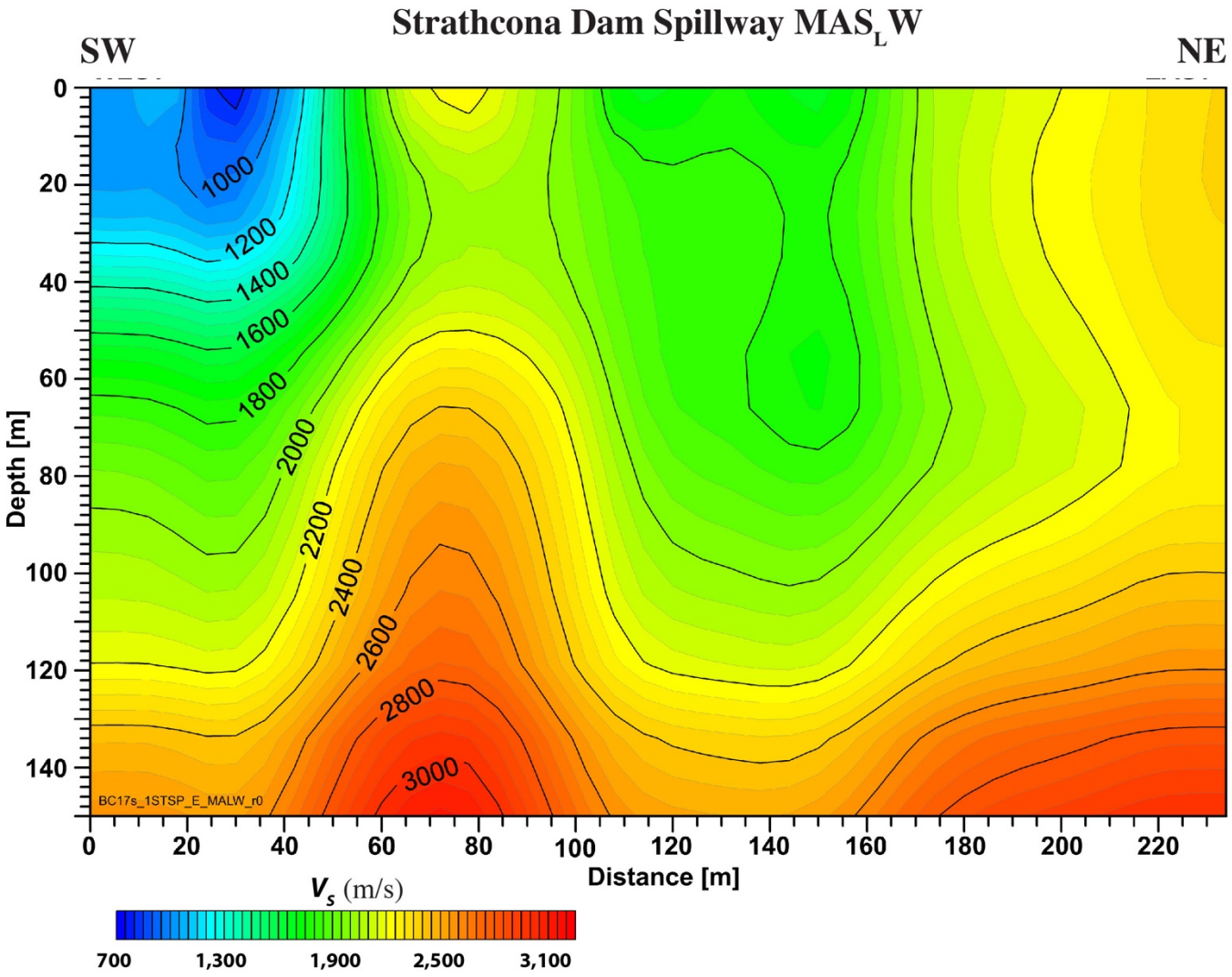

Figure 41. Diagram showing shear-wave-velocity (V_S) model along the seismic profile derived from multichannel analysis of surface waves using Love waves (MAS_LW) for Strathcona Dam Spillway, Vancouver Island, British Columbia, Canada (see fig. 6). SW, southwest; NE, northeast; m, meters.

Strathcona Dam Spillway V_{S30} Calculations and Models

Using the two V_S tomography models along the spillway (fig. 35*A* and 37*A*), we calculated V_{S30} at each meter along the profile (appendix 4, table 11) where the velocity model extended to at least 30 m depth (distance meters 48 to 183). For the model shown in for figure 35*A*, we calculated the maximum, minimum, and average tomographic V_{S30} values as 2,594, 2,128, and 2,369 m/s, respectively. For the model shown in figure 37*A*, we calculated the maximum, minimum, and average tomographic V_{S30} values as 2,483, 2,181, and 2,344 m/s, respectively. We also calculated 2D time-averaged models of $V_{S(z)}$ for the two models (figs. 35*B* and 37*B*). However, we again caution the spillway tomographic model may contain inaccurate values in parts of the model. However, the general range of V_{S30} values is likely representative of the range of V_{S30} at the spillway. Although we feel the MAS_RW and MAS_LW models are not well constrained, similar velocities are inferred by both the tomographic and surface-wave models.

Strathcona Dam Campground Models

For the Strathcona Dam Campground seismic profile, we could only develop a 2D V_P refraction tomography model and a 2D MAS$_L$W model, due to high noise levels. Because we lacked a 2D V_S refraction tomography model, we did not develop a 2D time-averaged $V_{S(z)}$ model.

Strathcona Dam Campground Tomography Model

The seismic data acquired along the Strathcona Campground seismic profile also include significant 60-Hz noise. As with the other Strathcona profiles, we stacked at least four hammer shots at each S-wave shot point, and we applied notch filters to remove the 60-Hz noise, but there remained significant noise on the S-wave shot gathers (see appendix 1, fig. 48). However, we used a Betsy Seisgun® to acquire P-wave data along the Campground profile, which resulted in relatively high signal-to-noise ratios. Thus, we were able to invert for a V_P model, but we could not invert for a V_S model. Based on our measured first arrivals, we determined V_P to range from about 1,500 m/s in parts of the near-surface to about 6,000 m/s in the upper 55 m, with significant lateral variations (fig. 42). This model likely represents the overall range of velocities, but fine details of the velocity structure may not be accurately captured. Because we could not develop a tomographic V_S model for the campground seismic profile, we could not develop tomographic V_P/V_S and Poisson's ratio models for this profile.

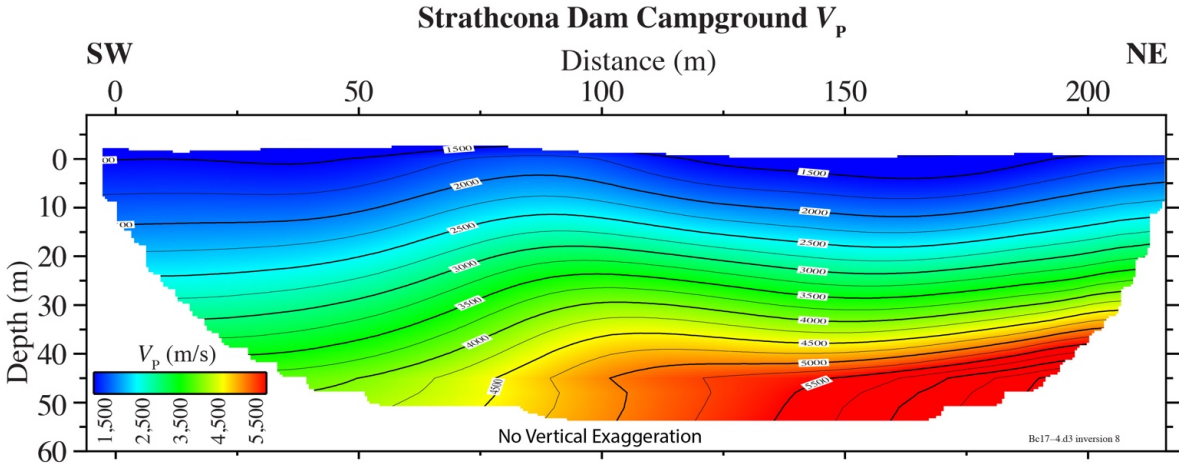

Figure 42. Diagram showing tomographic compressional-wave-velocity (V_P) model along the seismic profile for Strathcona Dam Campground, Vancouver Island, British Columbia, Canada (see fig. 6). The top of groundwater, as inferred by the 1,500 meter per second (m/s) velocity contour, is shown in white. SW, southwest; NE, northeast; m, meters.

Strathcona Dam Campground MAS$_L$W Model

We observed somewhat coherent dispersion curves along the Campground seismic profile from the Love-wave data (appendix 2; fig. 53) but not for the Rayleigh-wave data. As a result, using MAS$_L$W, we developed only a 2D V_S model along the Strathcona Campground seismic profile (fig. 43). Our MAS$_L$W V_S model suggests velocities ranging from about 400 m/s near the surface to about 1,900 m/s at about 60 m depth. Of the five seismic profiles evaluated in this report, the Strathcona Dam Campground profile has the least topographic relief and likely the least 3D complexities. Thus, the MAS$_L$W model may represent the velocity structure along the campground seismic profile reasonably

well. However, there are likely considerable lateral variations in V_S velocity structure, as suggested by the tomographic V_P model, which may affect parts of the MAS_LW model.

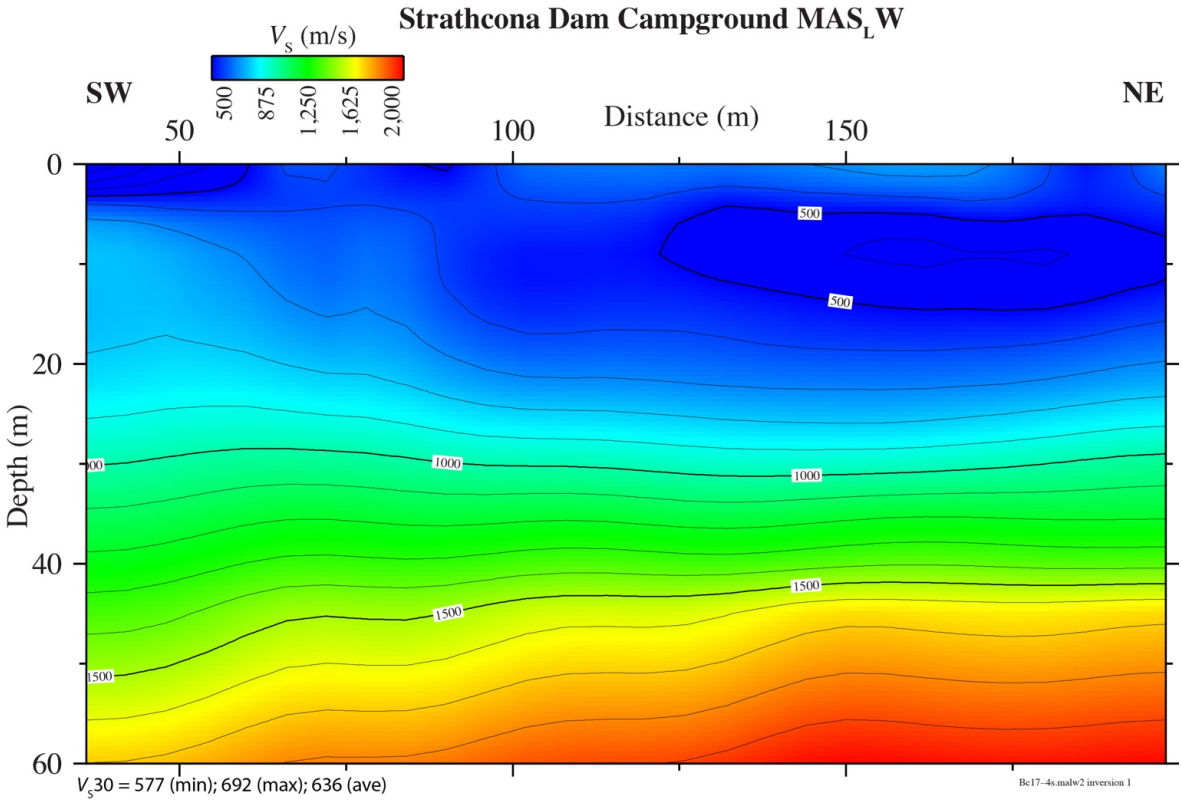

Figure 43. Diagram showing shear-wave-velocity (V_S) model along the seismic profile derived from multichannel analysis of surface waves using Love waves (MAS_LW) for Strathcona Dam Campground, Vancouver Island, British Columbia, Canada (see fig. 6). Lateral variations in time-averaged shear-wave velocity in the upper 30 meters (m) of the subsurface (V_{S30}) along the seismic profile (as inferred by MAS_LW modeling) range from a minimum of 577 meters per second (m/s) to a maximum of 692 m/s, with an average of 636 m/s. SW, southwest; NE, northeast; m, meters.

Strathcona Dam Campground V_{S30} Calculations and Models

From the MAS_LW V_S model (fig. 43), we calculated V_{S30} at each meter along the Strathcona Dam Campground seismic profile, and we found the maximum V_{S30} value to be 692 m/s, the minimum V_{S30} to be 577 m/s, and the average V_{S30} to be 636 m/s (appendix 4, table 12). We were not able to determine V_{S30} using the other analysis techniques.

Ambient Noise Model

We acquired passive-source data at each of the seismic acquisition sites at each dam. However, the passive-source dispersion curves were largely incoherent for all seismic sites except John Hart Dam (appendix 3, fig. 54). Passive data from the John Hart Dam profile provided partially coherent dispersion curves that infer shallow-depth V_S. On the basis of the passive-source data, V_{S30} at the John Hart Dam strong-motion station was calculated as 326 m/s, which is relatively low in comparison to

V_{S30} from the tomography model (577 m/s), the MAS_RW model (532 m/s), and the MAS_LW model (551 m/s).

Local and Regional Variation in Velocities

Seismic velocities (V_P and V_S) are highly variable in the Campbell River area due to variations in sediments, sedimentary rocks, and basement rocks. In the vicinity of the three dams where we acquired data, we found sediment thickness to be highly variable locally (~0 to 45 m thick), which greatly affected shallow (especially V_{S30}) velocities. However, we found that basement velocities were generally high, both with respect to V_P and V_S. V_P of basement rocks ranges from a minimum of about 1,500 m/s to a maximum of about 6,500 m/s in the upper 100 m, and V_S of basement rocks ranges from a minimum of about 800 m/s to a maximum of about 3,300 m/s in the upper 100 m.

V_S Acquisition and Evaluation Methods

On the basis of the data we acquired and evaluated from Vancouver Island, we suggest that the lithology and topographic variations render some methods less useful for evaluating V_S. In many locations, there is no or only a thin veneer of sediment or low-velocity materials overlying basement rocks, which consist largely of high-velocity basaltic and metamorphic rocks. In addition, some of the basement rocks may be layered, there are large lateral variations in velocity, and there are significant topographic variations. These conditions make it difficult to obtain good dispersion curves from the surface-wave data. As a result, evaluation methods such as MAS_RW, MAS_LW, and ambient noise frequently do not yield consistent 2D measures of V_S. In addition, the low signal-to-noise ratios of body-wave first arrivals, generated by low-power active sources (such as hammers), make it difficult to accurately measure first-arrival refractions, which could limit the applicability of tomographic methods. When using the tomographic method, the high velocities of basement rocks, combined with the relatively short lengths of the seismic profiles, require precise measurements of the first arrivals (few milliseconds). However, by applying higher power seismic sources (such as larger vertical and angled weight drops), high sampling rates, and shot stacking, we suggest that the tomography method can provide good measures of 2D variations in V_P and V_S in the Vancouver Island area.

References Cited

Aki, K., and Lee, W.H.K., 1976, Determination of three-dimensional velocity anomalies under a seismic array using P-arrival times from location earthquakes—I, A homogeneous initial model: Journal of Geophysical Research, v. 81, p. 4381–4399.

Atwater, B.F., Musumi-Rokkaku, S., Satake, K., Tsuji, Y., Ueda, K., and Yamaguchi, D.K., 2015, The orphan tsunami of 1700—Japanese clues to a parent earthquake in North America, 2nd ed.: Seattle, University of Washington Press, U.S. Geological Survey Professional Paper 1707, 135 p. [Also available at https://pubs.er.usgs.gov/publication/pp1707.]

BC Hydro, 2012a, Dam safety—Probabilistic seismic hazard analysis (PSHA) model volume 1—Methodology: British Columbia Hydro and Power Authority, Engineering Report E658, 124 p.

BC Hydro, 2012b, Dam safety—Probabilistic seismic hazard analysis (PSHA) model volume 2—Seismic Source Characterization (SSC)—Model: British Columbia Hydro and Power Authority, Engineering Report E658, WPR-3030.

BC Hydro, 2018, John Hart generation station replacement project site layout—Environmental and social considerations: British Columbia Hydro and Power Authority map, accessed December 14,

2018, at https://www.bchydro.com/content/dam/BCHydro/customer-portal/documents/projects/john-hart/john-hart-social-and-environmental-considerations-map.pdf.
Cardarelli, E., Cercato, M., and De Donno, G., 2014, Characterization of an earth-filled dam through the combined use of electrical resistivity tomography, P- and SH-wave seismic tomography, and surface wave data: Journal of Applied Geophysics, v. 106, p. 87–95.
Catchings, R.D., Goldman, M.R., Li, Y-G., and Chan, J.H., 2016, Continuity of the West Napa-Franklin Fault zone inferred from guided waves generated by earthquakes following the 24 August 2014 M_w 6.0 South Napa Earthquake: Bulletin of the Seismological Society of America, v. 106, p. 2721–2746, https://doi.org/10.1785/0120160154.
Catchings, R.D., Goldman, M.R., Trench, D., Buga, M., Chan, J.H., Criley, C.J., and Strayer, L.M., 2017, Shallow-depth location and geometry of the Piedmont Reverse splay of the Hayward Fault, Oakland, California: U.S. Geological Survey Open-File Report 2016–1123, 22 p., https://doi.org/10.3133/ofr20161123.
Catchings, R.D., Rymer, M.J., Goldman, M.R., Hole, J.A., Huggins, R., and Lippus, C., 2002, High-resolution seismic velocities and shallow structure of the San Andreas fault zone at Middle Mountain, Parkfield, California: Bulletin of the Seismological Society of America, v. 92, p. 2493–2503.
Catchings, R.D., Rymer, M.J., Goldman, M.R., Sickler, R.R., and Criley, C.J., 2014, A method and example of seismically imaging near-surface fault zones in geologically complex areas using V_P, V_S, and their ratios: Bulletin of the Seismological Society of America, v. 104, p. 1989–2006, https://doi.org/10.1785/0120130294.
Cormier, V.G., and Spudich, P., 1984, Amplification of ground motion and waveform complexity in fault zones—Examples form the San Andreas and Calaveras faults: Geophysical Journal of the Royal Astronomical Society, v. 79, p. 135–152.
Geosciences BC, 2013, Northern Vancouver Island project: Geosciences BC, geology map 2013-NVI-1-1, 1 sheet, scale 1:500,000, accessed December 18, 2018, at http://cdn.geosciencebc.com/pdf/Maps/NVI/NVI-1-1_geology.pdf.
Goldfinger, C., Hans Nelson, C., Morey, A.E., Johnson, J.E., Patton, J.R., Karabanov, E., Gutiérrez-Pastor, J., Eriksson, A.T., Gràcia, E., Dunhill, G., Enkin, R.J., Dallimore, A., and Vallier, T., 2012, Turbidite event history—Methods and implications for Holocene paleoseismicity of the Cascadia Subduction Zone, U.S. Geological Survey Professional Paper 1661–F, 184 p. [Also available at https://pubs.usgs.gov/pp/pp1661f/.]
Goldman, M.R., Catchings, R.D., Addo, K.O., Chan, J.H., Criley, C.J., and Sickler, R.R., 2018, 2017 U.S. Geological Survey/BC Hydro seismic data recorded at three dam sites on Vancouver Island, British Columbia, Canada: U.S. Geological Survey data release, https://doi.org/10.5066/P9PRGZ53.
Hayashi, K., 2008, Development of surface wave methods and its application to site investigations: Kyoto, Japan, Kyoto University, Ph.D. dissertation, 304 p., https://doi.org/10.14989/doctor.k13774.
Hayashi, K., and Suzuki, H., 2004, CMP cross-correlation analysis of multichannel surface-wave data: Exploration Geophysics, v. 35, p. 7–13, https://doi.org/10.1071/EG04007.
Healy, J., and Peake, L., 1975, Seismic velocity structure along a section of the San Andreas fault near Bear Valley, California: Bulletin of the Seismological Society of America, v. 65, p. 1177–1197.
Hole, J.A., 1992, Nonlinear high-resolution three-dimensional seismic traveltime tomography: Journal of Geophysical Research, v. 97, p. 6553–6562
Hu, Y., Xia, J., Mi, B., Cheng, F., and Shen, C., 2018, A pitfall of muting and removing bad traces in surface-wave analysis: Journal of Applied Geophysics, v. 153, p. 136–142.
Hyndman, R.D., 1979, Poisson's ratio in oceanic crust—A review, *in* Keen, C.E., ed., Crustal properties across passive margins: Tectonophysics, v. 59, p. 321–333.

Ivanov, J., Johnson, C.D., Lane, J.W., Miller, R.D., and Clemens, D., 2009, Near-surface evaluation of Ball Mountain Dam, Vermont, using multichannel analysis of surface waves (MASW) and refraction tomography seismic methods on land-streamer data: 2009 Society of Exploration Geophysicists Annual Meeting, October, 25–30, 2009, Houston Texas, Technical Program Expanded Abstracts 2009, p. 1454–1458, https://doi.org/10.1190/1.3255123.

Ivanov, J., Miller, R.D., Feigenbaum, D., Morton, S.L.C., Peterie, S.L., and Dunbar, J.B., 2017, Revisiting levees in southern Texas using Love-wave multichannel analysis of surface waves with the high-resolution linear Radon transform: Interpretation, v. 5, no. 3, p. T287–T298, https://doi.org/10.1190/INT-2016-0044.1.

Jarchow, C.M., Catchings, R.D., and Lutter, W.J., 1994, Large-explosive source, wide-recording aperture, seismic profiling on the Columbia Plateau, Washington: Geophysics, v. 59, p. 259–271.

Johnston, J.E., and Christensen, N.I., 1997, Seismic properties of layer 2 basalts: Geophysics Journal International, v. 128, p. 285–300.

Karl, L., Fechner, T., Schevenels, M., Francois, S., and Degrande, G., 2011, Geotechnical characterization of a river dyke by surface waves: Near Surface Geophysics, v. 9, p. 515–527.

Kim, D-S., Yoon, J-K., Lee, B-S., Park, H-C., 2001, Numerical studies for the application of the SASW method in an inclined soil layer: Journal of the Korean Geotechnical Society, v. 17, p.77– 84 [in Korean].

Lawrence, M., McCann, M., Ostenaa, D., Wong, I., Unruh, J., Hanson, K., Olig, S., Clague, J., LaForge, R., Lettis, W., Swan, B., Zachariasen, J., Youngs, R., and Addo, K., 2014, The BC Hydro SSHAC level 3 seismic source model: Earthquake Engineering Research Institute, Proceedings of the 10th National Conference on Earthquake Engineering, Anchorage, Alaska, 12 p.

Li, Y-G., Catchings, R.D., and Goldman, M.R., 2016, Subsurface fault damage zone of the 2014 M_w 6.0 South Napa, California, earthquake viewed from fault-zone trapped waves: Bulletin of the Seismological Society of America, v. 106, no. 6, 2747, https://doi.org/10.1785/0120160039.

Lou, J.K., Byrne, P.M., Garner, S.J., and Marcuson, W.F., III, 1991, Assessment of seismic stability of Dolphin Pool Slope of John Hart Dam: Missouri University of Science and Technology, Second International Conferences on Recent Advances in Geotechnical Earthquake Engineering and Soil Dynamics, session 7/5, March 11–15, 1991, accessed December 18, 2018, at http://scholarsmine.mst.edu/icrageesd/02icrageesd/session07/5.

Martin, A., Yong, A., Stephenson, W., Boatwright, J., and Diehl, J., 2017, Geophysical characterization of seismic station sites in the United States—The importance of a flexible, multi-method approach: Proceedings of the 16th World Conference on Earthquake Engineering, Santiago, Chile, January 9–13, 2017, paper no. 2160.

McCann, M.W., Jr., Addo, K., Lawrence, M., 2014, BC Hydro SSHAC level 3 study methodology: Earthquake Engineering Research Institute, Proceedings of the 10th National Conference on Earthquake Engineering, Anchorage, Alaska, 12 p.

Mayer-Rosa, D., 1973, Traveltime anomalies and distribution of earthquakes along the Calaveras fault zone, California: Bulletin of the Seismological Society of America, v. 72, p. 901–910.

Miller, R.D., Xia, J., Park, C.B., Ivanov, J.M., 1999, Multichannel analysis of surface waves to map bedrock. The Leading Edge, v. 18, p. 1392–1396.

Min, D-J. and Kim, H-S., 2006, Feasibility of the surface-wave method for the assessment of physical properties of a dam using numerical analysis: Journal of Applied Geophysics, v. 59, p. 236–243.

Mooney, W.D., and Ginzburg, A., 1986, Seismic measurements of the internal properties of fault zones: Pure Applied Geophysics, v. 124, p. 141–157.

Natural Resources Canada, 2018, Earthquakes Canada: Natural Resources Canada website, accessed December 18, 2018, at http://www.earthquakescanada.nrcan.gc.ca/index-en.php.
Park, C.B., Miller, R.D., and Xia, J., 1999, Multichannel analysis of surface waves: Geophysics, v. 64, no. 3, p. 800–808.
Pegah, E., and Liu, H., 2016, Application of near-surface refraction tomography and multichannel analysis of surface waves for geotechnical site characterizations—A case study: Engineering Geology, v. 208, p. 100–113.
Odum, J.K., Williams, R.A., Stephenson, W.J., and Worley, D.M., 2003, Near-surface S-wave and P-wave seismic velocities of primary geological formations of the Piedmont and Atlantic Coastal Plain of South Carolina, USA: U.S. Geological Survey Open-File Report 03–043, 23 p., accessed December 18, 2018, at https://pubs.usgs.gov/of/2003/ofr-03-043/.
Rogers, G.C., and Hasegawa, H.S., 1978, A second look at the British Columbia earthquake of June 23, 1946: : Bulletin of the Seismological Society of America, v. 68, p. 653–675.
Satake, K., Shimazaki, K., Tsuji, Y., and Ueda, U., 1996, Time and size of a giant earthquake in Cascadia inferred from Japanese tsunami records of January 1700: Nature, v. 379, p. 246–249.
Spudich, P., and Angstman, B., 1980, Lateral variations in velocity and Q structure in the region of the 1979 Coyote Lake, California, earthquake: Earthquake Notes, v. 50, p. 64.
Yamaguchi, D.K., Atwater, B.F., Bunker, D.E., Benson, B.E., and Reid, M.S., 1997, Tree-ring dating the 1700 Cascadia earthquake: Nature, v. 389, p. 922–923.
Yong, A., Martin, A., Stokoe, K., and Diehl, J., 2013, ARRA-funded V_{S30} measurements using multi-technique approach at strong-motion stations in California and central-eastern United States: U.S. Geological Survey Open-File Report 2013–1102, 60 p. and data files, accessed December 18, 2018, at https://pubs.usgs.gov/of/2013/1102/.
Wang, C.Y., Lin, W., and Wu, F.T., 1978, Constitution of the San Andreas fault zone at depth: Geophysical Research Letters, v. 5, p. 741–744.
Xia, J., Miller, R.D., and Park, C.B., 1999, Estimation of near-surface shear-wave velocity by inversion of Rayleigh waves: Geophysics, v. 64, p. 691–700.
Xia, J., Miller, R.D., Park, C.B., Hunter, J.A., Harris, J.B., and Ivanov, J., 2002, Comparing shear-wave velocity profiles inverted from multichannel surface wave with borehole measurements: Soil Dynamics and Earthquake Engineering, v. 22, p. 181–190.
Xia J, Xu Y, Luo Y, Miller R D, Cakir R., and Zeng, C., 2012, Advantages of using multichannel analysis of Love waves (MALW) to estimate near-surface shear-wave velocity: Surveys in Geophysics, p. 841–860.
Xia, J., 2014, Estimation of near-surface shear-wave velocities and quality factors using multichannel analysis of surface-wave methods: Journal of Applied Geophysics, v. 103, p. 140–151.
Yuan, J., 2011, Field Studies Comparing SASW, Beamforming, and MASW Test methods and characterization of geotechnical materials based on V_S: University of Texas at Austin, Ph.D. dissertation, 296 p.
Zeng, C., Xia, J., Miller, R.D., Tsoflias, G.P., and Wang, Z., 2012, Numerical investigation of MASW applications in presence of surface topography: Journal of Applied Geophysics, v. 84, p. 50–52.
Zhang, J.J., and Bentley, L.R., 2005, Factors determining Poisson's ratio: CREWES Research Report, v 17, p. 1–15, accessed December 18, 2018, at https://pdfs.semanticscholar.org/bcfd/3d741eb1b639965f388bc97443f436ed7022.pdf.

Appendix 1—Shot Gathers for the Seismic Profiles

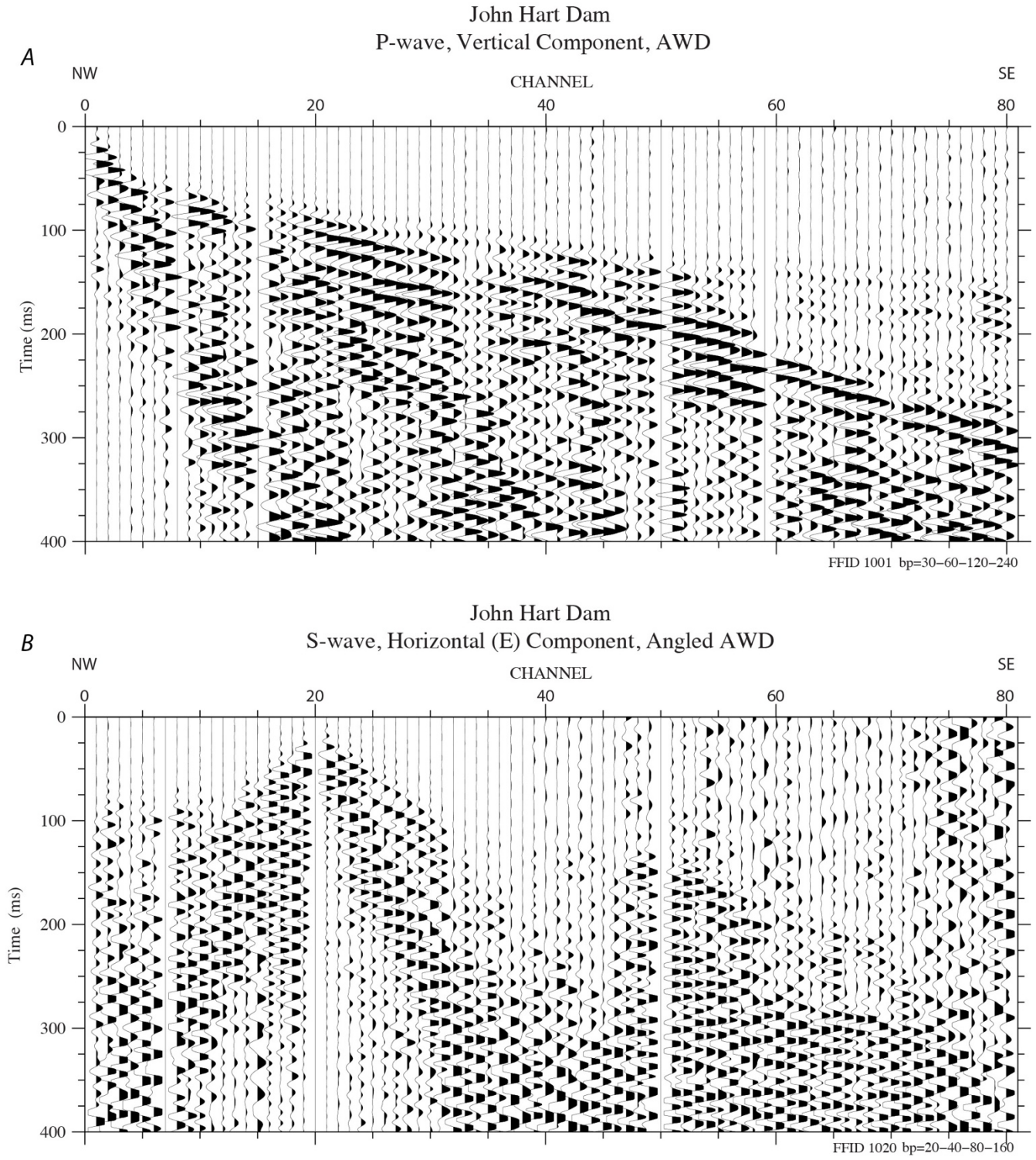

Figure 44. Diagram showing example shot gathers from the seismic profile for John Hart Dam, Vancouver Island, British Columbia, Canada. *A*, P-wave shot point near the northwestern end of the seismic profile. *B*, S-wave shot point near the northwestern end of profile. NW, northwest; SE, southeast; ms, milliseconds.

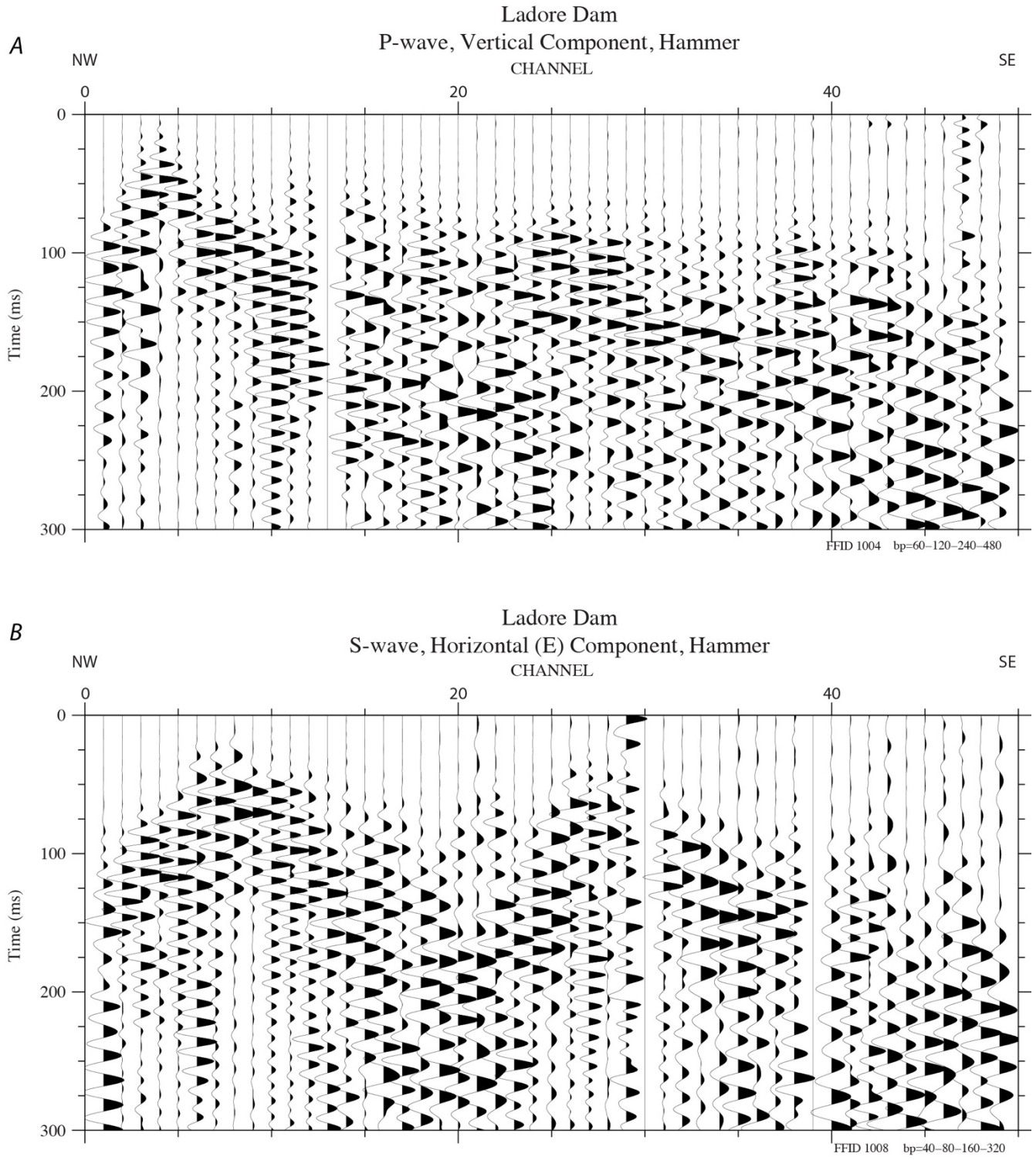

Figure 45. Diagram showing example shot gathers from the seismic profile for Ladore Dam, Vancouver Island, British Columbia, Canada. *A*, P-wave shot point near the northwestern end of the seismic profile. *B*, S-wave shot point near the northwestern end of profile. NW, northwest; SE, southeast; ms, milliseconds.

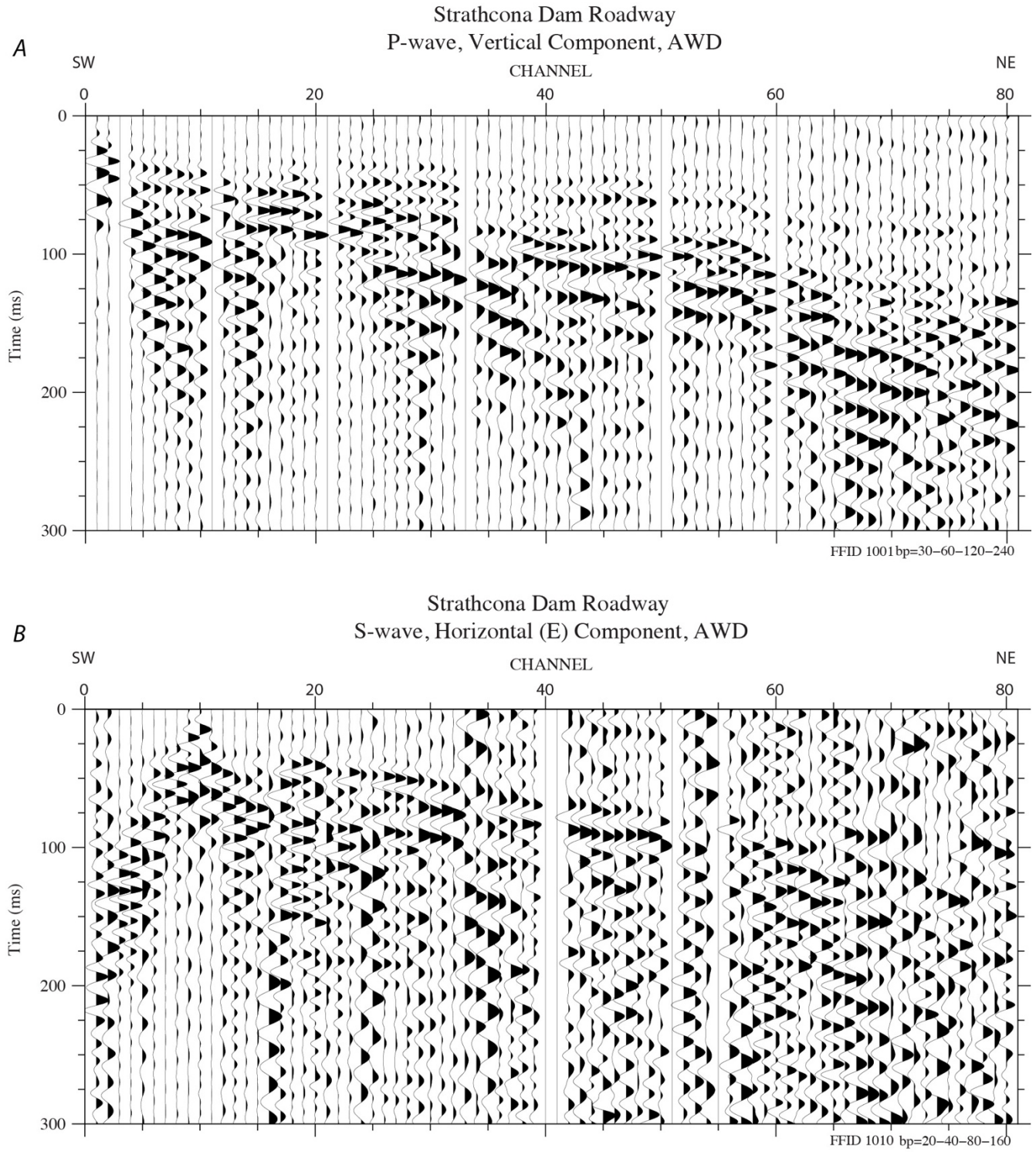

Figure 46. Diagram showing example shot gathers from the seismic profile for Strathcona Dam Roadway, Vancouver Island, British Columbia, Canada. *A*, P-wave shot point near the southwestern end of the seismic profile. *B*, S-wave shot point near the southwestern end of profile. SW, southwest; NE, northeast; ms, milliseconds.

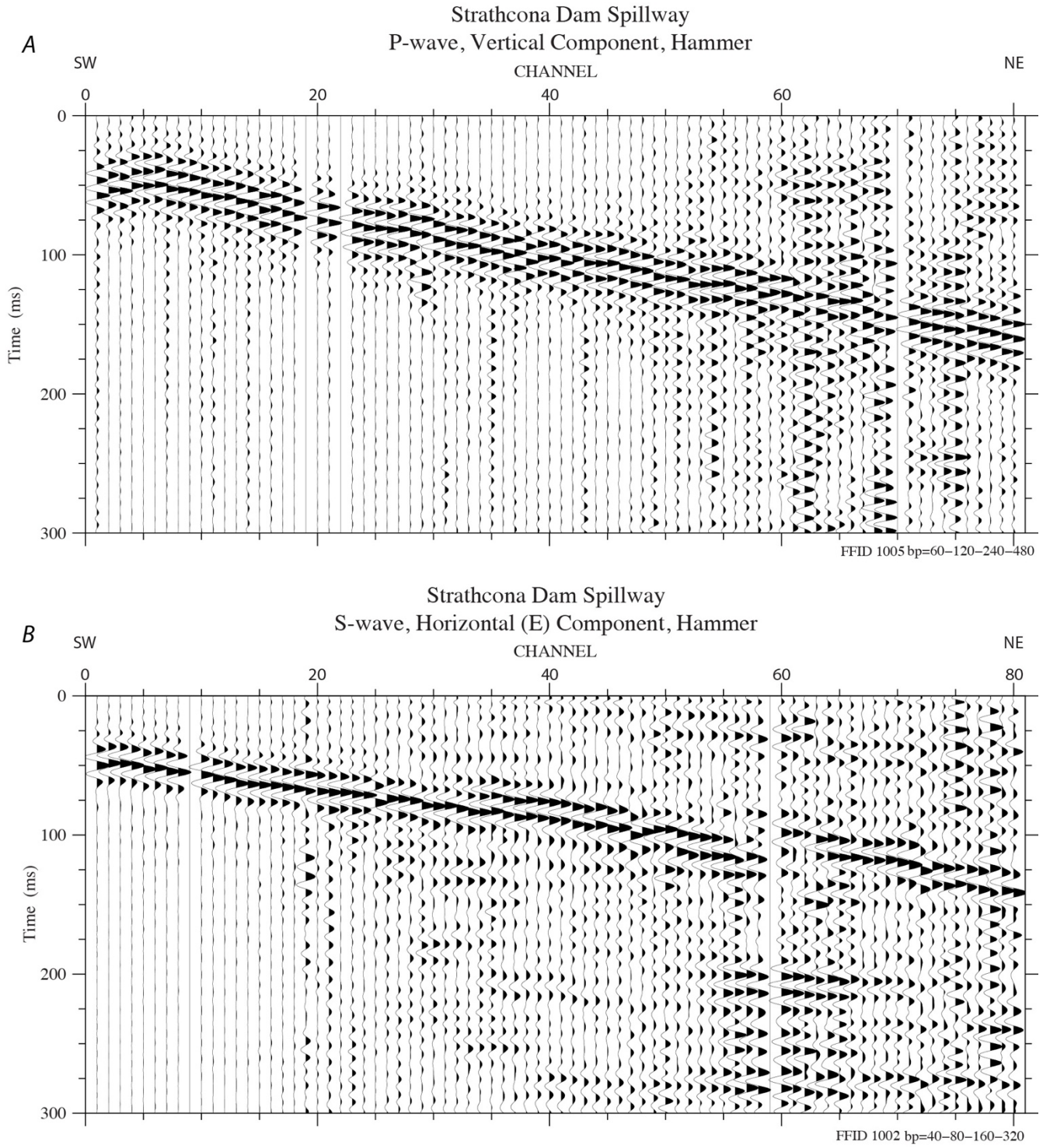

Figure 47. Diagram showing example shot gathers from the seismic profile for Strathcona Dam Spillway, Vancouver Island, British Columbia, Canada. *A*, P-wave shot point at the southwestern end of the seismic profile. *B*, S-wave shot point at the southwestern end of profile. SW, southwest; NE, northeast; ms, milliseconds.

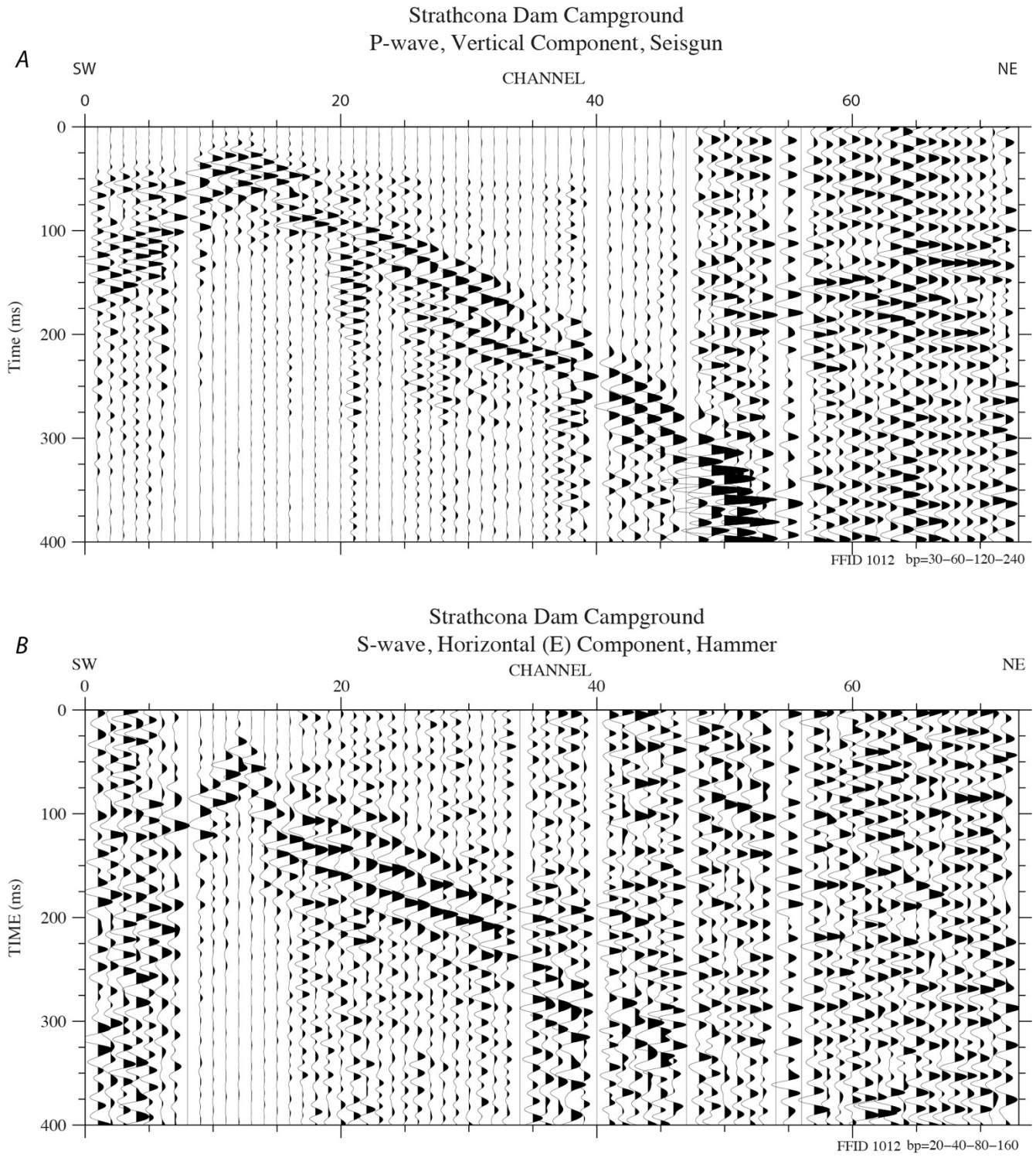

Figure 48. Diagram showing example shot gathers from the seismic profile for Strathcona Dam Campground, Vancouver Island, British Columbia, Canada. *A*, P-wave shot point at the southwestern end of the seismic profile. *B*, S-wave shot point at the southwestern end of profile. SW, southwest; NE, northeast; ms, milliseconds.

Appendix 2—MAS_RW/MAS_LW Dispersion Curves

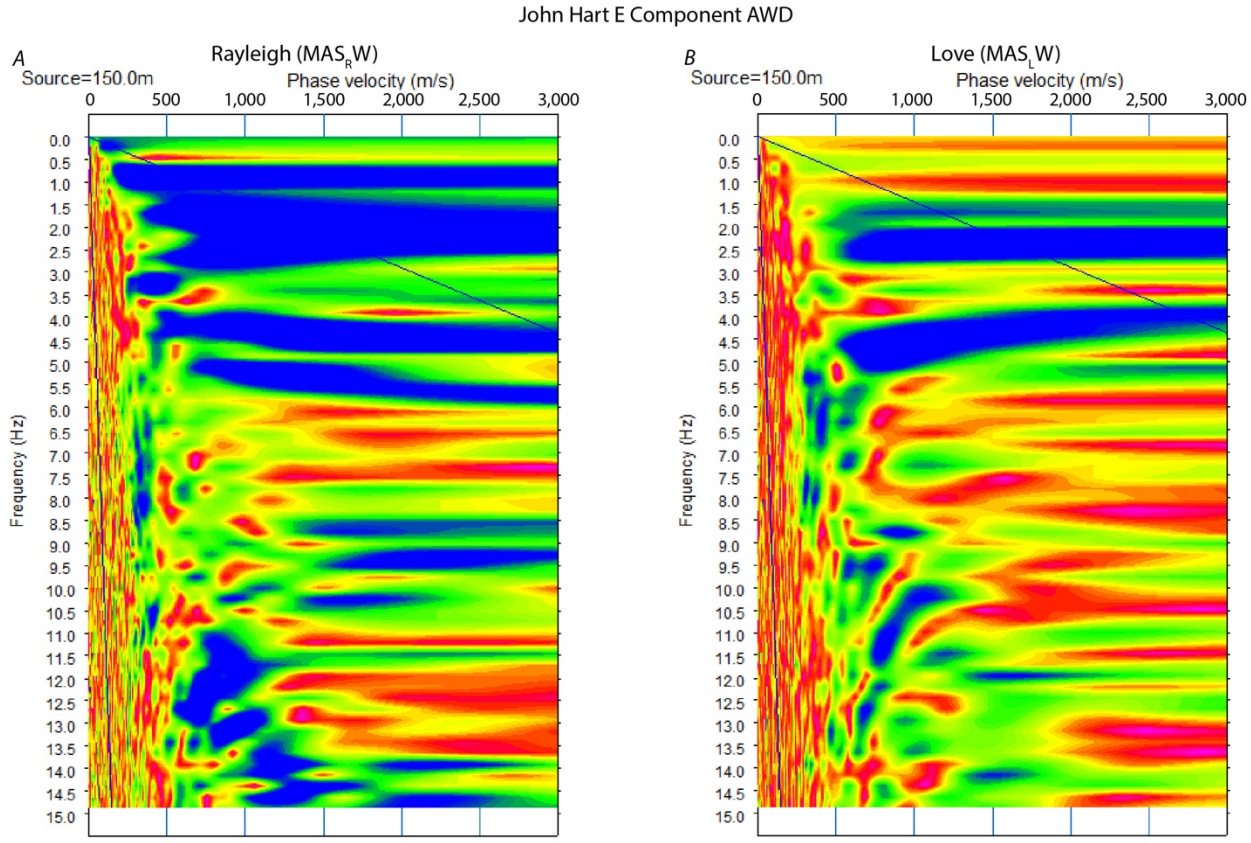

Figure 49. Diagram showing surface-wave dispersion curves from the seismic profile for John Hart Dam, Vancouver Island, British Columbia, Canada. *A*, Rayleigh wave dispersion curve. *B*, Love-wave dispersion curve. E component AWD, east component of accelerated weight drop; Hz, hertz; m, meters; ms, milliseconds.

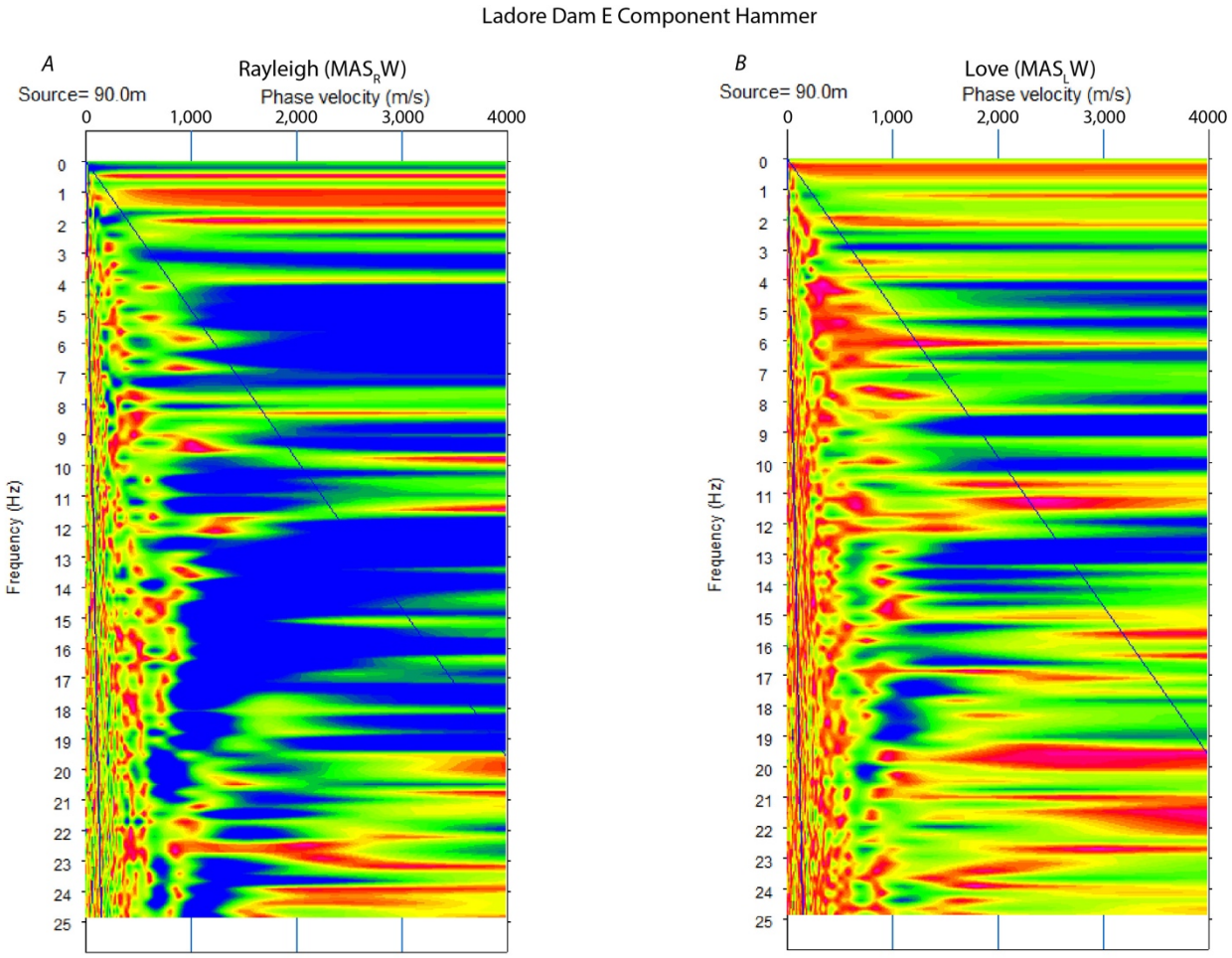

Figure 50. Diagram showing surface-wave dispersion curves from the seismic profile for Ladore Dam, Vancouver Island, British Columbia, Canada. *A*, Rayleigh wave dispersion curve. *B*, Love-wave dispersion curve. E component hammer, east component of hammer; Hz, hertz; m, meters; ms, milliseconds.

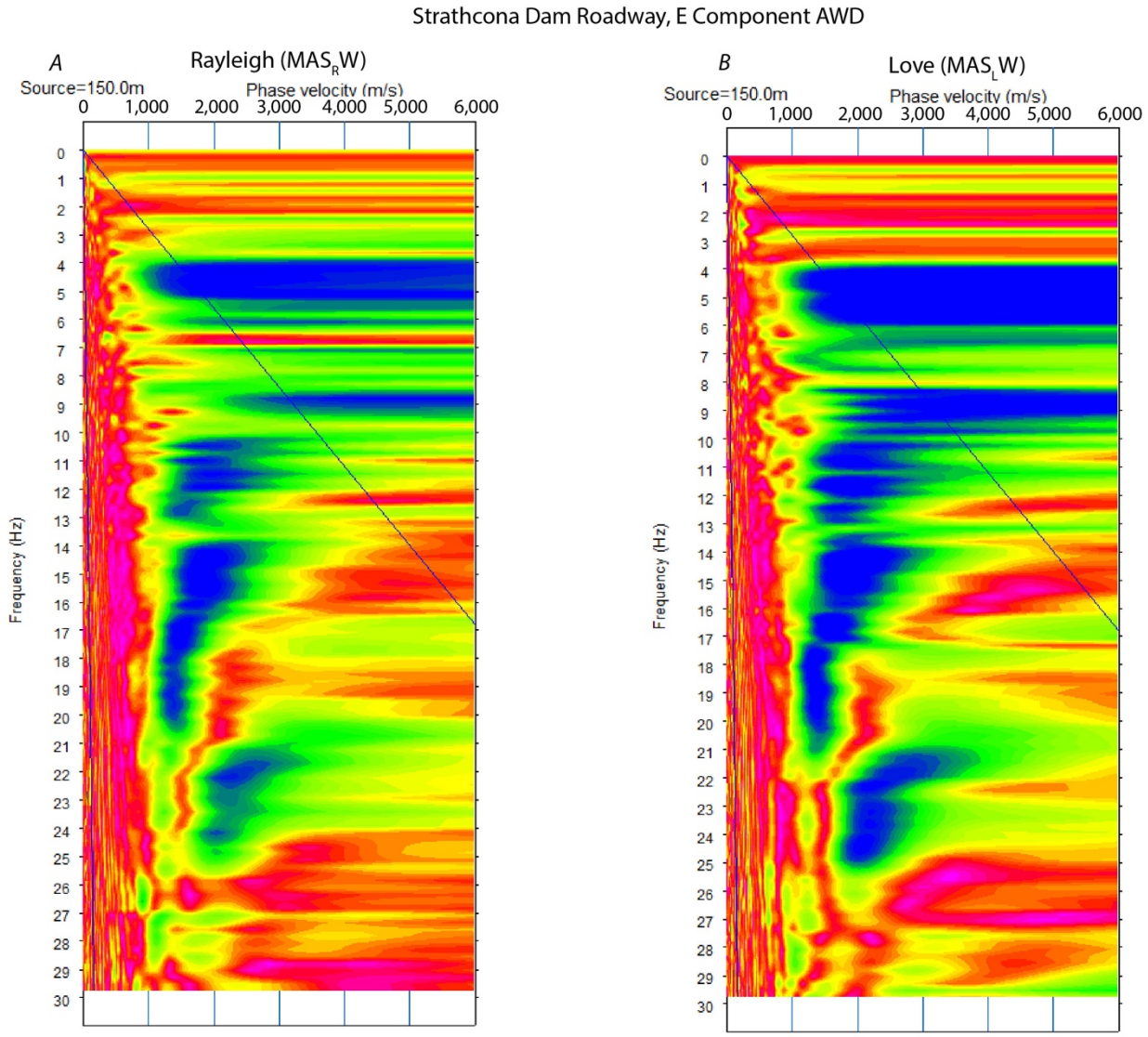

Figure 51. Diagram showing surface-wave dispersion curves from the seismic profile for Strathcona Dam Roadway, Vancouver Island, British Columbia, Canada. *A*, Rayleigh wave dispersion curve. *B*, Love-wave dispersion curve. E component AWD, east component of accelerated weight drop; Hz, hertz; m, meters; ms, milliseconds.

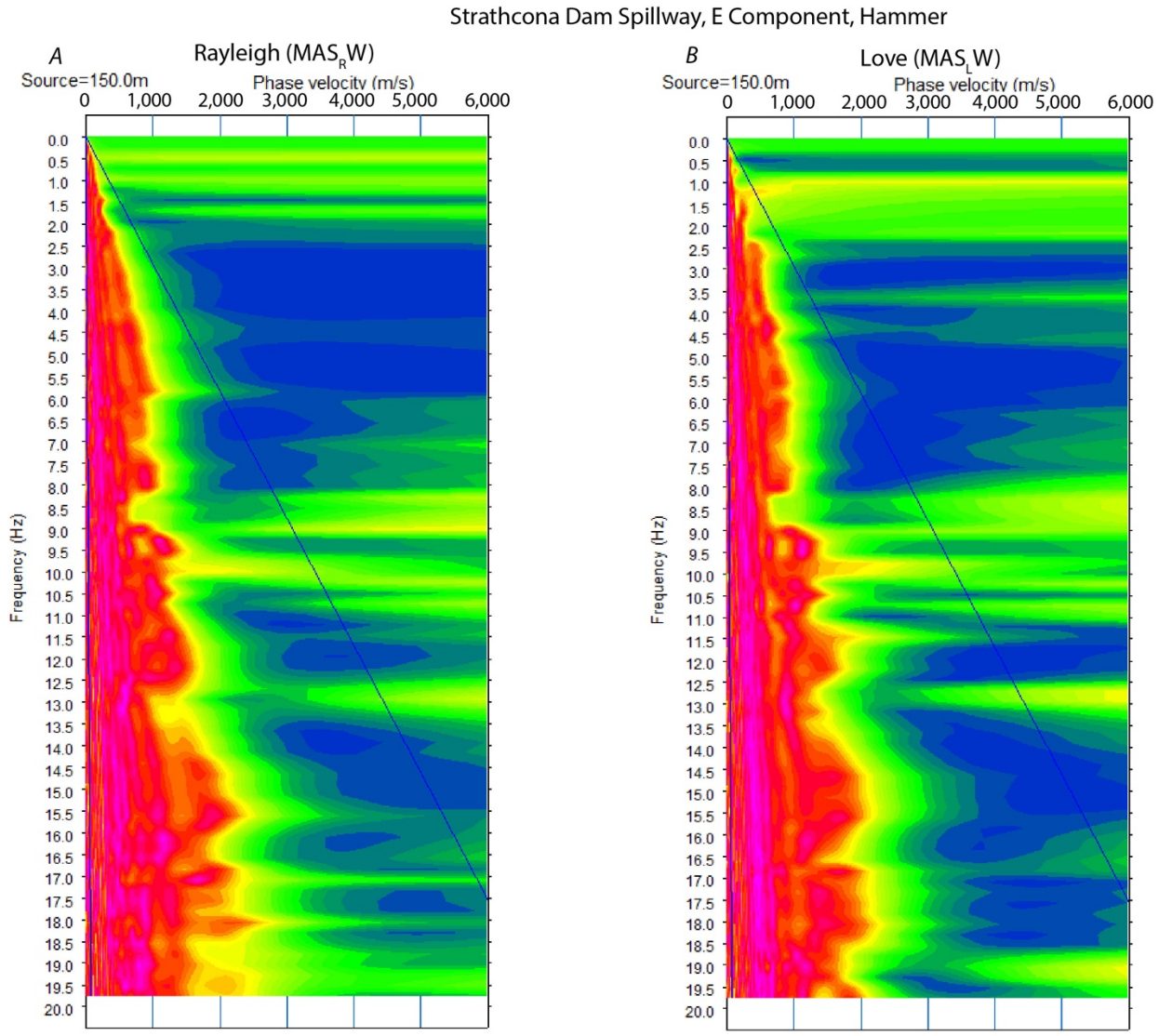

Figure 52. Diagram showing surface-wave dispersion curves from the seismic profile for Strathcona Dam Spillway, Vancouver Island, British Columbia, Canada. *A*, Rayleigh wave dispersion curve. *B*, Love-wave dispersion curve. E component hammer, east component of hammer; Hz, hertz; m, meters; ms, milliseconds.

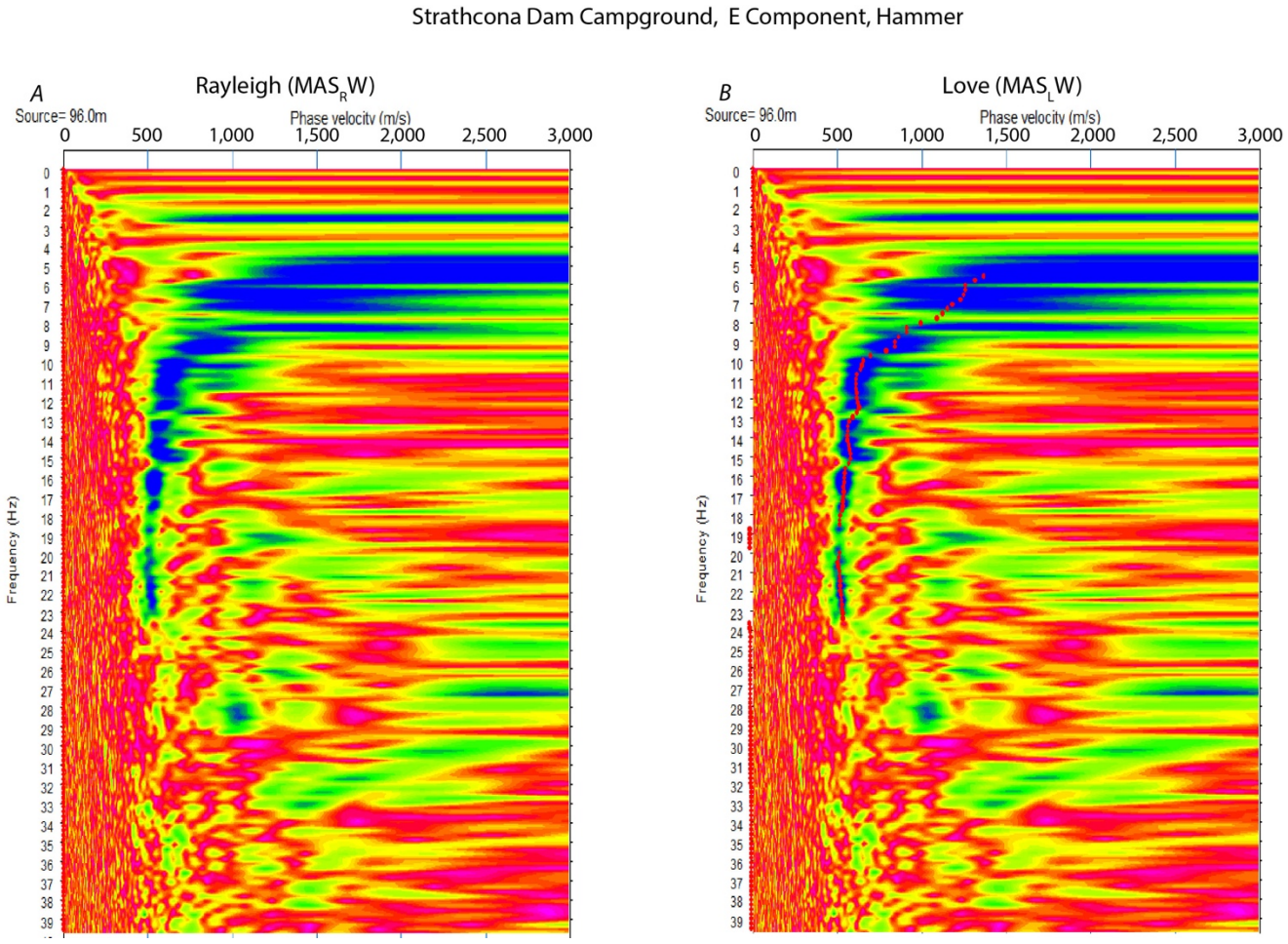

Figure 53. Diagram showing surface-wave dispersion curves from the seismic profile for Strathcona Dam Campground, Vancouver Island, British Columbia, Canada. *A*, Love-wave dispersion curve. *B*, Picked Love-wave dispersion curve. E component hammer, east component of hammer; Hz, hertz; m, meters; ms, milliseconds.

Appendix 3—Ambient-Noise (Passive-Source) Dispersion Curves

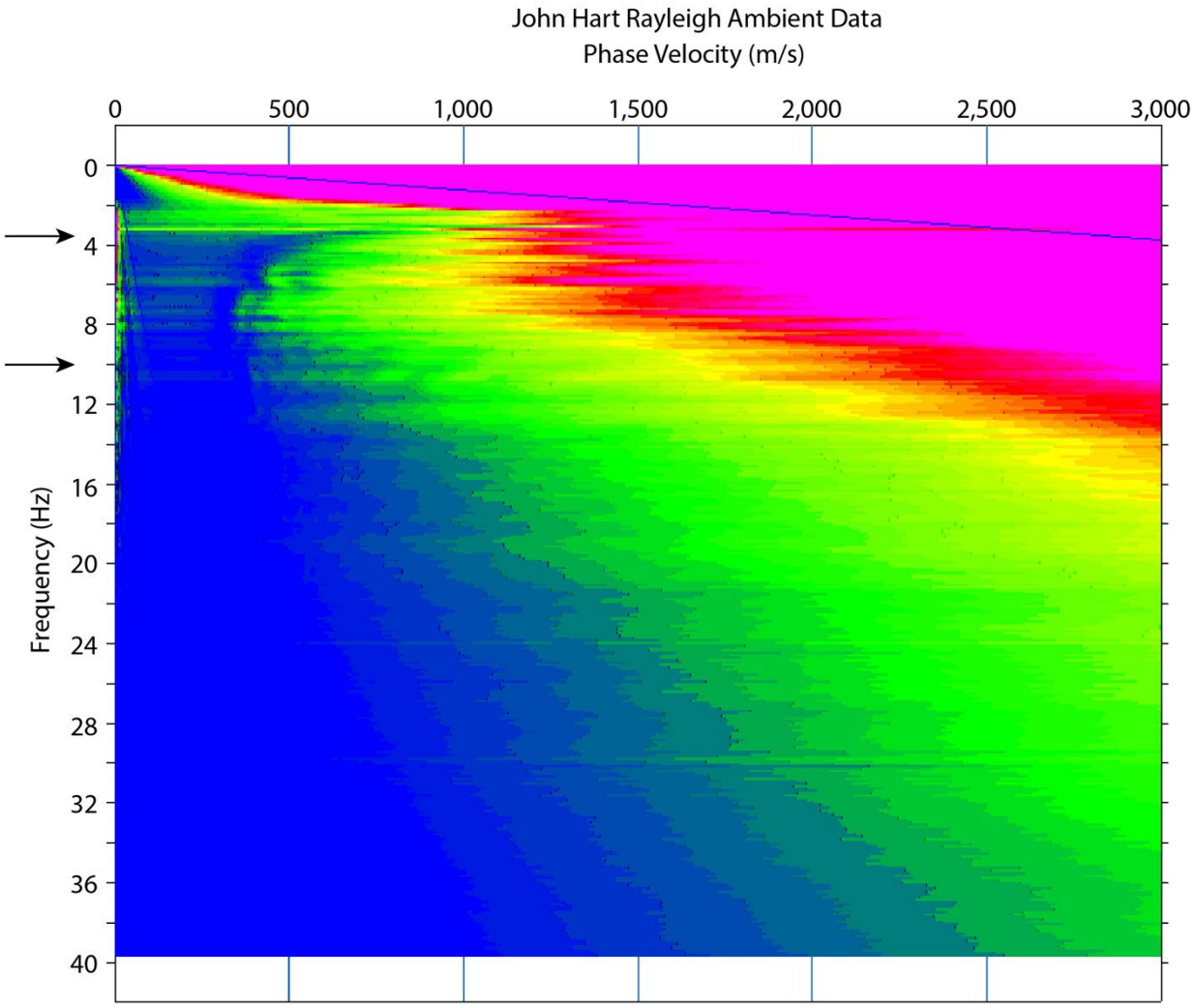

Figure 54. Diagram showing ambient-noise surface-wave dispersion curves from the seismic profile for John Hart Dam, Vancouver Island, British Columbia, Canada. Rayleigh wave dispersion curves (linear array). Hz, hertz; ms, milliseconds.

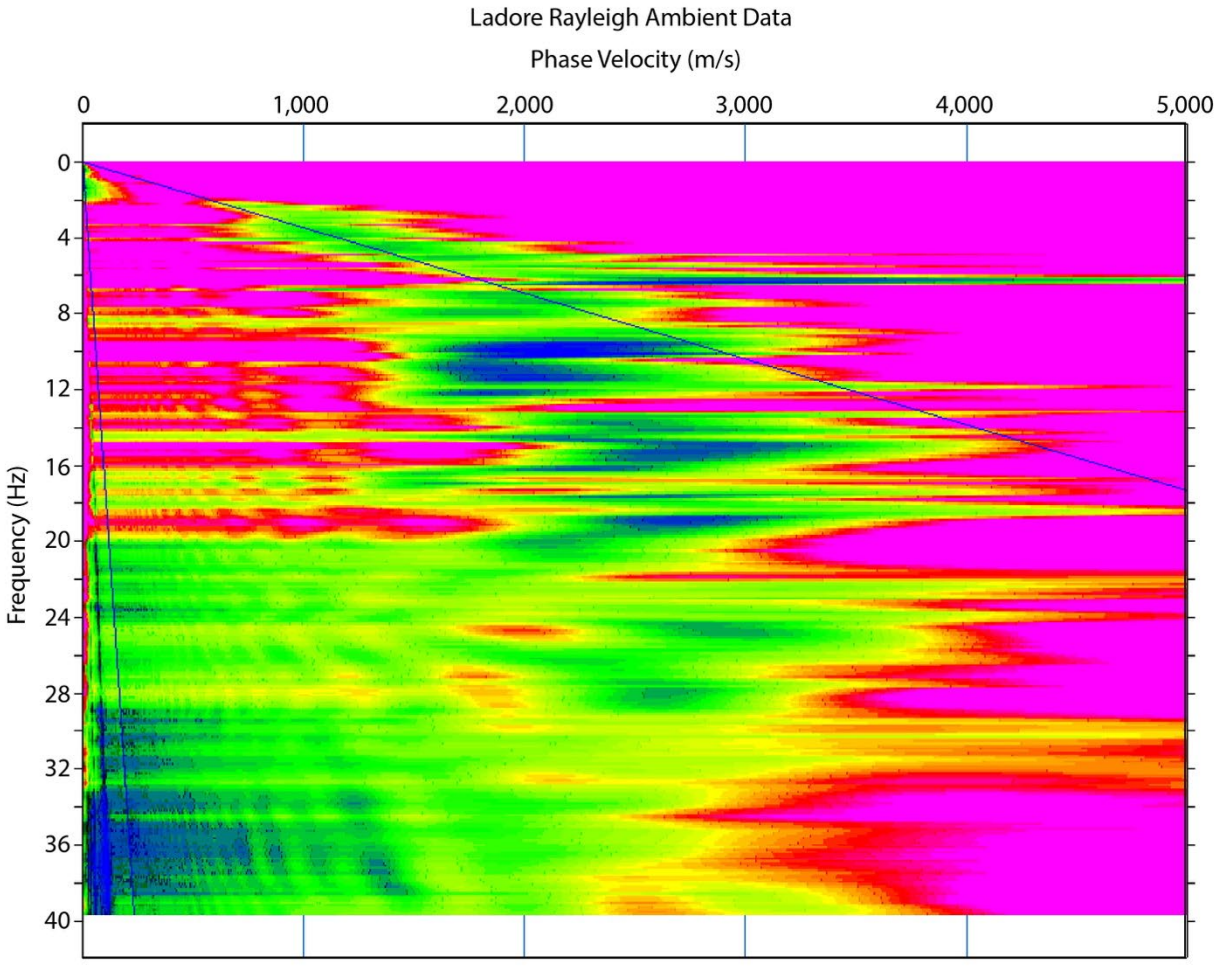

Figure 55. Diagram showing ambient-noise surface-wave dispersion curves from the seismic profile for Ladore Dam, Vancouver Island, British Columbia, Canada. Rayleigh wave dispersion curves (triangular array). Hz, hertz; ms, milliseconds.

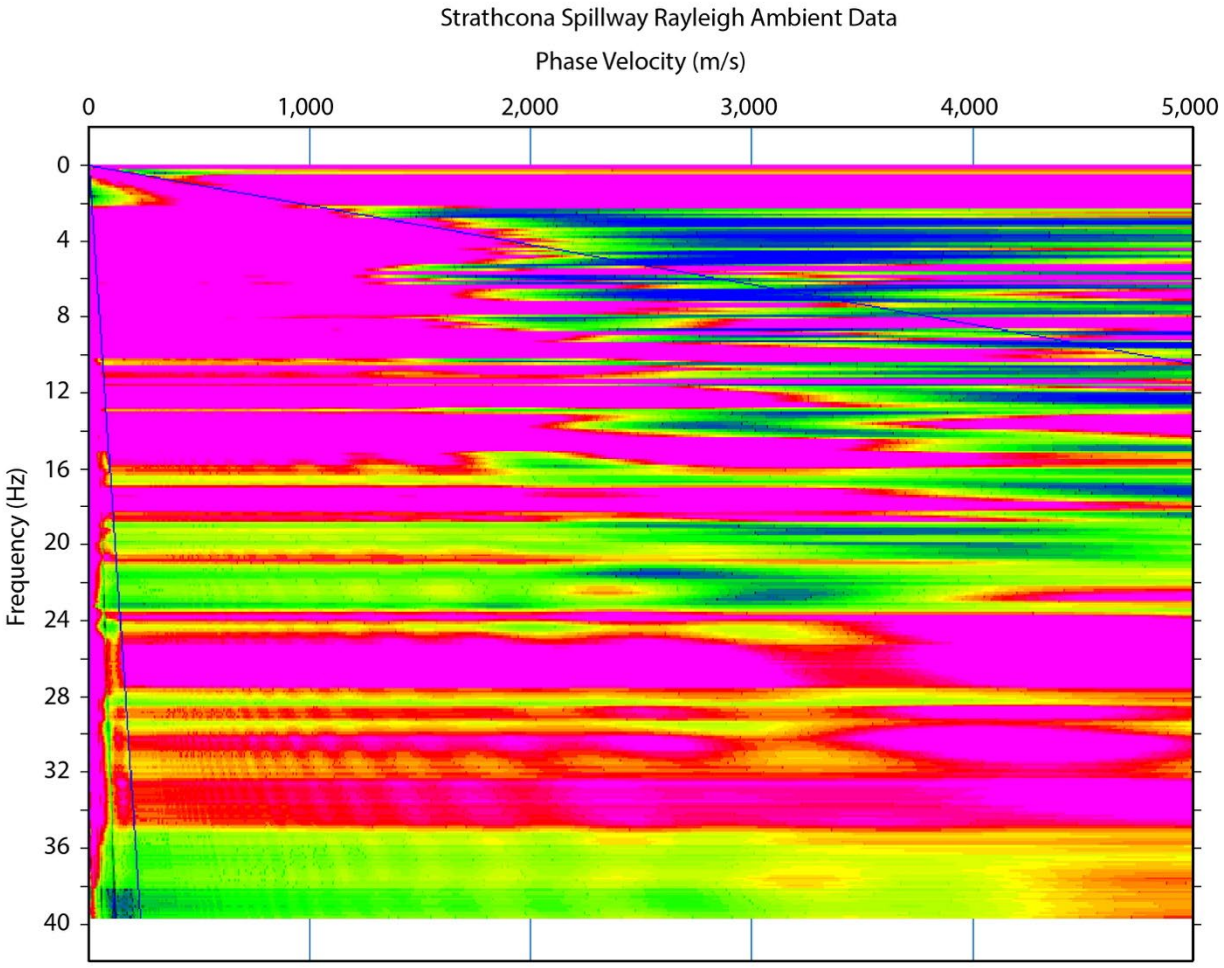

Figure 56. Diagram showing ambient-noise surface-wave dispersion curves from the seismic profile for Strathcona Dam Spillway, Vancouver Island, British Columbia, Canada. Rayleigh wave dispersion curves (linear array). Hz, hertz; ms, milliseconds.

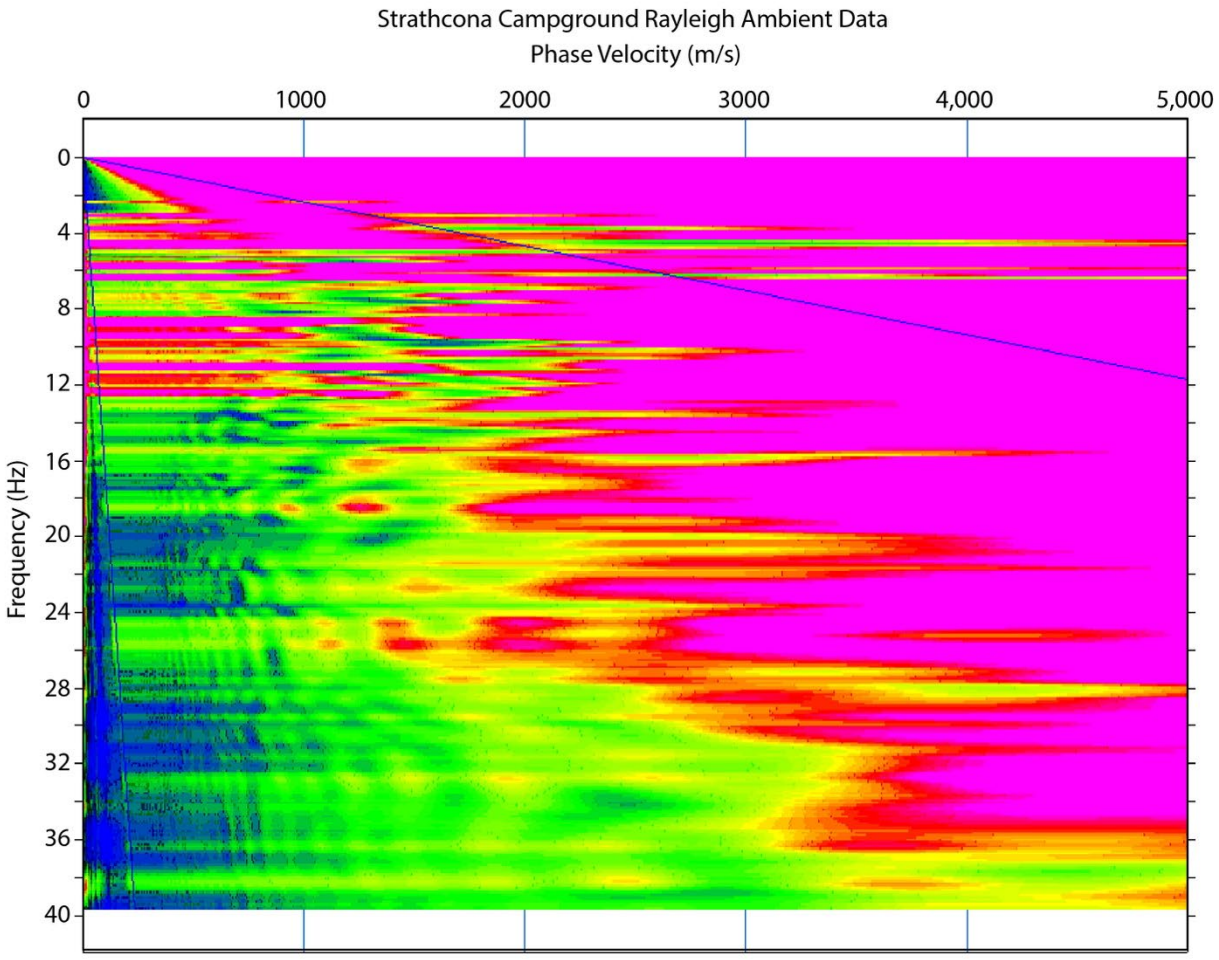

Figure 57. Diagram showing ambient-noise surface-wave dispersion curves from the Strathcona Dam Campground seismic profile for Strathcona Dam Campground, Vancouver Island, British Columbia, Canada. Rayleigh wave dispersion curves (triangular array). Hz, hertz; ms, milliseconds.

Appendix 4—Tables of V_{S30} Values

Table 1. Tomographically determined time-averaged shear-wave velocity in the upper 30 meters of the subsurface (V_{S30}) values along the John Hart Dam seismic profile, Vancouver Island, British Columbia, Canada.

Distance, in meters	Top and bottom, in meters	Number of layers	V_{S30}, in meters per second
–10	–0.79–29.21	0	0
–5	–1.18–28.82	0	0
0	–1.58–28.42	0	0
5	–1.98–28.02	0	0
10	–2.51–27.49	300	917
15	–3.09–26.91	300	862
20	–3.68–26.32	300	806
25	–3.98–26.02	300	763
30	–4.30–25.70	300	730
35	–4.49–25.51	300	709
40	–4.69–25.31	300	691
45	–4.60–25.40	300	679
50	–4.60–25.40	300	669
55	–4.69–25.31	300	658
60	–4.69–25.31	300	650
65	–4.79–25.21	300	641
70	–4.69–25.31	300	633
75	–4.69–25.31	300	626
80	–4.69–25.31	300	618
85	–4.69–25.31	300	612
90	–4.60–25.40	300	608
95	–4.48–25.52	300	605
100	–4.39–25.61	300	601
105	–4.30–25.70	300	597
110	–4.39–25.61	300	590
115	–4.48–25.52	300	583
120	–4.60–25.40	300	574
125	–4.69–25.31	300	564
130	–4.79–25.21	300	555
135	–4.79–25.21	300	547
140	–4.79–25.21	300	540
145	–4.79–25.21	300	533
150	–4.80–25.20	300	526
155	–4.89–25.11	300	519
160	–5.02–24.98	300	513
165	–5.19–24.81	300	508
170	–5.31–24.69	300	505
175	–5.40–24.60	300	504
180	–5.45–24.55	300	504
185	–5.25–24.75	300	509
190	–5.04–24.96	300	513
195	–4.78–25.22	300	521
200	–4.43–25.57	300	530
205	–4.22–25.78	300	537
210	–3.94–26.06	300	544
215	–3.78–26.22	300	549
220	–3.85–26.15	300	551
225	–4.10–25.90	300	549
230	–4.30–25.70	300	548
235	–4.83–25.17	300	542

Distance, in meters	Top and bottom, in meters	Number of layers	V_{S30}, in meters per second
240	–5.39–24.61	300	538
245	–5.83–24.17	300	535
250	–6.44–23.56	300	529
255	–7.03–22.97	300	521
260	–7.10–22.90	300	517
265	–6.71–23.29	300	517
270	–6.33–23.67	300	515
275	–6.03–23.97	300	511
280	–5.77–24.23	300	506
285	–5.70–24.30	300	500
290	–5.72–24.28	300	495
295	–5.81–24.19	300	490
300	–5.98–24.02	300	487
305	–6.10–23.90	300	487
310	–5.97–24.03	300	491
315	–5.97–24.03	300	492
320	–5.98–24.02	300	492
325	–6.18–23.82	300	484
330	–5.95–24.05	300	480
335	–5.68–24.32	300	475
340	–5.29–24.71	300	471
345	–4.85–25.15	300	472
350	–4.36–25.64	300	472
355	–3.68–26.32	300	474
360	–3.07–26.93	300	475
365	–2.48–27.52	300	477
370	–1.87–28.13	300	478
375	–1.47–28.53	300	473
380	–1.09–28.91	300	465
385	–0.66–29.34	0	0
390	–0.26–29.74	0	0
395	0.08–30.08	0	0
400	0.42–30.42	0	0
405	0.76–30.76	0	0
Minimum			465
Maximum			917
Average			559
Model Range, in meters			10–380

Table 2. Multichannel analysis of surface waves for Rayleigh waves (MAS_RW)-determined time-averaged shear-wave velocity in the upper 30 meters of the subsurface (V_{S30}) values along the John Hart seismic profile, Vancouver Island, British Columbia, Canada.

Distance, in meters	Top and bottom, in meters	Number of layers	V_{S30}, in meters per second
0	0.00–30.00	300	198
1	0.00–30.00	300	199
2	0.00–30.00	300	201
3	0.00–30.00	300	203
4	0.00–30.00	300	205
5	0.00–30.00	300	207
6	0.00–30.00	300	209
7	0.00–30.00	300	211
8	0.00–30.00	300	212
9	0.00–30.00	300	214
10	0.00–30.00	300	216
11	0.00–30.00	300	222
12	0.00–30.00	300	228
13	0.00–30.00	300	234
14	0.00–30.00	300	240
15	0.00–30.00	300	245
16	0.00–30.00	300	251
17	0.00–30.00	300	257
18	0.00–30.00	300	262
19	0.00–30.00	300	268
20	0.00–30.00	300	273
21	0.00–30.00	300	279
22	0.00–30.00	300	285
23	0.00–30.00	300	291
24	0.00–30.00	300	296
25	0.00–30.00	300	302
26	0.00–30.00	300	308
27	0.00–30.00	300	313
28	0.00–30.00	300	319
29	0.00–30.00	300	325
30	0.00–30.00	300	330
31	0.00–30.00	300	335
32	0.00–30.00	300	339
33	0.00–30.00	300	343
34	0.00–30.00	300	348
35	0.00–30.00	300	352
36	0.00–30.00	300	357
37	0.00–30.00	300	361
38	0.00–30.00	300	365
39	0.00–30.00	300	370
40	0.00–30.00	300	374
41	0.00–30.00	300	377
42	0.00–30.00	300	380
43	0.00–30.00	300	384
44	0.00–30.00	300	387
45	0.00–30.00	300	390
46	0.00–30.00	300	393
47	0.00–30.00	300	396
48	0.00–30.00	300	399
49	0.00–30.00	300	403
50	0.00–30.00	300	406

Distance, in meters	Top and bottom, in meters	Number of layers	V_{S30}, in meters per second
51	0.00–30.00	300	407
52	0.00–30.00	300	408
53	0.00–30.00	300	409
54	0.00–30.00	300	410
55	0.00–30.00	300	411
56	0.00–30.00	300	412
57	0.00–30.00	300	413
58	0.00–30.00	300	414
59	0.00–30.00	300	415
60	0.00–30.00	300	416
61	0.00–30.00	300	416
62	0.00–30.00	300	416
63	0.00–30.00	300	416
64	0.00–30.00	300	417
65	0.00–30.00	300	417
66	0.00–30.00	300	417
67	0.00–30.00	300	417
68	0.00–30.00	300	418
69	0.00–30.00	300	418
70	0.00–30.00	300	418
71	0.00–30.00	300	418
72	0.00–30.00	300	418
73	0.00–30.00	300	418
74	0.00–30.00	300	417
75	0.00–30.00	300	417
76	0.00–30.00	300	417
77	0.00–30.00	300	417
78	0.00–30.00	300	417
79	0.00–30.00	300	417
80	0.00–30.00	300	417
81	0.00–30.00	300	417
82	0.00–30.00	300	417
83	0.00–30.00	300	417
84	0.00–30.00	300	416
85	0.00–30.00	300	416
86	0.00–30.00	300	416
87	0.00–30.00	300	416
88	0.00–30.00	300	416
89	0.00–30.00	300	416
90	0.00–30.00	300	416
91	0.00–30.00	300	416
92	0.00–30.00	300	416
93	0.00–30.00	300	416
94	0.00–30.00	300	416
95	0.00–30.00	300	416
96	0.00–30.00	300	416
97	0.00–30.00	300	416
98	0.00–30.00	300	416
99	0.00–30.00	300	416
100	0.00–30.00	300	416
101	0.00–30.00	300	416
102	0.00–30.00	300	416
103	0.00–30.00	300	416
104	0.00–30.00	300	415
105	0.00–30.00	300	415

Distance, in meters	Top and bottom, in meters	Number of layers	V_{S30}, in meters per second
106	0.00–30.00	300	415
107	0.00–30.00	300	415
108	0.00–30.00	300	415
109	0.00–30.00	300	414
110	0.00–30.00	300	414
111	0.00–30.00	300	414
112	0.00–30.00	300	414
113	0.00–30.00	300	413
114	0.00–30.00	300	413
115	0.00–30.00	300	413
116	0.00–30.00	300	413
117	0.00–30.00	300	412
118	0.00–30.00	300	412
119	0.00–30.00	300	412
120	0.00–30.00	300	412
121	0.00–30.00	300	411
122	0.00–30.00	300	411
123	0.00–30.00	300	411
124	0.00–30.00	300	411
125	0.00–30.00	300	410
126	0.00–30.00	300	410
127	0.00–30.00	300	410
128	0.00–30.00	300	409
129	0.00–30.00	300	409
130	0.00–30.00	300	409
131	0.00–30.00	300	408
132	0.00–30.00	300	407
133	0.00–30.00	300	407
134	0.00–30.00	300	406
135	0.00–30.00	300	405
136	0.00–30.00	300	405
137	0.00–30.00	300	404
138	0.00–30.00	300	403
139	0.00–30.00	300	403
140	0.00–30.00	300	402
141	0.00–30.00	300	401
142	0.00–30.00	300	399
143	0.00–30.00	300	398
144	0.00–30.00	300	397
145	0.00–30.00	300	396
146	0.00–30.00	300	394
147	0.00–30.00	300	393
148	0.00–30.00	300	392
149	0.00–30.00	300	390
150	0.00–30.00	300	389
151	0.00–30.00	300	388
152	0.00–30.00	300	387
153	0.00–30.00	300	386
154	0.00–30.00	300	385
155	0.00–30.00	300	384
156	0.00–30.00	300	383
157	0.00–30.00	300	382
158	0.00–30.00	300	381
159	0.00–30.00	300	380
160	0.00–30.00	300	379

Distance, in meters	Top and bottom, in meters	Number of layers	V_{S30}, in meters per second
161	0.00–30.00	300	379
162	0.00–30.00	300	379
163	0.00–30.00	300	380
164	0.00–30.00	300	380
165	0.00–30.00	300	380
166	0.00–30.00	300	381
167	0.00–30.00	300	381
168	0.00–30.00	300	381
169	0.00–30.00	300	381
170	0.00–30.00	300	382
171	0.00–30.00	300	382
172	0.00–30.00	300	382
173	0.00–30.00	300	382
174	0.00–30.00	300	382
175	0.00–30.00	300	383
176	0.00–30.00	300	383
177	0.00–30.00	300	383
178	0.00–30.00	300	383
179	0.00–30.00	300	383
180	0.00–30.00	300	384
181	0.00–30.00	300	383
182	0.00–30.00	300	383
183	0.00–30.00	300	383
184	0.00–30.00	300	383
185	0.00–30.00	300	382
186	0.00–30.00	300	382
187	0.00–30.00	300	382
188	0.00–30.00	300	382
189	0.00–30.00	300	382
190	0.00–30.00	300	381
191	0.00–30.00	300	381
192	0.00–30.00	300	381
193	0.00–30.00	300	380
194	0.00–30.00	300	380
195	0.00–30.00	300	379
196	0.00–30.00	300	379
197	0.00–30.00	300	378
198	0.00–30.00	300	378
199	0.00–30.00	300	378
200	0.00–30.00	300	377
201	0.00–30.00	300	377
202	0.00–30.00	300	376
203	0.00–30.00	300	376
204	0.00–30.00	300	375
205	0.00–30.00	300	375
206	0.00–30.00	300	374
207	0.00–30.00	300	374
208	0.00–30.00	300	374
209	0.00–30.00	300	373
210	0.00–30.00	300	373
211	0.00–30.00	300	372
212	0.00–30.00	300	372
213	0.00–30.00	300	372
214	0.00–30.00	300	372
215	0.00–30.00	300	372

Distance, in meters	Top and bottom, in meters	Number of layers	V_{S30}, in meters per second
216	0.00–30.00	300	372
217	0.00–30.00	300	371
218	0.00–30.00	300	371
219	0.00–30.00	300	371
220	0.00–30.00	300	371
221	0.00–30.00	300	371
222	0.00–30.00	300	371
223	0.00–30.00	300	371
224	0.00–30.00	300	371
225	0.00–30.00	300	371
226	0.00–30.00	300	371
227	0.00–30.00	300	371
228	0.00–30.00	300	371
229	0.00–30.00	300	371
230	0.00–30.00	300	371
231	0.00–30.00	300	372
232	0.00–30.00	300	372
233	0.00–30.00	300	372
234	0.00–30.00	300	372
235	0.00–30.00	300	372
236	0.00–30.00	300	372
237	0.00–30.00	300	372
238	0.00–30.00	300	372
239	0.00–30.00	300	372
240	0.00–30.00	300	372
241	0.00–30.00	300	372
242	0.00–30.00	300	372
243	0.00–30.00	300	372
244	0.00–30.00	300	372
245	0.00–30.00	300	372
246	0.00–30.00	300	372
247	0.00–30.00	300	372
248	0.00–30.00	300	372
249	0.00–30.00	300	372
250	0.00–30.00	300	372
251	0.00–30.00	300	372
252	0.00–30.00	300	371
253	0.00–30.00	300	371
254	0.00–30.00	300	371
255	0.00–30.00	300	371
256	0.00–30.00	300	371
257	0.00–30.00	300	370
258	0.00–30.00	300	370
259	0.00–30.00	300	370
260	0.00–30.00	300	370
261	0.00–30.00	300	370
262	0.00–30.00	300	370
263	0.00–30.00	300	369
264	0.00–30.00	300	369
265	0.00–30.00	300	369
266	0.00–30.00	300	369
267	0.00–30.00	300	369
268	0.00–30.00	300	368
269	0.00–30.00	300	368
270	0.00–30.00	300	368

Distance, in meters	Top and bottom, in meters	Number of layers	V_{S30}, in meters per second
271	0.00–30.00	300	368
272	0.00–30.00	300	368
273	0.00–30.00	300	368
274	0.00–30.00	300	368
275	0.00–30.00	300	368
276	0.00–30.00	300	368
277	0.00–30.00	300	368
278	0.00–30.00	300	368
279	0.00–30.00	300	368
280	0.00–30.00	300	368
281	0.00–30.00	300	369
282	0.00–30.00	300	369
283	0.00–30.00	300	370
284	0.00–30.00	300	370
285	0.00–30.00	300	370
286	0.00–30.00	300	371
287	0.00–30.00	300	371
288	0.00–30.00	300	372
289	0.00–30.00	300	372
290	0.00–30.00	300	372
291	0.00–30.00	300	373
292	0.00–30.00	300	374
293	0.00–30.00	300	374
294	0.00–30.00	300	375
295	0.00–30.00	300	375
296	0.00–30.00	300	376
297	0.00–30.00	300	377
298	0.00–30.00	300	377
299	0.00–30.00	300	378
300	0.00–30.00	300	378
301	0.00–30.00	300	379
302	0.00–30.00	300	379
303	0.00–30.00	300	380
304	0.00–30.00	300	380
305	0.00–30.00	300	380
306	0.00–30.00	300	381
307	0.00–30.00	300	381
308	0.00–30.00	300	382
309	0.00–30.00	300	382
310	0.00–30.00	300	382
311	0.00–30.00	300	383
312	0.00–30.00	300	383
313	0.00–30.00	300	383
314	0.00–30.00	300	384
315	0.00–30.00	300	384
316	0.00–30.00	300	384
317	0.00–30.00	300	384
318	0.00–30.00	300	385
319	0.00–30.00	300	385
320	0.00–30.00	300	385
321	0.00–30.00	300	385
322	0.00–30.00	300	385
323	0.00–30.00	300	385
324	0.00–30.00	300	385
325	0.00–30.00	300	385

Distance, in meters	Top and bottom, in meters	Number of layers	V_{S30}, in meters per second
326	0.00–30.00	300	384
327	0.00–30.00	300	384
328	0.00–30.00	300	384
329	0.00–30.00	300	384
330	0.00–30.00	300	384
331	0.00–30.00	300	383
332	0.00–30.00	300	382
333	0.00–30.00	300	381
334	0.00–30.00	300	381
335	0.00–30.00	300	380
336	0.00–30.00	300	379
337	0.00–30.00	300	378
338	0.00–30.00	300	377
339	0.00–30.00	300	376
340	0.00–30.00	300	376
341	0.00–30.00	300	375
342	0.00–30.00	300	375
343	0.00–30.00	300	375
344	0.00–30.00	300	374
345	0.00–30.00	300	374
346	0.00–30.00	300	374
347	0.00–30.00	300	373
348	0.00–30.00	300	373
349	0.00–30.00	300	373
350	0.00–30.00	300	372
351	0.00–30.00	300	372
352	0.00–30.00	300	372
353	0.00–30.00	300	372
354	0.00–30.00	300	372
355	0.00–30.00	300	372
356	0.00–30.00	300	372
357	0.00–30.00	300	372
358	0.00–30.00	300	372
359	0.00–30.00	300	372
360	0.00–30.00	300	372
361	0.00–30.00	300	371
362	0.00–30.00	300	371
363	0.00–30.00	300	370
364	0.00–30.00	300	370
365	0.00–30.00	300	369
366	0.00–30.00	300	369
367	0.00–30.00	300	369
368	0.00–30.00	300	368
369	0.00–30.00	300	368
370	0.00–30.00	300	367
371	0.00–30.00	300	367
372	0.00–30.00	300	367
373	0.00–30.00	300	366
374	0.00–30.00	300	366
375	0.00–30.00	300	366
376	0.00–30.00	300	366
377	0.00–30.00	300	366
378	0.00–30.00	300	365
379	0.00–30.00	300	365
380	0.00–30.00	300	365

Distance, in meters	Top and bottom, in meters	Number of layers	V_{S30}, in meters per second
381	0.00–30.00	300	365
382	0.00–30.00	300	365
383	0.00–30.00	300	365
384	0.00–30.00	300	365
385	0.00–30.00	300	365
386	0.00–30.00	300	364
387	0.00–30.00	300	364
388	0.00–30.00	300	364
389	0.00–30.00	300	364
390	0.00–30.00	300	364
Minimum			198
Maximum			418
Average			374

Table 3. Multichannel analysis of surface waves for Love waves (MAS_LW)-determined time-averaged shear-wave velocity in the upper 30 meters of the subsurface (V_{S30}) values along the John Hart Dam seismic profile, Vancouver Island, British Columbia, Canada.

Distance, in meters	Top and bottom, in meters	Number of layers	V_{S30}, in meters per second
0	0.00–30.00	300	196
1	0.00–30.00	300	197
2	0.00–30.00	300	198
3	0.00–30.00	300	198
4	0.00–30.00	300	199
5	0.00–30.00	300	200
6	0.00–30.00	300	201
7	0.00–30.00	300	202
8	0.00–30.00	300	202
9	0.00–30.00	300	203
10	0.00–30.00	300	204
11	0.00–30.00	300	211
12	0.00–30.00	300	218
13	0.00–30.00	300	225
14	0.00–30.00	300	231
15	0.00–30.00	300	238
16	0.00–30.00	300	244
17	0.00–30.00	300	250
18	0.00–30.00	300	256
19	0.00–30.00	300	262
20	0.00–30.00	300	268
21	0.00–30.00	300	275
22	0.00–30.00	300	282
23	0.00–30.00	300	289
24	0.00–30.00	300	296
25	0.00–30.00	300	303
26	0.00–30.00	300	310
27	0.00–30.00	300	316
28	0.00–30.00	300	323
29	0.00–30.00	300	329
30	0.00–30.00	300	336
31	0.00–30.00	300	342
32	0.00–30.00	300	349
33	0.00–30.00	300	355
34	0.00–30.00	300	362

Distance, in meters	Top and bottom, in meters	Number of layers	V_{S30}, in meters per second
35	0.00–30.00	300	368
36	0.00–30.00	300	374
37	0.00–30.00	300	380
38	0.00–30.00	300	386
39	0.00–30.00	300	392
40	0.00–30.00	300	399
41	0.00–30.00	300	404
42	0.00–30.00	300	409
43	0.00–30.00	300	414
44	0.00–30.00	300	419
45	0.00–30.00	300	424
46	0.00–30.00	300	429
47	0.00–30.00	300	434
48	0.00–30.00	300	439
49	0.00–30.00	300	444
50	0.00–30.00	300	449
51	0.00–30.00	300	451
52	0.00–30.00	300	453
53	0.00–30.00	300	455
54	0.00–30.00	300	457
55	0.00–30.00	300	459
56	0.00–30.00	300	461
57	0.00–30.00	300	463
58	0.00–30.00	300	464
59	0.00–30.00	300	466
60	0.00–30.00	300	468
61	0.00–30.00	300	469
62	0.00–30.00	300	471
63	0.00–30.00	300	472
64	0.00–30.00	300	473
65	0.00–30.00	300	474
66	0.00–30.00	300	475
67	0.00–30.00	300	476
68	0.00–30.00	300	477
69	0.00–30.00	300	478
70	0.00–30.00	300	480
71	0.00–30.00	300	480
72	0.00–30.00	300	481
73	0.00–30.00	300	481
74	0.00–30.00	300	481
75	0.00–30.00	300	482
76	0.00–30.00	300	482
77	0.00–30.00	300	483
78	0.00–30.00	300	483
79	0.00–30.00	300	484
80	0.00–30.00	300	484
81	0.00–30.00	300	484
82	0.00–30.00	300	484
83	0.00–30.00	300	483
84	0.00–30.00	300	483
85	0.00–30.00	300	483
86	0.00–30.00	300	482
87	0.00–30.00	300	482
88	0.00–30.00	300	482
89	0.00–30.00	300	481

Distance, in meters	Top and bottom, in meters	Number of layers	V_{S30}, in meters per second
90	0.00–30.00	300	481
91	0.00–30.00	300	480
92	0.00–30.00	300	478
93	0.00–30.00	300	477
94	0.00–30.00	300	475
95	0.00–30.00	300	474
96	0.00–30.00	300	472
97	0.00–30.00	300	470
98	0.00–30.00	300	469
99	0.00–30.00	300	467
100	0.00–30.00	300	466
101	0.00–30.00	300	462
102	0.00–30.00	300	458
103	0.00–30.00	300	454
104	0.00–30.00	300	450
105	0.00–30.00	300	446
106	0.00–30.00	300	442
107	0.00–30.00	300	437
108	0.00–30.00	300	433
109	0.00–30.00	300	429
110	0.00–30.00	300	425
111	0.00–30.00	300	421
112	0.00–30.00	300	417
113	0.00–30.00	300	413
114	0.00–30.00	300	409
115	0.00–30.00	300	405
116	0.00–30.00	300	401
117	0.00–30.00	300	397
118	0.00–30.00	300	392
119	0.00–30.00	300	388
120	0.00–30.00	300	384
121	0.00–30.00	300	382
122	0.00–30.00	300	381
123	0.00–30.00	300	380
124	0.00–30.00	300	379
125	0.00–30.00	300	377
126	0.00–30.00	300	376
127	0.00–30.00	300	375
128	0.00–30.00	300	373
129	0.00–30.00	300	372
130	0.00–30.00	300	371
131	0.00–30.00	300	371
132	0.00–30.00	300	371
133	0.00–30.00	300	371
134	0.00–30.00	300	372
135	0.00–30.00	300	372
136	0.00–30.00	300	372
137	0.00–30.00	300	372
138	0.00–30.00	300	372
139	0.00–30.00	300	373
140	0.00–30.00	300	373
141	0.00–30.00	300	374
142	0.00–30.00	300	375
143	0.00–30.00	300	376
144	0.00–30.00	300	377

Distance, in meters	Top and bottom, in meters	Number of layers	V_{S30}, in meters per second
145	0.00–30.00	300	378
146	0.00–30.00	300	379
147	0.00–30.00	300	380
148	0.00–30.00	300	381
149	0.00–30.00	300	383
150	0.00–30.00	300	384
151	0.00–30.00	300	384
152	0.00–30.00	300	384
153	0.00–30.00	300	384
154	0.00–30.00	300	384
155	0.00–30.00	300	384
156	0.00–30.00	300	385
157	0.00–30.00	300	385
158	0.00–30.00	300	385
159	0.00–30.00	300	385
160	0.00–30.00	300	385
161	0.00–30.00	300	385
162	0.00–30.00	300	385
163	0.00–30.00	300	385
164	0.00–30.00	300	385
165	0.00–30.00	300	384
166	0.00–30.00	300	384
167	0.00–30.00	300	384
168	0.00–30.00	300	384
169	0.00–30.00	300	384
170	0.00–30.00	300	383
171	0.00–30.00	300	382
172	0.00–30.00	300	382
173	0.00–30.00	300	381
174	0.00–30.00	300	380
175	0.00–30.00	300	379
176	0.00–30.00	300	378
177	0.00–30.00	300	377
178	0.00–30.00	300	376
179	0.00–30.00	300	375
180	0.00–30.00	300	374
181	0.00–30.00	300	373
182	0.00–30.00	300	372
183	0.00–30.00	300	371
184	0.00–30.00	300	370
185	0.00–30.00	300	369
186	0.00–30.00	300	368
187	0.00–30.00	300	367
188	0.00–30.00	300	366
189	0.00–30.00	300	365
190	0.00–30.00	300	364
191	0.00–30.00	300	364
192	0.00–30.00	300	363
193	0.00–30.00	300	363
194	0.00–30.00	300	362
195	0.00–30.00	300	362
196	0.00–30.00	300	361
197	0.00–30.00	300	361
198	0.00–30.00	300	360
199	0.00–30.00	300	360

Distance, in meters	Top and bottom, in meters	Number of layers	V_{S30}, in meters per second
200	0.00–30.00	300	359
201	0.00–30.00	300	359
202	0.00–30.00	300	358
203	0.00–30.00	300	358
204	0.00–30.00	300	357
205	0.00–30.00	300	356
206	0.00–30.00	300	356
207	0.00–30.00	300	355
208	0.00–30.00	300	355
209	0.00–30.00	300	354
210	0.00–30.00	300	354
211	0.00–30.00	300	353
212	0.00–30.00	300	353
213	0.00–30.00	300	353
214	0.00–30.00	300	353
215	0.00–30.00	300	353
216	0.00–30.00	300	353
217	0.00–30.00	300	353
218	0.00–30.00	300	353
219	0.00–30.00	300	353
220	0.00–30.00	300	353
221	0.00–30.00	300	354
222	0.00–30.00	300	354
223	0.00–30.00	300	355
224	0.00–30.00	300	355
225	0.00–30.00	300	356
226	0.00–30.00	300	356
227	0.00–30.00	300	357
228	0.00–30.00	300	357
229	0.00–30.00	300	358
230	0.00–30.00	300	358
231	0.00–30.00	300	359
232	0.00–30.00	300	361
233	0.00–30.00	300	362
234	0.00–30.00	300	364
235	0.00–30.00	300	365
236	0.00–30.00	300	366
237	0.00–30.00	300	368
238	0.00–30.00	300	369
239	0.00–30.00	300	370
240	0.00–30.00	300	372
241	0.00–30.00	300	372
242	0.00–30.00	300	372
243	0.00–30.00	300	372
244	0.00–30.00	300	372
245	0.00–30.00	300	373
246	0.00–30.00	300	373
247	0.00–30.00	300	373
248	0.00–30.00	300	373
249	0.00–30.00	300	373
250	0.00–30.00	300	373
251	0.00–30.00	300	373
252	0.00–30.00	300	373
253	0.00–30.00	300	372
254	0.00–30.00	300	372

Distance, in meters	Top and bottom, in meters	Number of layers	V_{S30}, in meters per second
255	0.00–30.00	300	371
256	0.00–30.00	300	371
257	0.00–30.00	300	371
258	0.00–30.00	300	370
259	0.00–30.00	300	370
260	0.00–30.00	300	369
261	0.00–30.00	300	369
262	0.00–30.00	300	369
263	0.00–30.00	300	369
264	0.00–30.00	300	369
265	0.00–30.00	300	369
266	0.00–30.00	300	368
267	0.00–30.00	300	368
268	0.00–30.00	300	368
269	0.00–30.00	300	368
270	0.00–30.00	300	368
271	0.00–30.00	300	369
272	0.00–30.00	300	369
273	0.00–30.00	300	370
274	0.00–30.00	300	371
275	0.00–30.00	300	372
276	0.00–30.00	300	372
277	0.00–30.00	300	373
278	0.00–30.00	300	374
279	0.00–30.00	300	375
280	0.00–30.00	300	375
281	0.00–30.00	300	376
282	0.00–30.00	300	376
283	0.00–30.00	300	376
284	0.00–30.00	300	376
285	0.00–30.00	300	376
286	0.00–30.00	300	376
287	0.00–30.00	300	376
288	0.00–30.00	300	376
289	0.00–30.00	300	376
290	0.00–30.00	300	377
291	0.00–30.00	300	375
292	0.00–30.00	300	374
293	0.00–30.00	300	373
294	0.00–30.00	300	372
295	0.00–30.00	300	371
296	0.00–30.00	300	370
297	0.00–30.00	300	368
298	0.00–30.00	300	367
299	0.00–30.00	300	366
300	0.00–30.00	300	365
301	0.00–30.00	300	365
302	0.00–30.00	300	365
303	0.00–30.00	300	366
304	0.00–30.00	300	366
305	0.00–30.00	300	366
306	0.00–30.00	300	366
307	0.00–30.00	300	366
308	0.00–30.00	300	367
309	0.00–30.00	300	367

Distance, in meters	Top and bottom, in meters	Number of layers	V_{S30}, in meters per second
310	0.00–30.00	300	367
311	0.00–30.00	300	367
312	0.00–30.00	300	367
313	0.00–30.00	300	367
314	0.00–30.00	300	367
315	0.00–30.00	300	367
316	0.00–30.00	300	367
317	0.00–30.00	300	367
318	0.00–30.00	300	367
319	0.00–30.00	300	367
320	0.00–30.00	300	367
321	0.00–30.00	300	367
322	0.00–30.00	300	368
323	0.00–30.00	300	369
324	0.00–30.00	300	370
325	0.00–30.00	300	371
326	0.00–30.00	300	371
327	0.00–30.00	300	372
328	0.00–30.00	300	373
329	0.00–30.00	300	374
330	0.00–30.00	300	375
331	0.00–30.00	300	376
332	0.00–30.00	300	377
333	0.00–30.00	300	378
334	0.00–30.00	300	379
335	0.00–30.00	300	380
336	0.00–30.00	300	381
337	0.00–30.00	300	382
338	0.00–30.00	300	383
339	0.00–30.00	300	384
340	0.00–30.00	300	385
341	0.00–30.00	300	384
342	0.00–30.00	300	382
343	0.00–30.00	300	381
344	0.00–30.00	300	379
345	0.00–30.00	300	378
346	0.00–30.00	300	376
347	0.00–30.00	300	375
348	0.00–30.00	300	373
349	0.00–30.00	300	372
350	0.00–30.00	300	370
351	0.00–30.00	300	369
352	0.00–30.00	300	367
353	0.00–30.00	300	366
354	0.00–30.00	300	364
355	0.00–30.00	300	363
356	0.00–30.00	300	362
357	0.00–30.00	300	360
358	0.00–30.00	300	359
359	0.00–30.00	300	357
360	0.00–30.00	300	356
361	0.00–30.00	300	358
362	0.00–30.00	300	359
363	0.00–30.00	300	361
364	0.00–30.00	300	362

Distance, in meters	Top and bottom, in meters	Number of layers	V_{S30}, in meters per second
365	0.00–30.00	300	363
366	0.00–30.00	300	365
367	0.00–30.00	300	366
368	0.00–30.00	300	368
369	0.00–30.00	300	369
370	0.00–30.00	300	370
371	0.00–30.00	300	370
372	0.00–30.00	300	370
373	0.00–30.00	300	370
374	0.00–30.00	300	370
375	0.00–30.00	300	370
376	0.00–30.00	300	370
377	0.00–30.00	300	370
378	0.00–30.00	300	370
379	0.00–30.00	300	370
380	0.00–30.00	300	370
381	0.00–30.00	300	368
382	0.00–30.00	300	367
383	0.00–30.00	300	365
384	0.00–30.00	300	364
385	0.00–30.00	300	362
386	0.00–30.00	300	361
387	0.00–30.00	300	359
388	0.00–30.00	300	358
389	0.00–30.00	300	356
390	0.00–30.00	300	355
Minimum			196
Maximum			484
Average			378

Table 4. Tomographically determined time-averaged shear-wave velocity in the upper 30 meters of the subsurface (V_{S30}) values along the Ladore seismic profile, Vancouver Island, British Columbia, Canada.

Distance, in meters	Top and bottom, in meters	Number of layers	V_{S30}, in meters per second
–6	–6.90–23.10	300	728
–3	–7.10–22.90	300	728
0	–7.30–22.70	300	726
3	–7.50–22.50	300	723
6	–7.70–22.30	300	735
9	–8.00–22.00	300	752
12	–8.09–21.91	300	779
15	–7.80–22.20	300	821
18	–7.60–22.40	300	859
21	–7.50–22.50	300	895
24	–7.40–22.60	300	930
27	–7.50–22.50	300	961
30	–7.60–22.40	300	990
33	–7.71–22.29	300	1,011
36	–7.91–22.09	300	1,012
39	–8.01–21.99	300	1,004
42	–8.22–21.78	300	982
45	–8.51–21.49	300	956
48	–8.73–21.27	300	944
51	–9.13–20.87	300	924
54	–9.53–20.47	300	914
57	–9.84–20.16	300	916
60	–10.17–19.83	300	927
63	–9.87–20.13	300	999
66	–9.56–20.44	300	1,085
69	–9.15–20.85	300	1,171
72	–8.75–21.25	300	1,278
75	–8.34–21.66	300	1,378
78	–7.83–22.17	300	1,475
81	–7.36–22.64	300	1,536
84	–7.03–22.97	300	1,540
87	–6.50–23.50	300	1,479
90	–5.79–24.21	300	1,381
93	–5.07–24.93	300	1,250
96	–4.29–25.71	300	1,092
99	–3.58–26.42	300	933
102	–2.85–27.15	300	861
105	–2.01–27.99	300	813
108	–1.53–28.47	300	776
111	–1.14–28.86	300	751
114	–0.86–29.14	300	734
117	–0.64–29.36	300	718
120	–0.36–29.64	300	707
123	–0.18–29.82	300	696
126	–0.08–29.92	300	681
129	–0.02–29.98	300	669
132	–0.12–29.88	300	655
135	–0.20–29.80	300	640
138	–0.20–29.80	300	627
141	–0.22–29.78	300	610
144	–0.32–29.68	300	602
147	–0.42–29.58	300	591

Distance, in meters	Top and bottom, in meters	Number of layers	V_{S30}, in meters per second
150	–0.52–29.48	300	575
Minimum			575
Maximum			1,540
Average			915

Table 5. Multichannel analysis of surface waves for Rayleigh waves (MAS_RW)-determined time-averaged shear-wave velocity in the upper 30 meters of the subsurface (V_{S30}) values along the Ladore seismic profile, Vancouver Island, British Columbia, Canada.

Distance, in meters	Top and bottom, in meters	Number of layers	V_{S30}, in meters per second
0	0.00–30.00	300	1,932
1	0.00–30.00	300	1,929
2	0.00–30.00	300	1,925
3	0.00–30.00	300	1,921
4	0.00–30.00	300	1,918
5	0.00–30.00	300	1,914
6	0.00–30.00	300	1,910
7	0.00–30.00	300	1,887
8	0.00–30.00	300	1,865
9	0.00–30.00	300	1,842
10	0.00–30.00	300	1,819
11	0.00–30.00	300	1,796
12	0.00–30.00	300	1,773
13	0.00–30.00	300	1,770
14	0.00–30.00	300	1,767
15	0.00–30.00	300	1,764
16	0.00–30.00	300	1,761
17	0.00–30.00	300	1,758
18	0.00–30.00	300	1,755
19	0.00–30.00	300	1,780
20	0.00–30.00	300	1,804
21	0.00–30.00	300	1,829
22	0.00–30.00	300	1,853
23	0.00–30.00	300	1,878
24	0.00–30.00	300	1,902
25	0.00–30.00	300	1,917
26	0.00–30.00	300	1,932
27	0.00–30.00	300	1,947
28	0.00–30.00	300	1,962
29	0.00–30.00	300	1,978
30	0.00–30.00	300	1,993
31	0.00–30.00	300	2,000
32	0.00–30.00	300	2,007
33	0.00–30.00	300	2,013
34	0.00–30.00	300	2,020
35	0.00–30.00	300	2,027
36	0.00–30.00	300	2,034
37	0.00–30.00	300	2,045
38	0.00–30.00	300	2,055
39	0.00–30.00	300	2,065
40	0.00–30.00	300	2,076
41	0.00–30.00	300	2,086
42	0.00–30.00	300	2,097
43	0.00–30.00	300	2,108
44	0.00–30.00	300	2,119
45	0.00–30.00	300	2,130
46	0.00–30.00	300	2,141
47	0.00–30.00	300	2,152
48	0.00–30.00	300	2,163
49	0.00–30.00	300	2,155
50	0.00–30.00	300	2,147

Distance, in meters	Top and bottom, in meters	Number of layers	V_{S30}, in meters per second
51	0.00–30.00	300	2,139
52	0.00–30.00	300	2,131
53	0.00–30.00	300	2,123
54	0.00–30.00	300	2,114
55	0.00–30.00	300	2,098
56	0.00–30.00	300	2,081
57	0.00–30.00	300	2,064
58	0.00–30.00	300	2,048
59	0.00–30.00	300	2,031
60	0.00–30.00	300	2,014
61	0.00–30.00	300	1,989
62	0.00–30.00	300	1,964
63	0.00–30.00	300	1,938
64	0.00–30.00	300	1,913
65	0.00–30.00	300	1,887
66	0.00–30.00	300	1,862
67	0.00–30.00	300	1,811
68	0.00–30.00	300	1,760
69	0.00–30.00	300	1,708
70	0.00–30.00	300	1,655
71	0.00–30.00	300	1,601
72	0.00–30.00	300	1,546
73	0.00–30.00	300	1,497
74	0.00–30.00	300	1,448
75	0.00–30.00	300	1,398
76	0.00–30.00	300	1,347
77	0.00–30.00	300	1,296
78	0.00–30.00	300	1,244
79	0.00–30.00	300	1,234
80	0.00–30.00	300	1,222
81	0.00–30.00	300	1,210
82	0.00–30.00	300	1,196
83	0.00–30.00	300	1,181
84	0.00–30.00	300	1,165
85	0.00–30.00	300	1,162
86	0.00–30.00	300	1,160
87	0.00–30.00	300	1,157
88	0.00–30.00	300	1,155
89	0.00–30.00	300	1,152
90	0.00–30.00	300	1,149
91	0.00–30.00	300	1,147
92	0.00–30.00	300	1,145
93	0.00–30.00	300	1,143
94	0.00–30.00	300	1,140
95	0.00–30.00	300	1,138
96	0.00–30.00	300	1,135
97	0.00–30.00	300	1,130
98	0.00–30.00	300	1,125
99	0.00–30.00	300	1,120
100	0.00–30.00	300	1,115
101	0.00–30.00	300	1,109
102	0.00–30.00	300	1,104
103	0.00–30.00	300	1,087
104	0.00–30.00	300	1,069
105	0.00–30.00	300	1,050

Distance, in meters	Top and bottom, in meters	Number of layers	V_{S30}, in meters per second
106	0.00–30.00	300	1,031
107	0.00–30.00	300	1,010
108	0.00–30.00	300	988
109	0.00–30.00	300	965
110	0.00–30.00	300	941
111	0.00–30.00	300	916
112	0.00–30.00	300	890
113	0.00–30.00	300	862
114	0.00–30.00	300	833
115	0.00–30.00	300	823
116	0.00–30.00	300	813
117	0.00–30.00	300	803
118	0.00–30.00	300	793
119	0.00–30.00	300	783
120	0.00–30.00	300	773
121	0.00–30.00	300	766
122	0.00–30.00	300	760
123	0.00–30.00	300	753
124	0.00–30.00	300	747
125	0.00–30.00	300	740
126	0.00–30.00	300	733
127	0.00–30.00	300	727
128	0.00–30.00	300	721
129	0.00–30.00	300	714
130	0.00–30.00	300	708
131	0.00–30.00	300	701
132	0.00–30.00	300	694
133	0.00–30.00	300	694
134	0.00–30.00	300	693
135	0.00–30.00	300	693
136	0.00–30.00	300	693
137	0.00–30.00	300	693
138	0.00–30.00	300	692
139	0.00–30.00	300	693
140	0.00–30.00	300	694
141	0.00–30.00	300	695
142	0.00–30.00	300	695
143	0.00–30.00	300	696
144	0.00–30.00	300	697
Minimum			692
Maximum			2,163
Average			1,458

Table 6. Multichannel analysis of surface waves for Love waves (MAS_LW)-determined time-averaged shear-wave velocity in the upper 30 meters of the subsurface (V_{S30}) values along the Ladore seismic profile, Vancouver Island, British Columbia, Canada.

Distance, in meters	Top and bottom, in meters	Number of layers	V_{S30}, in meters per second
0	0.00–30.00	300	1,459
1	0.00–30.00	300	1,464
2	0.00–30.00	300	1,470
3	0.00–30.00	300	1,475
4	0.00–30.00	300	1,481
5	0.00–30.00	300	1,486
6	0.00–30.00	300	1,491
7	0.00–30.00	300	1,502
8	0.00–30.00	300	1,512
9	0.00–30.00	300	1,522
10	0.00–30.00	300	1,532
11	0.00–30.00	300	1,542
12	0.00–30.00	300	1,552
13	0.00–30.00	300	1,556
14	0.00–30.00	300	1,560
15	0.00–30.00	300	1,565
16	0.00–30.00	300	1,569
17	0.00–30.00	300	1,572
18	0.00–30.00	300	1,576
19	0.00–30.00	300	1,578
20	0.00–30.00	300	1,580
21	0.00–30.00	300	1,582
22	0.00–30.00	300	1,583
23	0.00–30.00	300	1,584
24	0.00–30.00	300	1,586
25	0.00–30.00	300	1,592
26	0.00–30.00	300	1,599
27	0.00–30.00	300	1,606
28	0.00–30.00	300	1,612
29	0.00–30.00	300	1,619
30	0.00–30.00	300	1,625
31	0.00–30.00	300	1,624
32	0.00–30.00	300	1,622
33	0.00–30.00	300	1,621
34	0.00–30.00	300	1,619
35	0.00–30.00	300	1,616
36	0.00–30.00	300	1,614
37	0.00–30.00	300	1,598
38	0.00–30.00	300	1,582
39	0.00–30.00	300	1,565
40	0.00–30.00	300	1,548
41	0.00–30.00	300	1,530
42	0.00–30.00	300	1,511
43	0.00–30.00	300	1,502
44	0.00–30.00	300	1,493
45	0.00–30.00	300	1,484
46	0.00–30.00	300	1,475
47	0.00–30.00	300	1,466
48	0.00–30.00	300	1,457
49	0.00–30.00	300	1,449
50	0.00–30.00	300	1,441

Distance, in meters	Top and bottom, in meters	Number of layers	V_{S30}, in meters per second
51	0.00–30.00	300	1,432
52	0.00–30.00	300	1,424
53	0.00–30.00	300	1,416
54	0.00–30.00	300	1,408
55	0.00–30.00	300	1,393
56	0.00–30.00	300	1,378
57	0.00–30.00	300	1,363
58	0.00–30.00	300	1,348
59	0.00–30.00	300	1,332
60	0.00–30.00	300	1,316
61	0.00–30.00	300	1,302
62	0.00–30.00	300	1,288
63	0.00–30.00	300	1,274
64	0.00–30.00	300	1,259
65	0.00–30.00	300	1,244
66	0.00–30.00	300	1,230
67	0.00–30.00	300	1,216
68	0.00–30.00	300	1,203
69	0.00–30.00	300	1,190
70	0.00–30.00	300	1,177
71	0.00–30.00	300	1,163
72	0.00–30.00	300	1,150
73	0.00–30.00	300	1,148
74	0.00–30.00	300	1,147
75	0.00–30.00	300	1,145
76	0.00–30.00	300	1,144
77	0.00–30.00	300	1,142
78	0.00–30.00	300	1,140
79	0.00–30.00	300	1,138
80	0.00–30.00	300	1,135
81	0.00–30.00	300	1,133
82	0.00–30.00	300	1,131
83	0.00–30.00	300	1,128
84	0.00–30.00	300	1,126
85	0.00–30.00	300	1,115
86	0.00–30.00	300	1,104
87	0.00–30.00	300	1,092
88	0.00–30.00	300	1,081
89	0.00–30.00	300	1,069
90	0.00–30.00	300	1,057
91	0.00–30.00	300	1,054
92	0.00–30.00	300	1,052
93	0.00–30.00	300	1,049
94	0.00–30.00	300	1,046
95	0.00–30.00	300	1,042
96	0.00–30.00	300	1,039
97	0.00–30.00	300	1,039
98	0.00–30.00	300	1,038
99	0.00–30.00	300	1,037
100	0.00–30.00	300	1,036
101	0.00–30.00	300	1,035
102	0.00–30.00	300	1,034
103	0.00–30.00	300	1,017
104	0.00–30.00	300	999
105	0.00–30.00	300	982

Distance, in meters	Top and bottom, in meters	Number of layers	V_{S30}, in meters per second
106	0.00–30.00	300	964
107	0.00–30.00	300	946
108	0.00–30.00	300	929
109	0.00–30.00	300	897
110	0.00–30.00	300	864
111	0.00–30.00	300	831
112	0.00–30.00	300	796
113	0.00–30.00	300	761
114	0.00–30.00	300	724
115	0.00–30.00	300	703
116	0.00–30.00	300	682
117	0.00–30.00	300	660
118	0.00–30.00	300	637
119	0.00–30.00	300	611
120	0.00–30.00	300	584
121	0.00–30.00	300	588
122	0.00–30.00	300	593
123	0.00–30.00	300	597
124	0.00–30.00	300	601
125	0.00–30.00	300	605
126	0.00–30.00	300	608
127	0.00–30.00	300	607
128	0.00–30.00	300	606
129	0.00–30.00	300	605
130	0.00–30.00	300	604
131	0.00–30.00	300	602
132	0.00–30.00	300	601
133	0.00–30.00	300	598
134	0.00–30.00	300	594
135	0.00–30.00	300	591
136	0.00–30.00	300	587
137	0.00–30.00	300	583
138	0.00–30.00	300	580
139	0.00–30.00	300	580
140	0.00–30.00	300	580
141	0.00–30.00	300	580
142	0.00–30.00	300	581
143	0.00–30.00	300	581
144	0.00–30.00	300	581
Minimum			580
Maximum			1,625
Average			1,164

Table 7. Tomographically determined time-averaged shear-wave velocity in the upper 30 meters of the subsurface (V_{S30}) values along the Strathcona Dam Roadway seismic profile, Vancouver Island, British Columbia, Canada.

Distance, in meters	Top and bottom, in meters	Number of layers	V_{S30}, in meters per second
–6	1.02–31.02	0	0
–3	0.51–30.51	0	0
0	0.00–30.00	0	0
3	–0.51–29.49	0	0
6	–0.93–29.07	0	0
9	–1.53–28.47	0	0
12	–2.01–27.99	0	0
15	–2.23–27.77	0	0
18	–2.36–27.64	0	0
21	–2.29–27.71	0	0
24	–2.03–27.97	0	0
27	–1.92–28.08	0	0
30	–1.68–28.32	0	0
33	–1.62–28.38	300	1,294
36	–1.69–28.31	300	1,312
39	–1.78–28.22	300	1,325
42	–1.97–28.03	300	1,332
45	–2.30–27.70	300	1,325
48	–2.56–27.44	300	1,321
51	–2.74–27.26	300	1,319
54	–2.80–27.20	300	1,324
57	–2.74–27.26	300	1,338
60	–2.45–27.55	300	1,367
63	–2.10–27.90	300	1,400
66	–1.86–28.14	300	1,424
69	–1.74–28.26	300	1,436
72	–1.71–28.29	300	1,442
75	–1.71–28.29	300	1,447
78	–1.78–28.22	300	1,445
81	–1.90–28.10	300	1,438
84	–2.08–27.92	300	1,425
87	–2.58–27.42	300	1,382
90	–2.79–27.21	300	1,363
93	–2.92–27.08	300	1,351
96	–2.71–27.29	300	1,369
99	–2.50–27.50	300	1,388
102	–2.41–27.59	300	1,396
105	–2.41–27.59	300	1,393
108	–2.40–27.60	300	1,392
111	–2.23–27.77	300	1,406
114	–2.25–27.75	300	1,404
117	–2.33–27.67	300	1,396
120	–2.02–27.98	300	1,425
123	–2.18–27.82	300	1,409
126	–2.53–27.47	300	1,377
129	–2.56–27.44	300	1,372
132	–2.30–27.70	300	1,390
135	–2.01–27.99	300	1,408
138	–1.81–28.19	300	1,419
141	–1.71–28.29	300	1,415
144	–1.63–28.37	300	1,414

Distance, in meters	Top and bottom, in meters	Number of layers	V_{S30}, in meters per second
147	–1.70–28.30	300	1,399
150	–1.97–28.03	300	1,368
153	–2.20–27.80	300	1,339
156	–2.30–27.70	300	1,322
159	–2.46–27.54	300	1,300
162	–2.65–27.35	300	1,273
165	–2.71–27.29	300	1,254
168	–2.56–27.44	300	1,249
171	–2.58–27.42	300	1,231
174	–2.80–27.20	300	1,197
177	–3.07–26.93	300	1,162
180	–3.30–26.70	300	1,137
183	–3.60–26.40	300	1,102
186	–3.95–26.05	300	1,063
189	–4.26–25.74	300	1,028
192	–4.42–25.58	300	1,002
195	–4.74–25.26	300	965
198	–5.32–24.68	300	915
201	–5.74–24.26	300	875
204	–5.67–24.33	300	864
207	–5.76–24.24	300	846
210	–5.63–24.37	300	839
213	–5.66–24.34	300	828
216	–5.43–24.57	0	0
219	–5.48–24.52	0	0
222	–5.70–24.30	0	0
225	–6.07–23.93	0	0
228	–6.57–23.43	0	0
231	–7.07–22.93	0	0
234	–7.50–22.50	0	0
237	–8.00–22.00	0	0
240	–8.49–21.51	0	0
243	–8.99–21.01	0	0
Minimum			828
Maximum			1,447
Average			1,281

Table 8. Multichannel analysis of surface waves for Rayleigh waves ($MASW_R$)-determined time-averaged shear-wave velocity in the upper 30 meters of the subsurface (V_{S30}) values along the Strathcona Dam Roadway seismic profile, Vancouver Island, British Columbia, Canada.

Distance, in meters	Top and bottom, in meters	Number of layers	V_{S30}, in meters per second
0	0.00–30.00	300	315
1	0.00–30.00	300	315
2	0.00–30.00	300	314
3	0.00–30.00	300	313
4	0.00–30.00	300	312
5	0.00–30.00	300	312
6	0.00–30.00	300	311
7	0.00–30.00	300	312
8	0.00–30.00	300	313
9	0.00–30.00	300	313
10	0.00–30.00	300	314
11	0.00–30.00	300	315
12	0.00–30.00	300	316
13	0.00–30.00	300	321
14	0.00–30.00	300	326
15	0.00–30.00	300	331
16	0.00–30.00	300	336
17	0.00–30.00	300	341
18	0.00–30.00	300	346
19	0.00–30.00	300	349
20	0.00–30.00	300	352
21	0.00–30.00	300	354
22	0.00–30.00	300	356
23	0.00–30.00	300	359
24	0.00–30.00	300	361
25	0.00–30.00	300	357
26	0.00–30.00	300	354
27	0.00–30.00	300	350
28	0.00–30.00	300	347
29	0.00–30.00	300	343
30	0.00–30.00	300	339
31	0.00–30.00	300	344
32	0.00–30.00	300	348
33	0.00–30.00	300	353
34	0.00–30.00	300	357
35	0.00–30.00	300	361
36	0.00–30.00	300	365
37	0.00–30.00	300	366
38	0.00–30.00	300	366
39	0.00–30.00	300	366
40	0.00–30.00	300	367
41	0.00–30.00	300	367
42	0.00–30.00	300	367
43	0.00–30.00	300	372
44	0.00–30.00	300	377
45	0.00–30.00	300	382
46	0.00–30.00	300	386
47	0.00–30.00	300	391
48	0.00–30.00	300	395
49	0.00–30.00	300	407
50	0.00–30.00	300	419

Distance, in meters	Top and bottom, in meters	Number of layers	V_{S30}, in meters per second
51	0.00–30.00	300	432
52	0.00–30.00	300	444
53	0.00–30.00	300	455
54	0.00–30.00	300	467
55	0.00–30.00	300	473
56	0.00–30.00	300	478
57	0.00–30.00	300	482
58	0.00–30.00	300	485
59	0.00–30.00	300	488
60	0.00–30.00	300	489
61	0.00–30.00	300	592
62	0.00–30.00	300	682
63	0.00–30.00	300	767
64	0.00–30.00	300	847
65	0.00–30.00	300	925
66	0.00–30.00	300	1,000
67	0.00–30.00	300	1,063
68	0.00–30.00	300	1,125
69	0.00–30.00	300	1,185
70	0.00–30.00	300	1,244
71	0.00–30.00	300	1,302
72	0.00–30.00	300	1,360
73	0.00–30.00	300	1,367
74	0.00–30.00	300	1,374
75	0.00–30.00	300	1,381
76	0.00–30.00	300	1,387
77	0.00–30.00	300	1,394
78	0.00–30.00	300	1,401
79	0.00–30.00	300	1,405
80	0.00–30.00	300	1,408
81	0.00–30.00	300	1,411
82	0.00–30.00	300	1,414
83	0.00–30.00	300	1,417
84	0.00–30.00	300	1,419
85	0.00–30.00	300	1,416
86	0.00–30.00	300	1,413
87	0.00–30.00	300	1,410
88	0.00–30.00	300	1,406
89	0.00–30.00	300	1,403
90	0.00–30.00	300	1,400
91	0.00–30.00	300	1,400
92	0.00–30.00	300	1,400
93	0.00–30.00	300	1,400
94	0.00–30.00	300	1,400
95	0.00–30.00	300	1,400
96	0.00–30.00	300	1,400
97	0.00–30.00	300	1,413
98	0.00–30.00	300	1,426
99	0.00–30.00	300	1,439
100	0.00–30.00	300	1,452
101	0.00–30.00	300	1,465
102	0.00–30.00	300	1,477
103	0.00–30.00	300	1,490
104	0.00–30.00	300	1,502
105	0.00–30.00	300	1,514

Distance, in meters	Top and bottom, in meters	Number of layers	V_{S30}, in meters per second
106	0.00–30.00	300	1,527
107	0.00–30.00	300	1,539
108	0.00–30.00	300	1,551
109	0.00–30.00	300	1,547
110	0.00–30.00	300	1,542
111	0.00–30.00	300	1,537
112	0.00–30.00	300	1,533
113	0.00–30.00	300	1,528
114	0.00–30.00	300	1,523
115	0.00–30.00	300	1,513
116	0.00–30.00	300	1,502
117	0.00–30.00	300	1,492
118	0.00–30.00	300	1,481
119	0.00–30.00	300	1,469
120	0.00–30.00	300	1,457
121	0.00–30.00	300	1,453
122	0.00–30.00	300	1,448
123	0.00–30.00	300	1,444
124	0.00–30.00	300	1,439
125	0.00–30.00	300	1,435
126	0.00–30.00	300	1,430
127	0.00–30.00	300	1,434
128	0.00–30.00	300	1,438
129	0.00–30.00	300	1,441
130	0.00–30.00	300	1,444
131	0.00–30.00	300	1,447
132	0.00–30.00	300	1,450
133	0.00–30.00	300	1,442
134	0.00–30.00	300	1,434
135	0.00–30.00	300	1,427
136	0.00–30.00	300	1,419
137	0.00–30.00	300	1,412
138	0.00–30.00	300	1,404
139	0.00–30.00	300	1,389
140	0.00–30.00	300	1,374
141	0.00–30.00	300	1,359
142	0.00–30.00	300	1,343
143	0.00–30.00	300	1,328
144	0.00–30.00	300	1,312
145	0.00–30.00	300	1,305
146	0.00–30.00	300	1,297
147	0.00–30.00	300	1,290
148	0.00–30.00	300	1,283
149	0.00–30.00	300	1,276
150	0.00–30.00	300	1,268
151	0.00–30.00	300	1,269
152	0.00–30.00	300	1,271
153	0.00–30.00	300	1,272
154	0.00–30.00	300	1,273
155	0.00–30.00	300	1,274
156	0.00–30.00	300	1,275
157	0.00–30.00	300	1,272
158	0.00–30.00	300	1,269
159	0.00–30.00	300	1,266
160	0.00–30.00	300	1,262

Distance, in meters	Top and bottom, in meters	Number of layers	V_{S30}, in meters per second
161	0.00–30.00	300	1,259
162	0.00–30.00	300	1,256
163	0.00–30.00	300	1,266
164	0.00–30.00	300	1,275
165	0.00–30.00	300	1,285
166	0.00–30.00	300	1,294
167	0.00–30.00	300	1,303
168	0.00–30.00	300	1,311
169	0.00–30.00	300	1,326
170	0.00–30.00	300	1,340
171	0.00–30.00	300	1,354
172	0.00–30.00	300	1,367
173	0.00–30.00	300	1,379
174	0.00–30.00	300	1,392
175	0.00–30.00	300	1,388
176	0.00–30.00	300	1,384
177	0.00–30.00	300	1,381
178	0.00–30.00	300	1,377
179	0.00–30.00	300	1,373
180	0.00–30.00	300	1,369
181	0.00–30.00	300	1,361
182	0.00–30.00	300	1,352
183	0.00–30.00	300	1,343
184	0.00–30.00	300	1,335
185	0.00–30.00	300	1,326
186	0.00–30.00	300	1,317
187	0.00–30.00	300	1,314
188	0.00–30.00	300	1,311
189	0.00–30.00	300	1,308
190	0.00–30.00	300	1,305
191	0.00–30.00	300	1,301
192	0.00–30.00	300	1,298
193	0.00–30.00	300	1,290
194	0.00–30.00	300	1,282
195	0.00–30.00	300	1,274
196	0.00–30.00	300	1,265
197	0.00–30.00	300	1,256
198	0.00–30.00	300	1,248
199	0.00–30.00	300	1,242
200	0.00–30.00	300	1,236
201	0.00–30.00	300	1,229
202	0.00–30.00	300	1,223
203	0.00–30.00	300	1,217
204	0.00–30.00	300	1,210
205	0.00–30.00	300	1,215
206	0.00–30.00	300	1,220
207	0.00–30.00	300	1,224
208	0.00–30.00	300	1,229
209	0.00–30.00	300	1,234
210	0.00–30.00	300	1,238
211	0.00–30.00	300	1,244
212	0.00–30.00	300	1,250
213	0.00–30.00	300	1,256
214	0.00–30.00	300	1,261
215	0.00–30.00	300	1,267

Distance, in meters	Top and bottom, in meters	Number of layers	V_{S30}, in meters per second
216	0.00–30.00	300	1,272
217	0.00–30.00	300	1,269
218	0.00–30.00	300	1,266
219	0.00–30.00	300	1,262
220	0.00–30.00	300	1,259
221	0.00–30.00	300	1,255
222	0.00–30.00	300	1,252
223	0.00–30.00	300	1,250
224	0.00–30.00	300	1,248
225	0.00–30.00	300	1,246
226	0.00–30.00	300	1,244
227	0.00–30.00	300	1,242
228	0.00–30.00	300	1,240
229	0.00–30.00	300	1,244
230	0.00–30.00	300	1,248
231	0.00–30.00	300	1,252
232	0.00–30.00	300	1,256
233	0.00–30.00	300	1,260
234	0.00–30.00	300	1,264
Minimum			311
Maximum			1,551
Average			1,078

Table 9. Multichannel analysis of surface waves for Love waves (MAS_LW)-determined time-averaged shear-wave velocity in the upper 30 meters of the subsurface (V_{S30}) values along the Strathcona Roadway seismic profile (model 1), Vancouver Island, British Columbia, Canada.

Distance, in meters	Top and bottom, in meters	Number of layers	V_{S30}, in meters per second
0	0.00–30.00	300	359
1	0.00–30.00	300	358
2	0.00–30.00	300	357
3	0.00–30.00	300	356
4	0.00–30.00	300	355
5	0.00–30.00	300	354
6	0.00–30.00	300	353
7	0.00–30.00	300	355
8	0.00–30.00	300	357
9	0.00–30.00	300	359
10	0.00–30.00	300	361
11	0.00–30.00	300	363
12	0.00–30.00	300	365
13	0.00–30.00	300	367
14	0.00–30.00	300	369
15	0.00–30.00	300	371
16	0.00–30.00	300	373
17	0.00–30.00	300	376
18	0.00–30.00	300	378
19	0.00–30.00	300	401
20	0.00–30.00	300	424
21	0.00–30.00	300	447
22	0.00–30.00	300	469
23	0.00–30.00	300	492
24	0.00–30.00	300	514
25	0.00–30.00	300	522
26	0.00–30.00	300	531
27	0.00–30.00	300	540
28	0.00–30.00	300	549
29	0.00–30.00	300	558
30	0.00–30.00	300	566
31	0.00–30.00	300	554
32	0.00–30.00	300	542
33	0.00–30.00	300	530
34	0.00–30.00	300	518
35	0.00–30.00	300	505
36	0.00–30.00	300	493
37	0.00–30.00	300	485
38	0.00–30.00	300	478
39	0.00–30.00	300	471
40	0.00–30.00	300	463
41	0.00–30.00	300	456
42	0.00–30.00	300	448
43	0.00–30.00	300	445
44	0.00–30.00	300	442
45	0.00–30.00	300	438
46	0.00–30.00	300	435
47	0.00–30.00	300	431
48	0.00–30.00	300	427
49	0.00–30.00	300	438
50	0.00–30.00	300	449

Distance, in meters	Top and bottom, in meters	Number of layers	V_{S30}, in meters per second
51	0.00–30.00	300	459
52	0.00–30.00	300	470
53	0.00–30.00	300	480
54	0.00–30.00	300	491
55	0.00–30.00	300	530
56	0.00–30.00	300	568
57	0.00–30.00	300	604
58	0.00–30.00	300	640
59	0.00–30.00	300	675
60	0.00–30.00	300	710
61	0.00–30.00	300	749
62	0.00–30.00	300	787
63	0.00–30.00	300	825
64	0.00–30.00	300	862
65	0.00–30.00	300	898
66	0.00–30.00	300	934
67	0.00–30.00	300	926
68	0.00–30.00	300	917
69	0.00–30.00	300	909
70	0.00–30.00	300	900
71	0.00–30.00	300	890
72	0.00–30.00	300	880
73	0.00–30.00	300	862
74	0.00–30.00	300	844
75	0.00–30.00	300	825
76	0.00–30.00	300	806
77	0.00–30.00	300	787
78	0.00–30.00	300	767
79	0.00–30.00	300	762
80	0.00–30.00	300	756
81	0.00–30.00	300	751
82	0.00–30.00	300	746
83	0.00–30.00	300	740
84	0.00–30.00	300	735
85	0.00–30.00	300	728
86	0.00–30.00	300	721
87	0.00–30.00	300	714
88	0.00–30.00	300	706
89	0.00–30.00	300	698
90	0.00–30.00	300	690
91	0.00–30.00	300	715
92	0.00–30.00	300	738
93	0.00–30.00	300	762
94	0.00–30.00	300	784
95	0.00–30.00	300	806
96	0.00–30.00	300	828
97	0.00–30.00	300	850
98	0.00–30.00	300	872
99	0.00–30.00	300	893
100	0.00–30.00	300	914
101	0.00–30.00	300	934
102	0.00–30.00	300	955
103	0.00–30.00	300	953
104	0.00–30.00	300	952
105	0.00–30.00	300	950

Distance, in meters	Top and bottom, in meters	Number of layers	V_{S30}, in meters per second
106	0.00–30.00	300	948
107	0.00–30.00	300	946
108	0.00–30.00	300	945
109	0.00–30.00	300	936
110	0.00–30.00	300	927
111	0.00–30.00	300	917
112	0.00–30.00	300	906
113	0.00–30.00	300	893
114	0.00–30.00	300	879
115	0.00–30.00	300	893
116	0.00–30.00	300	907
117	0.00–30.00	300	920
118	0.00–30.00	300	934
119	0.00–30.00	300	947
120	0.00–30.00	300	961
121	0.00–30.00	300	1,007
122	0.00–30.00	300	1,051
123	0.00–30.00	300	1,093
124	0.00–30.00	300	1,134
125	0.00–30.00	300	1,173
126	0.00–30.00	300	1,211
127	0.00–30.00	300	1,236
128	0.00–30.00	300	1,261
129	0.00–30.00	300	1,285
130	0.00–30.00	300	1,308
131	0.00–30.00	300	1,332
132	0.00–30.00	300	1,355
133	0.00–30.00	300	1,359
134	0.00–30.00	300	1,363
135	0.00–30.00	300	1,368
136	0.00–30.00	300	1,372
137	0.00–30.00	300	1,377
138	0.00–30.00	300	1,381
139	0.00–30.00	300	1,380
140	0.00–30.00	300	1,378
141	0.00–30.00	300	1,377
142	0.00–30.00	300	1,376
143	0.00–30.00	300	1,374
144	0.00–30.00	300	1,373
145	0.00–30.00	300	1,371
146	0.00–30.00	300	1,369
147	0.00–30.00	300	1,366
148	0.00–30.00	300	1,364
149	0.00–30.00	300	1,362
150	0.00–30.00	300	1,360
151	0.00–30.00	300	1,357
152	0.00–30.00	300	1,355
153	0.00–30.00	300	1,353
154	0.00–30.00	300	1,350
155	0.00–30.00	300	1,348
156	0.00–30.00	300	1,345
157	0.00–30.00	300	1,343
158	0.00–30.00	300	1,341
159	0.00–30.00	300	1,338
160	0.00–30.00	300	1,336

Distance, in meters	Top and bottom, in meters	Number of layers	V_{S30}, in meters per second
161	0.00–30.00	300	1,334
162	0.00–30.00	300	1,332
163	0.00–30.00	300	1,331
164	0.00–30.00	300	1,330
165	0.00–30.00	300	1,330
166	0.00–30.00	300	1,329
167	0.00–30.00	300	1,328
168	0.00–30.00	300	1,328
169	0.00–30.00	300	1,326
170	0.00–30.00	300	1,325
171	0.00–30.00	300	1,323
172	0.00–30.00	300	1,321
173	0.00–30.00	300	1,320
174	0.00–30.00	300	1,318
175	0.00–30.00	300	1,314
176	0.00–30.00	300	1,310
177	0.00–30.00	300	1,305
178	0.00–30.00	300	1,301
179	0.00–30.00	300	1,296
180	0.00–30.00	300	1,292
181	0.00–30.00	300	1,274
182	0.00–30.00	300	1,255
183	0.00–30.00	300	1,235
184	0.00–30.00	300	1,215
185	0.00–30.00	300	1,194
186	0.00–30.00	300	1,172
187	0.00–30.00	300	1,164
188	0.00–30.00	300	1,155
189	0.00–30.00	300	1,147
190	0.00–30.00	300	1,139
191	0.00–30.00	300	1,130
192	0.00–30.00	300	1,122
193	0.00–30.00	300	1,130
194	0.00–30.00	300	1,138
195	0.00–30.00	300	1,146
196	0.00–30.00	300	1,153
197	0.00–30.00	300	1,160
198	0.00–30.00	300	1,168
199	0.00–30.00	300	1,166
200	0.00–30.00	300	1,164
201	0.00–30.00	300	1,162
202	0.00–30.00	300	1,160
203	0.00–30.00	300	1,158
204	0.00–30.00	300	1,156
205	0.00–30.00	300	1,160
206	0.00–30.00	300	1,165
207	0.00–30.00	300	1,170
208	0.00–30.00	300	1,174
209	0.00–30.00	300	1,179
210	0.00–30.00	300	1,183
211	0.00–30.00	300	1,183
212	0.00–30.00	300	1,183
213	0.00–30.00	300	1,182
214	0.00–30.00	300	1,182
215	0.00–30.00	300	1,181

Distance, in meters	Top and bottom, in meters	Number of layers	V_{S30}, in meters per second
216	0.00–30.00	300	1,181
217	0.00–30.00	300	1,162
218	0.00–30.00	300	1,144
219	0.00–30.00	300	1,125
220	0.00–30.00	300	1,106
221	0.00–30.00	300	1,086
222	0.00–30.00	300	1,067
223	0.00–30.00	300	1,055
224	0.00–30.00	300	1,044
225	0.00–30.00	300	1,032
226	0.00–30.00	300	1,021
227	0.00–30.00	300	1,009
228	0.00–30.00	300	998
229	0.00–30.00	300	1,001
230	0.00–30.00	300	1,004
231	0.00–30.00	300	1,007
232	0.00–30.00	300	1,011
233	0.00–30.00	300	1,014
234	0.00–30.00	300	1,017
Minimum			399
Maximum			1,545
Average			1,027

Table 10. Multichannel analysis of surface waves for Rayleigh waves ($MASW_R$)-determined time-averaged shear-wave velocity in the upper 30 meters of the subsurface (V_{S30}) values along the Strathcona Dam Roadway seismic profile, Vancouver Island, British Columbia, Canada.

Distance, in meters	Top and bottom, in meters	Number of layers	V_{S30}, in meters per second
0	0.00–30.00	300	405
1	0.00–30.00	300	411
2	0.00–30.00	300	418
3	0.00–30.00	300	425
4	0.00–30.00	300	432
5	0.00–30.00	300	438
6	0.00–30.00	300	445
7	0.00–30.00	300	449
8	0.00–30.00	300	453
9	0.00–30.00	300	457
10	0.00–30.00	300	460
11	0.00–30.00	300	464
12	0.00–30.00	300	468
13	0.00–30.00	300	468
14	0.00–30.00	300	468
15	0.00–30.00	300	467
16	0.00–30.00	300	467
17	0.00–30.00	300	467
18	0.00–30.00	300	466
19	0.00–30.00	300	473
20	0.00–30.00	300	480
21	0.00–30.00	300	487
22	0.00–30.00	300	494
23	0.00–30.00	300	501
24	0.00–30.00	300	508
25	0.00–30.00	300	512
26	0.00–30.00	300	517
27	0.00–30.00	300	521
28	0.00–30.00	300	525
29	0.00–30.00	300	530
30	0.00–30.00	300	534
31	0.00–30.00	300	524
32	0.00–30.00	300	515
33	0.00–30.00	300	505
34	0.00–30.00	300	496
35	0.00–30.00	300	486
36	0.00–30.00	300	476
37	0.00–30.00	300	464
38	0.00–30.00	300	452
39	0.00–30.00	300	440
40	0.00–30.00	300	428
41	0.00–30.00	300	415
42	0.00–30.00	300	403
43	0.00–30.00	300	402
44	0.00–30.00	300	402
45	0.00–30.00	300	401
46	0.00–30.00	300	401
47	0.00–30.00	300	400
48	0.00–30.00	300	399
49	0.00–30.00	300	407
50	0.00–30.00	300	414

Distance, in meters	Top and bottom, in meters	Number of layers	V_{S30}, in meters per second
51	0.00–30.00	300	421
52	0.00–30.00	300	428
53	0.00–30.00	300	435
54	0.00–30.00	300	442
55	0.00–30.00	300	450
56	0.00–30.00	300	457
57	0.00–30.00	300	465
58	0.00–30.00	300	473
59	0.00–30.00	300	480
60	0.00–30.00	300	488
61	0.00–30.00	300	489
62	0.00–30.00	300	490
63	0.00–30.00	300	491
64	0.00–30.00	300	492
65	0.00–30.00	300	493
66	0.00–30.00	300	494
67	0.00–30.00	300	492
68	0.00–30.00	300	490
69	0.00–30.00	300	488
70	0.00–30.00	300	485
71	0.00–30.00	300	483
72	0.00–30.00	300	480
73	0.00–30.00	300	483
74	0.00–30.00	300	487
75	0.00–30.00	300	490
76	0.00–30.00	300	492
77	0.00–30.00	300	494
78	0.00–30.00	300	496
79	0.00–30.00	300	587
80	0.00–30.00	300	666
81	0.00–30.00	300	739
82	0.00–30.00	300	808
83	0.00–30.00	300	874
84	0.00–30.00	300	937
85	0.00–30.00	300	1,007
86	0.00–30.00	300	1,075
87	0.00–30.00	300	1,141
88	0.00–30.00	300	1,205
89	0.00–30.00	300	1,269
90	0.00–30.00	300	1,331
91	0.00–30.00	300	1,356
92	0.00–30.00	300	1,381
93	0.00–30.00	300	1,406
94	0.00–30.00	300	1,431
95	0.00–30.00	300	1,456
96	0.00–30.00	300	1,481
97	0.00–30.00	300	1,491
98	0.00–30.00	300	1,501
99	0.00–30.00	300	1,512
100	0.00–30.00	300	1,522
101	0.00–30.00	300	1,532
102	0.00–30.00	300	1,542
103	0.00–30.00	300	1,542
104	0.00–30.00	300	1,543
105	0.00–30.00	300	1,543

Distance, in meters	Top and bottom, in meters	Number of layers	V_{S30}, in meters per second
106	0.00–30.00	300	1,544
107	0.00–30.00	300	1,544
108	0.00–30.00	300	1,545
109	0.00–30.00	300	1,543
110	0.00–30.00	300	1,541
111	0.00–30.00	300	1,539
112	0.00–30.00	300	1,538
113	0.00–30.00	300	1,536
114	0.00–30.00	300	1,534
115	0.00–30.00	300	1,531
116	0.00–30.00	300	1,528
117	0.00–30.00	300	1,526
118	0.00–30.00	300	1,523
119	0.00–30.00	300	1,520
120	0.00–30.00	300	1,517
121	0.00–30.00	300	1,516
122	0.00–30.00	300	1,515
123	0.00–30.00	300	1,514
124	0.00–30.00	300	1,513
125	0.00–30.00	300	1,512
126	0.00–30.00	300	1,511
127	0.00–30.00	300	1,512
128	0.00–30.00	300	1,513
129	0.00–30.00	300	1,514
130	0.00–30.00	300	1,515
131	0.00–30.00	300	1,515
132	0.00–30.00	300	1,516
133	0.00–30.00	300	1,518
134	0.00–30.00	300	1,520
135	0.00–30.00	300	1,521
136	0.00–30.00	300	1,523
137	0.00–30.00	300	1,525
138	0.00–30.00	300	1,527
139	0.00–30.00	300	1,528
140	0.00–30.00	300	1,529
141	0.00–30.00	300	1,530
142	0.00–30.00	300	1,531
143	0.00–30.00	300	1,532
144	0.00–30.00	300	1,533
145	0.00–30.00	300	1,532
146	0.00–30.00	300	1,532
147	0.00–30.00	300	1,532
148	0.00–30.00	300	1,531
149	0.00–30.00	300	1,531
150	0.00–30.00	300	1,530
151	0.00–30.00	300	1,529
152	0.00–30.00	300	1,529
153	0.00–30.00	300	1,528
154	0.00–30.00	300	1,527
155	0.00–30.00	300	1,526
156	0.00–30.00	300	1,525
157	0.00–30.00	300	1,525
158	0.00–30.00	300	1,524
159	0.00–30.00	300	1,524
160	0.00–30.00	300	1,523

Distance, in meters	Top and bottom, in meters	Number of layers	V_{S30}, in meters per second
161	0.00–30.00	300	1,522
162	0.00–30.00	300	1,522
163	0.00–30.00	300	1,521
164	0.00–30.00	300	1,519
165	0.00–30.00	300	1,518
166	0.00–30.00	300	1,516
167	0.00–30.00	300	1,515
168	0.00–30.00	300	1,514
169	0.00–30.00	300	1,511
170	0.00–30.00	300	1,508
171	0.00–30.00	300	1,506
172	0.00–30.00	300	1,503
173	0.00–30.00	300	1,500
174	0.00–30.00	300	1,497
175	0.00–30.00	300	1,490
176	0.00–30.00	300	1,482
177	0.00–30.00	300	1,474
178	0.00–30.00	300	1,466
179	0.00–30.00	300	1,458
180	0.00–30.00	300	1,450
181	0.00–30.00	300	1,431
182	0.00–30.00	300	1,413
183	0.00–30.00	300	1,395
184	0.00–30.00	300	1,377
185	0.00–30.00	300	1,359
186	0.00–30.00	300	1,341
187	0.00–30.00	300	1,320
188	0.00–30.00	300	1,299
189	0.00–30.00	300	1,278
190	0.00–30.00	300	1,257
191	0.00–30.00	300	1,236
192	0.00–30.00	300	1,215
193	0.00–30.00	300	1,197
194	0.00–30.00	300	1,179
195	0.00–30.00	300	1,161
196	0.00–30.00	300	1,144
197	0.00–30.00	300	1,126
198	0.00–30.00	300	1,108
199	0.00–30.00	300	1,091
200	0.00–30.00	300	1,075
201	0.00–30.00	300	1,058
202	0.00–30.00	300	1,042
203	0.00–30.00	300	1,026
204	0.00–30.00	300	1,009
205	0.00–30.00	300	1,001
206	0.00–30.00	300	992
207	0.00–30.00	300	984
208	0.00–30.00	300	976
209	0.00–30.00	300	967
210	0.00–30.00	300	959
211	0.00–30.00	300	954
212	0.00–30.00	300	949
213	0.00–30.00	300	944
214	0.00–30.00	300	939
215	0.00–30.00	300	933

Distance, in meters	Top and bottom, in meters	Number of layers	V_{S30}, in meters per second
216	0.00–30.00	300	928
217	0.00–30.00	300	922
218	0.00–30.00	300	916
219	0.00–30.00	300	910
220	0.00–30.00	300	903
221	0.00–30.00	300	897
222	0.00–30.00	300	891
223	0.00–30.00	300	889
224	0.00–30.00	300	887
225	0.00–30.00	300	885
226	0.00–30.00	300	883
227	0.00–30.00	300	881
228	0.00–30.00	300	879
229	0.00–30.00	300	879
230	0.00–30.00	300	879
231	0.00–30.00	300	879
232	0.00–30.00	300	878
233	0.00–30.00	300	878
234	0.00–30.00	300	878
Minimum			353
Maximum			1,381
Average			932

Table 11. Tomographically determined time-averaged shear-wave velocity in the upper 30 meters of the subsurface (V_{S30}) values along the Strathcona Dam Spillway seismic profile, Vancouver Island, British Columbia, Canada.

Distance, in meters	Top and bottom, in meters	Number of layers	V_{S30}, in meters per second
–6	–29.02–0.98	0	0
–3	–28.61–1.39	0	0
0	–28.20–1.80	0	0
3	–27.79–2.21	0	0
6	–27.49–2.51	0	0
9	–27.17–2.83	0	0
12	–26.84–3.16	0	0
15	–26.48–3.52	0	0
18	–26.17–3.83	0	0
21	–25.69–4.31	0	0
24	–25.70–4.30	0	0
27	–25.20–4.80	300	2,255
30	–24.90–5.10	300	2,253
33	–24.59–5.41	300	2,240
36	–24.14–5.86	300	2,208
39	–23.74–6.26	300	2,219
42	–23.63–6.37	300	2,188
45	–23.31–6.69	300	2,181
48	–22.85–7.15	300	2,189
51	–22.33–7.67	300	2,204
54	–22.10–7.90	300	2,202
57	–21.90–8.10	300	2,210
60	–21.90–8.10	300	2,209
63	–21.82–8.18	300	2,220
66	–21.47–8.53	300	2,254
69	–21.08–8.92	300	2,261
72	–20.72–9.28	300	2,320
75	–20.50–9.50	300	2,337
78	–20.29–9.71	300	2,349
81	–19.90–10.10	300	2,369
84	–19.76–10.24	300	2,361
87	–19.60–10.40	300	2,356
90	–19.37–10.63	300	2,363
93	–19.05–10.95	300	2,382
96	–18.70–11.30	300	2,405
99	–18.37–11.63	300	2,421
102	–17.98–12.02	300	2,440
105	–17.50–12.50	300	2,463
108	–17.12–12.88	300	2,476
111	–16.82–13.18	300	2,480
114	–16.55–13.45	300	2,480
117	–16.22–13.78	300	2,483
120	–15.92–14.08	300	2,482
123	–15.60–14.40	300	2,483
126	–15.28–14.72	300	2,480
129	–14.95–15.05	300	2,479
132	–14.75–15.25	300	2,466
135	–14.61–15.39	300	2,451
138	–14.42–15.58	300	2,444
141	–14.30–15.70	300	2,427
144	–14.17–15.83	300	2,408

Distance, in meters	Top and bottom, in meters	Number of layers	V_{S30}, in meters per second
147	–13.96–16.04	300	2,397
150	–13.71–16.29	300	2,386
153	–13.44–16.56	300	2,374
156	–13.15–16.85	300	2,361
159	–12.79–17.21	300	2,350
162	–12.36–17.64	300	2,337
165	–11.90–18.10	300	2,325
168	–11.34–18.66	300	2,323
171	–10.77–19.23	300	2,328
174	–10.34–19.66	300	2,326
177	–10.26–19.74	300	2,302
180	–9.87–20.13	300	2,300
183	–9.41–20.59	300	2,301
186	–8.94–21.06	300	2,300
189	–8.36–21.64	300	2,316
192	–7.95–22.05	300	2,319
195	–7.54–22.46	0	0
198	–7.24–22.76	0	0
201	–6.84–23.16	0	0
204	–6.39–23.61	0	0
207	–5.99–24.01	0	0
210	–5.46–24.54	0	0
213	–4.69–25.31	0	0
216	–4.19–25.81	0	0
219	–3.65–26.35	0	0
222	–2.96–27.04	0	0
225	–2.30–27.70	0	0
228	–1.54–28.46	0	0
231	–0.89–29.11	0	0
234	–0.19–29.81	0	0
237	0.54–30.54	0	0
240	1.28–31.28	0	0
Minimum			2,181
Maximum			2,483
Average			2,344

Table 12. Multichannel analysis of surface waves for Love waves (MAS_LW)-determined time-averaged shear-wave velocity in the upper 30 meters of the subsurface (V_{S30}) values along the Strathcona Dam Campground seismic profile, Vancouver Island, British Columbia, Canada.

Distance, in meters	Top and bottom, in meters	Number of layers	V_{S30}, in meters per second
36	0.00–30.00	300	633
37	0.00–30.00	300	646
38	0.00–30.00	300	657
39	0.00–30.00	300	666
40	0.00–30.00	300	675
41	0.00–30.00	300	682
42	0.00–30.00	300	689
43	0.00–30.00	300	696
44	0.00–30.00	300	702
45	0.00–30.00	300	708
46	0.00–30.00	300	713
47	0.00–30.00	300	718
48	0.00–30.00	300	722
49	0.00–30.00	300	722
50	0.00–30.00	300	722
51	0.00–30.00	300	722
52	0.00–30.00	300	723
53	0.00–30.00	300	723
54	0.00–30.00	300	723
55	0.00–30.00	300	724
56	0.00–30.00	300	726
57	0.00–30.00	300	727
58	0.00–30.00	300	729
59	0.00–30.00	300	730
60	0.00–30.00	300	731
61	0.00–30.00	300	731
62	0.00–30.00	300	731
63	0.00–30.00	300	731
64	0.00–30.00	300	730
65	0.00–30.00	300	730
66	0.00–30.00	300	729
67	0.00–30.00	300	727
68	0.00–30.00	300	726
69	0.00–30.00	300	724
70	0.00–30.00	300	722
71	0.00–30.00	300	721
72	0.00–30.00	300	719
73	0.00–30.00	300	719
74	0.00–30.00	300	720
75	0.00–30.00	300	720
76	0.00–30.00	300	721
77	0.00–30.00	300	721
78	0.00–30.00	300	722
79	0.00–30.00	300	718
80	0.00–30.00	300	714
81	0.00–30.00	300	711
82	0.00–30.00	300	707
83	0.00–30.00	300	703
84	0.00–30.00	300	699
85	0.00–30.00	300	693
86	0.00–30.00	300	687

Distance, in meters	Top and bottom, in meters	Number of layers	V_{S30}, in meters per second
87	0.00–30.00	300	680
88	0.00–30.00	300	674
89	0.00–30.00	300	667
90	0.00–30.00	300	661
91	0.00–30.00	300	659
92	0.00–30.00	300	656
93	0.00–30.00	300	653
94	0.00–30.00	300	651
95	0.00–30.00	300	648
96	0.00–30.00	300	645
97	0.00–30.00	300	644
98	0.00–30.00	300	643
99	0.00–30.00	300	641
100	0.00–30.00	300	640
101	0.00–30.00	300	639
102	0.00–30.00	300	637
103	0.00–30.00	300	638
104	0.00–30.00	300	638
105	0.00–30.00	300	638
106	0.00–30.00	300	638
107	0.00–30.00	300	639
108	0.00–30.00	300	639
109	0.00–30.00	300	639
110	0.00–30.00	300	640
111	0.00–30.00	300	640
112	0.00–30.00	300	640
113	0.00–30.00	300	640
114	0.00–30.00	300	641
115	0.00–30.00	300	640
116	0.00–30.00	300	638
117	0.00–30.00	300	637
118	0.00–30.00	300	636
119	0.00–30.00	300	635
120	0.00–30.00	300	634
121	0.00–30.00	300	631
122	0.00–30.00	300	627
123	0.00–30.00	300	624
124	0.00–30.00	300	621
125	0.00–30.00	300	617
126	0.00–30.00	300	614
127	0.00–30.00	300	610
128	0.00–30.00	300	605
129	0.00–30.00	300	601
130	0.00–30.00	300	597
131	0.00–30.00	300	593
132	0.00–30.00	300	588
133	0.00–30.00	300	587
134	0.00–30.00	300	586
135	0.00–30.00	300	585
136	0.00–30.00	300	585
137	0.00–30.00	300	584
138	0.00–30.00	300	583
139	0.00–30.00	300	582
140	0.00–30.00	300	582
141	0.00–30.00	300	582

Distance, in meters	Top and bottom, in meters	Number of layers	V_{S30}, in meters per second
142	0.00–30.00	300	582
143	0.00–30.00	300	582
144	0.00–30.00	300	582
145	0.00–30.00	300	580
146	0.00–30.00	300	579
147	0.00–30.00	300	578
148	0.00–30.00	300	577
149	0.00–30.00	300	576
150	0.00–30.00	300	574
151	0.00–30.00	300	573
152	0.00–30.00	300	572
153	0.00–30.00	300	571
154	0.00–30.00	300	570
155	0.00–30.00	300	568
156	0.00–30.00	300	567
157	0.00–30.00	300	567
158	0.00–30.00	300	567
159	0.00–30.00	300	567
160	0.00–30.00	300	567
161	0.00–30.00	300	567
162	0.00–30.00	300	566
163	0.00–30.00	300	569
164	0.00–30.00	300	571
165	0.00–30.00	300	573
166	0.00–30.00	300	576
167	0.00–30.00	300	578
168	0.00–30.00	300	580
169	0.00–30.00	300	580
170	0.00–30.00	300	580
171	0.00–30.00	300	579
172	0.00–30.00	300	579
173	0.00–30.00	300	579
174	0.00–30.00	300	579
175	0.00–30.00	300	577
176	0.00–30.00	300	576
177	0.00–30.00	300	575
178	0.00–30.00	300	574
179	0.00–30.00	300	573
180	0.00–30.00	300	571
181	0.00–30.00	300	573
182	0.00–30.00	300	574
183	0.00–30.00	300	575
184	0.00–30.00	300	576
185	0.00–30.00	300	577
186	0.00–30.00	300	578
187	0.00–30.00	300	584
188	0.00–30.00	300	589
189	0.00–30.00	300	594
190	0.00–30.00	300	600
191	0.00–30.00	300	605
192	0.00–30.00	300	610
193	0.00–30.00	300	615
194	0.00–30.00	300	619
195	0.00–30.00	300	624
196	0.00–30.00	300	628

Distance, in meters	Top and bottom, in meters	Number of layers	V_{S30}, in meters per second
197	0.00–30.00	300	632
198	0.00–30.00	300	637
Minimum			566
Maximum			731
Average			638

ISSN 2331-1258 (online)
https://doi.org/10.3133/ofr20191015